



Durham E-Theses

Second order nonlinear optical properties of poled polymeric thin Films

Karakus, Yusuf

How to cite:

Karakus, Yusuf (1993) *Second order nonlinear optical properties of poled polymeric thin Films*, Durham theses, Durham University. Available at Durham E-Theses Online: <http://etheses.dur.ac.uk/5656/>

Use policy

The full-text may be used and/or reproduced, and given to third parties in any format or medium, without prior permission or charge, for personal research or study, educational, or not-for-profit purposes provided that:

- a full bibliographic reference is made to the original source
- a [link](#) is made to the metadata record in Durham E-Theses
- the full-text is not changed in any way

The full-text must not be sold in any format or medium without the formal permission of the copyright holders.

Please consult the [full Durham E-Theses policy](#) for further details.

The copyright of this thesis rests with the author.
No quotation from it should be published without
his prior written consent and information derived
from it should be acknowledged.

Second order Nonlinear Optical Properties
of Poled Polymeric Thin Films

A thesis submitted for the degree of
Doctor of Philosophy

by

Yusuf Karkuş (BSc)

University of Durham
Applied Physics Group
Department of Physics

May 1993



2 JUL 1993

Declaration

I hereby declare that the work reported in this thesis has not previously been submitted for any degree and is not being currently submitted in candidature for any other degree.

The work reported in this thesis was carried out by the candidate. Any work not carried out by the candidate is acknowledged in the main text.

Candidate

Statement of Copyright

The copyright of this thesis rests with the author. No quotation should be published without his prior written consent and information derived from it should be acknowledged.

ACKNOWLEDGEMENTS

I would like to thank Professor Bloor for his supervision, guidance and support throughout the project. I would like to express my gratitude to Dr. G.H. Cross for his valuable help and continuous assistance. I also would like to thank members of Durham Opto-electronics Group, especially Mr. D. Gray for their valuable comments and help. I would like to thank Dr. J. Hutson for AM1 calculations and to Mr. G.M. Forrest for DSC measurements. Special thanks are due to The Turkish Scientific and Technical Research Council (TUBITAK) for sponsorship. Finally, I would like to thank my wife, my parents and my friends for their encouragement.

ABSTRACT

In this thesis the electrical poling and second order non-linear optical, NLO properties of guest-host, side-chain and main-chain polymers are studied. In bisphenol-A polycarbonate, BPA-PC guest-host systems an enhancement in both the thermal stability and linear electro-optic coefficient can be observed. This can occur in guest-host systems where hydrogen bonding can arise. One example is DAN/BPA-PC guest-host polymer.

In side-chain materials a commercially available polymer P-4VP can be poled. This material shows moderate electro-optic response following poling.

A novel main-chain type material, where the NLO group is rigidly bonded to the main-chain in a 'V' shape is studied for its poling and second-order NLO properties. The rigidity of the polymer is so high that only chain-end groups contribute to the response.

TABLE OF CONTENTS

I- INTRODUCTION	1
1.1 Background	1
1.1.1 Molecular Basis for NLO	3
1.1.2 The Non-linear Effects Associated with $\chi^{(2)}$ and $\chi^{(3)}$	3
1.1.3 $\chi^{(2)}$ Effects	4
1.2 Use of NLO in Device Applications	5
1.3 Material Requirements	6
1.4 Origin of Non-linearity in Organic Materials	8
1.4.1 Relationship Between $\chi^{(2)}$ and Electro-optic Coefficient	8
1.4.2 Different Types of Polymeric Systems	9
1.5 References	11
II- ELECTRICAL POLING AND STABILITY	13
2.1 Electrical Poling	13
2.2 Local Field Correction Factor	16
2.3 Free Gas Model	17
2.4 Optimisation of $\chi^{(2)}$	18
2.4.1 Increasing N	18
2.4.2 Molecular Design	19
2.4.3 Increasing Poling Field	21
2.5 Thermal Stability	21
2.5.1 Introduction	21
2.5.2 Thermal relaxation in Poled Polymers	22
2.6 Models of Relaxation Phenomena	23
2.6.1 Temperature Dependence of Relaxation	24
2.7 Attempts to Increase Thermal Stability of Poled Polymer Films	26
2.7.1 Physical ageing	26
2.7.2 Annealing	26
2.7.3 Chemical Cross-linking	27
2.7.4 Hydrogen Bonding	28
2.8 References	29
III- EXPERIMENTAL TECHNIQUES	32
3.1 Introduction	32
3.2 Sample Preparation	32
3.2.1 Spin Coating	32
3.2.2 Dip Coating	33
3.3 Characterisation of Samples	34

3.3.1 Prism Coupling	35
3.3.2 Relative Permittivity Measurements	38
3.4 Electrical poling	38
3.4.1 Parallel Plate Poling	38
3.4.2 Corona Discharge Poling	40
3.5 Uniform Field Distribution of Corona Discharge Poling	41
3.6 Electro-optic Reflection Technique	42
3.7 Maker Fringe Analysis Technique for Second Harmonic Generation Measurements	46
3.8 References	49
IV- GUEST-HOST SYSTEMS	51
4.1 Introduction	51
4.2 Physical Properties of Materials Used	51
4.2.1 Guest Molecules	51
4.2.2 Host Polymers	53
4.3 Sample Preparation and Characterisation	54
4.4 Linear and Quadratic Electro-optic Response	57
4.5 Plasticizing Effects in DAN/BPA-PC and DAN/PMMA Films	59
4.6 Thermal Relaxation in a Poled 20 % DAN/BPA-PC Sample	64
4.7 Electrical Poling of DAN Doped BPA-PC and PMMA Thin Films	65
4.7.1 Poling at Different Temperatures	65
4.7.2 Poling at Different Fields	66
4.7.3 Effect of varying Poling Time	68
4.8 Current Density versus Temperature	69
4.9 Comparative Poling Study of DAN Doped BPA-PC and PMMA	70
4.9.1 Contribution of BPA-PC	72
4.9.2 Loss of Dopant	73
4.9.3 Guest-host Interaction	79
4.10 Poling Stability	80
4.11 Hydrogen Bonding in DAN/BPA-PC Systems	82
4.12 Second Harmonic Generation Measurements	85
4.13 Conclusions	86
4.14 References	87
V- SIDE-CHAIN POLYMERS	89
5.1 Introduction	89
5.2 Sample preparation and Characterisation	92
5.3 Poling of P-4VP	94
5.3.1 Initial studies	94

5.3.2	Current Density versus Temperature Characteristics	96
5.3.3	Poling at Different Temperatures	97
5.3.4	Poling of 'dry' and 'wet' P-4VP Samples at Various Fields	99
5.3.5	Stability of Polar Alignment in Poled 'dry' and 'wet' P-4VP	99
5.3.6	Theoretical comparison	101
5.4	Poling of MO3ONS	102
5.5	Conclusions	105
5.6	References	105
VI-	MAIN-CHAIN POLYMERS	107
6.1	Introduction	107
6.2	Synthesis and film deposition	109
6.3	Poling of Rigid 'V' Main-Chain Polymer	112
6.4	Thermal stability of poled rigid 'V' film	113
6.5	SHG Measurements on Corona Poled Samples	113
6.6	Comparison with theory	114
6.7	Conclusion	115
6.8	References	118
VII-	CONCLUSIONS	119
7.1	Summary of The Work	119
7.2	Ideas For Future Work	122
	APPENDIX I	124
	APPENDIX II	126

List of Figure Captions

Chapter 1

Figure 1.1: The basic molecular structure required for 2nd order NLO.

Chapter 2

Figure 2.1: Position of a dipole moment in spherical coordinates

Figure 2.2 Structure formulae of the materials used in table 2.1

Figure 2.3: Temperature dependence of the specific free volume of typical glassy polymers (after Man and Yoon [31])

Chapter 3

Figure 3.1 : Dip coating apparatus.

Figure 3.2 : Schematic diagram of prism coupling set-up.

Figure 3.3 : The bulk refractive index and the thickness of a 10% w/w DAN/BPA-PC film.

Figure 3.4 : (a) The parallel plate poling experimental set-up (C, chopper; CC, chopper controller; P, polarizer; SBC, Soleil-Babinet compensator; S, sample; TC, temperature controller; A, analyser; D, detector; LA, lock-in amplifier; O, oscilloscope; M, modulator; Am, amplifier; AC, AC signal generator; DC, DC power supply),
(b) Electrical connections

Figure 3.5 : The experimental arrangement for corona poling (HVS stands for high voltage supplier)

Figure 3.6 : The optical configuration of the EO reflection technique.

Figure 3.7 : Transmission factor of a cross-polarised EO modulator as a function of an applied voltage (Yariv, Optical Electronics, New York, 1985, p: 293)The path of the HeNe radiation in EO reflection technique.

Figure 3.8 : The second harmonic generation (Maker fringe) experimental set-up

Chapter 4

Figure 4.1: Structural formulae of materials used (a) guest molecules (b) host polymers

- Figure 4.2:** α , β , γ -relaxation in bisphenol-A polycarbonate measured by dynamical mechanical analysis (G' = storage modulus, G'' = loss modulus (adapted from [14])
- Figure 4.3:** Modulation intensity (I_m) vs. drive field characteristic of DAN/BPA-PC film at ω
- Figure 4.4:** Modulation intensity (I_m) vs. drive field characteristic of DAN/BPA-PC film at 2ω
- Figure 4.5:** a) Circular polarisation ($V_m=0$), b) Elliptical polarisation ($V_m>0$)
- Figure 4.6:** DSC of un-doped BPA-PC film
- Figure 4.7:** DSC of un-doped PMMA film
- Figure 4.8:** DSC of 20% DAN/BPA-PC film
- Figure 4.9:** DSC of 20% DAN/PMMA film
- Figure 4.10:** DSC of 25% NMBA/BPA-PC film
- Figure 4.11:** T_g of DAN/BPA-PC films vs. weight fraction of DAN
- Figure 4.12:** Normalised EO response (r_{33}) vs. temperature for 20% DAN/BPA-PC thin film
- Figure 4.13:** (a) EO coefficient (r_{33}) vs. poling temperature ($^{\circ}\text{C}$) of 20% DAN/BPA-PC and 20% DAN/PMMA films (b) r_{33} vs. T_p of two different 20% DAN/BPA-PC samples
- Figure 4.14:** EO coefficient (r_{33}) vs. poling field for 20% DAN doped BPA-PC and PMMA
- Figure 4.15:** Current density/ temperature relationships for guest-host polymers. Note that the decrease in current density between cycles occurs over the poling time of 15 minutes
- Figure 4.16:** J/T of BPA-PC and 20% DAN doped BPA-PC sample
- Figure 4.17:** Absorption spectrum of 20% DAN/PMMA films (before and after drying)
- Figure 4.18:** Absorption spectrum of 20% DAN/BPA-PC films (before and after drying)
- Figure 4.19:** Absorption spectrum of 20% DAN/PMMA film at different temperatures
- Figure 4.19:** Absorption spectrum of 20% DAN/PMMA film at different temperatures
- Figure 4.21:** r_{33} vs. poling temperature for two different 20% DAN doped PMMA samples
- Figure 4.22:** Normalised EO coefficient (r_{33}) vs. time for poled 20% DAN doped PMMA and BPA-PC
- Figure 4.23:** Normalised r_{33} of poled 20% DAN/BPA-PC, NMBA/PMMA and NMBA/BPA-PC samples

Figure 4.24: KWW plot of 20% DAN/BPA-PC and an annealed side-chain polymer

Figure 4.25: Infrared spectrum of a 20% (w/w) DAN/BPA-PC thin film

Figure 4.26: The normalised SH intensity of p-polarised fundamental and second harmonic light versus θ

Chapter 5

Figure 5.1 : The structural formulae of these side-chain polymers, (a) P-4VP, and (b) MO3ONS

Figure 5.2 : The absorption spectrum of P-4VP thin film

Figure 5.3 : DSC of P-4VP (heating rate 10 °C minutes⁻¹)

Figure 5.4 : The absorption spectrum of MO3ONS film

Figure 5.5 : Possible mechanism for quarternisation of P-4VP

Figure 5.6: The current density/temperature relationship of (a) 'wet' P-4VP (open circles, heating; open squares cooling cycle), and (b) 'dry' P-4VP (open squares, heating; open circles cooling cycle).

Figure 5.7: The r_{33} vs. poling temperature for a poled ($E_p = 21 \text{ V}\mu\text{m}^{-1}$) 'wet' P-4VP sample

Figure 5.8: The r_{33} vs. poling field relationship of 'wet' and 'dry' P-4VP samples (T_p : 120 °C in both samples)

Figure 5.9: The thermal relaxation of polar alignment in 'wet' and 'dry' P-4VP samples at $T = 20 \text{ °C}$ (poling conditions for the 'wet' P-4VP, $E_p = 88 \text{ V}\mu\text{m}^{-1}$, $T_p = 120 \text{ °C}$ and 'dry' P-4VP, $E_p = 28 \text{ V}\mu\text{m}^{-1}$, $T_p = 125 \text{ °C}$)

Figure 5.10 : The thermal relaxation of polar alignment in MO3ONS with compared to 'wet' P-4VP (at $T = 20 \text{ °C}$).

Chapter 6

Figure 6.1 : (a) Head-to-tail type dipolar arrangement, (b) Random coil conformation in a main-chain which has a flexible segments.

Figure 6.2 : Structure of the rigid 'V' main-chain polymer.

Figure 6.3: DSC scan of rigid 'V' (heating rate is 10 °C minutes⁻¹)

Figure 6.4 : The absorption spectrum of the rigid 'V' main-chain polymer.

Figure 6.5 : The current density/temperature relationship of rigid 'V' main-chain polymer.

Figure 6.6 : The r_{33} vs. T_p of rigid 'V' main-chain polymer ($E_p = 11.7 \text{ V}\mu\text{m}^{-1}$).

Figure 6.7 : The r_{33} vs. E_p of rigid 'V' main-chain polymer ($T_p = 85$ °C).

Figure 6.8 : The thermal relaxation of poled rigid 'V' main-chain polymer (at room temperature)

Figure 6.9 : The angular dependence of the second harmonic light (for 'p' incident and 'p' transmitted)

List of Tables

Chapter 1

Table 1.1: Electro-optic properties of some organic and inorganic materials (MNA represent 2-methyl-4-nitroaniline, [1] Ermer S., J.F. Valley, R. Lytel, G.F. Lipscomb, T.E. Van Eck, and D.G. Girton, Appl. Phys. Lett. 61, (1992), 2272-2274, [2] : Shuto Y., M. Amano, and T. Kaino, IEEE, Transactions photonics technology lett., 3, (1991), 1003, [3] : Xu C., B. Wu, L.R. Dalton, P.M. R., Y Shi, and W.H. Steier, Macromolecules, 25, (1992), 6716-6718)

Chapter 2

Table 2.1: Value of the product $\mu\beta$ determined from EFISH measurements for a series of molecules (β in 10^{-30} esu, μ in Debyes, $\lambda = 1.356$ μm) Katz et al. in "Introduction to Non-linear Optical Effects in Molecules and Polymers", Eds. Prasad and Williams, (1991), John Wiley & Sons, New York [5]. The molecular structure of the compounds are shown in figure 2.2

Chapter 4

Table 4.1: Refractive index versus doping level for polycarbonate guest-host films

Table 4.2 : ω and 2ω response of poled DAN/BPA-PC

Table 4.3 : r_{33} \poling time relationship of 20% DAN/PMMA sample

Table 4.4: Poling conditions and electro-optic response obtained at 633 nm for DAN-doped polymers

Table 4.5: Poling conditions and the measured EO responses of NMBA and DAN doped BPA-PC thin films [12]

Chapter 5

Table 5.1: Measured EO responses (at 632.8 nm) for the poled P-4VP samples (1-6 fixed electrode poled samples, 7 corona poled sample)

Table 5.2: The poling conditions and the measured EO coefficients at 632.8

1.1 Background

Although certain non-linear optical (NLO) effects such as the Kerr effect and Pockels effect were discovered in the 19th century, the demonstration of most other non-linear effects (all optical effects) awaited the invention of the laser by Maiman in 1960 [1]. One year after this Franken et al. [2] demonstrated second-harmonic generation (SHG) from a crystal of quartz using a ruby laser. The origins of non-linear optical effects lie in the way in which a beam of light interacts with a material. When light interacts with a material, a polarisation response is obtained. At the microscopic level, the applied field displaces the charges from their equilibrium positions and induces a dipole moment μ_{ind} given by

$$\mu_{\text{ind}} = -q\mathbf{r} \quad 1.1$$

where q is the charge and \mathbf{r} is the field induced displacement.

At the macroscopic level the bulk polarisation, \mathbf{P} , resulting from the total induced dipoles is given as

$$\mathbf{P} = Nq\mathbf{r} \quad 1.2$$

where N is the electron density in the medium.

The negative sign is due to the fact that the direction of polarisation is opposite to the electron displacement direction. When the applied field strength is small in comparison to the atomic field (10^{11} Vm^{-1}) the induced polarisation is linearly dependent on the field. This linear dependence is shown below

$$\mathbf{P} = \chi^{(1)} \mathbf{E} \quad 1.3$$

where $\chi^{(1)}$ is the linear susceptibility of the material and is independent of the field. $\chi^{(1)}$ is a second rank tensor and relates the components of polarisation vector to the components of the electric field vector. $\chi^{(1)}$ is related to the relative permittivity, ϵ_r , through

$$\chi^{(1)} = \epsilon_0 (\epsilon_r - 1) \quad 1.4$$

where ϵ_0 is the permittivity of free space.

However at higher fields (fields which are not entirely negligible in comparison to the atomic field strength), the induced polarisation becomes nonlinearly dependent on the field.

The total polarisation could now be expressed in terms of an effective susceptibility i.e.

$$\mathbf{P} = \chi_{\text{eff}} \mathbf{E} \quad 1.5$$

The difference between equations 1.3 and 1.5 is that χ_{eff} is field dependent in the latter.

The bulk polarisation can then be expressed in a power series of the field strength E as

$$P_i = P_o + \sum_J \chi_{ij}^{(1)} E_j + \sum_{j,k} \chi_{ijk}^{(2)} E_j E_k + \sum_{j,k,l} \chi_{ijkl}^{(3)} E_j E_k E_l + \dots \quad 1.6$$

where P_o is the permanent polarisation in the material, $\chi^{(2)}$ and $\chi^{(3)}$ are the second and the third order non-linear susceptibility of the medium. $\chi^{(2)}$ is a third rank tensor and $\chi^{(3)}$, a fourth rank tensor. The subscripts I,J,K etc. refer to Cartesian coordinates in the laboratory frame of reference.

1.1.1 Molecular Basis for NLO

The properties of a solid can be investigated through the structural subunits (molecules or other groups) of the solid. On the microscopic level the linear and non-linear optical properties can be discussed using a power series expansion of the induced dipole moment, p , in powers of the electric field

$$p_i = \mu_o + \sum_j \alpha_{ij} E_j + \sum_{j,k} \beta_{ijk} E_j E_k + \sum_{j,k,l} \gamma_{ijkl} E_j E_k E_l + \dots \quad 1.7$$

where μ_o is permanent dipole moment, α is the linear polarisability, β is the second and γ is the third order polarisability and $E_{j,(k,l)}$ are the local electric field components.

This transformation from the molecular microscopic level to the macroscopic level can be achieved by using an oriented gas model. A detailed explanation of this model is given in Chapter 2, section 2.3. In this model one assumes that molecules forming a solid preserve all their properties and interactions can be taken account of by introducing parameters, such as local field correction factors. The relationship between the local fields and fields applied is given in Chapter 2 section 2.2.

1.1.2 The Non-linear Effects Associated with $\chi^{(2)}$ and $\chi^{(3)}$

Non-linear optical phenomena can be divided into two general groups as $\chi^{(2)}$ effects and $\chi^{(3)}$ effects respectively. $\chi^{(2)}$ effects occur only in noncentrosymmetric materials. By contrast $\chi^{(3)}$ effects do not require any symmetry consideration.

For second order effects the most well known is SHG which is indicated by $\chi^{(2)}(-2\omega; \omega, \omega)$. Here (-) sign indicates energy radiation. SHG is a special case of sum-frequency generation, $\chi^{(2)}(-\omega_3; \omega_1, \omega_2)$ where $\omega_1 = \omega_2 = \omega$ and $\omega_3 = 2\omega$. $\chi^{(2)}(-\omega_3; \omega_1, -\omega_2)$ indicates difference frequency generation where $\omega_3 = \omega_1 - \omega_2$ and optical rectification occurs where $\omega_1 = \omega_2$, $\omega_3 = 0$. Another well known second order effect is the linear electro-optic effect (or Pockels effect) which is characterised by $\chi^{(2)}(-\omega; \omega, 0)$ here ω_2 is a zero frequency, dc, field.

$\chi^{(3)}(-\omega_4; \omega_1, \omega_2, \omega_3)$ describes four wave mixing. Third harmonic generation is a special case of sum-frequency four wave mixing where $\omega_1 = \omega_2 = \omega_3 = \omega$, $\omega_4 = 3\omega$. Another well known $\chi^{(3)}$ effect is the DC Kerr effect, $\chi^{(3)}(-\omega; \omega, 0, 0)$. Here two zero frequency dc fields interact with an optical field in the material. One other third order effect is the electric field induced second harmonic generation (EFISH), which is represented by $\chi^{(3)}(-2\omega; \omega_1, \omega_2, 0)$. This effect is used to measure the microscopic second order hyperpolarisability of an organic molecule in liquid solution.

1.1.3 $\chi^{(2)}$ Effects

$\chi^{(2)}$ effects are of special consideration in the work presented herein. When an optical field $E(t) = E_0 \cos(\omega t)$ and a dc field ($E(0)$) are applied to a noncentrosymmetric material, the second order polarisation may be given as

$$P^{(2)} = \epsilon_0 \chi^{(2)} [E_0 \cos(\omega t) + E(0)]^2 \quad 1.8$$

After carrying out the arithmetic and expanding the first term by applying appropriate trigonometric identities, equation 1.8 takes the form

$$P^{(2)} = \epsilon_0 \chi^{(2)} \left[\frac{E_0^2}{2} (1 + \cos(2\omega t)) + 2E_0 \cos(\omega t) E(0) + E(0)^2 \right] \quad 1.9$$

Since the contributions to the refractive index at ω are the focus of the attention, the third term in the above equation is not taken into consideration. The first term contains 2ω , as well as a frequency independent term. The 2ω term represents second harmonic generation. In the case of second harmonic generation two fields of equivalent frequency interact in the material and a field with twice the frequency of the incoming fields is produced. For example, the Nd:YAG laser operates in the near infrared at a wavelength of 1.064 μm . Second harmonic generation is routinely used to convert the wavelength of the radiation to 0.532 μm , in the middle of the visible spectrum.

The second term indicates the linear EO effect. The linear EO effect is the change in the indices of the ordinary and extraordinary rays that is caused by, and proportional to, an applied electric field. In the case of the linear EO effect the noncentrosymmetric material is subject to a static electric field as well as the monochromatic incident light of frequency ω . In this context it suffices for the 'static' field to oscillate at a frequency well below optical frequencies ($10^3 \text{ Hz} \ll 10^{14} \text{ Hz}$). In the refractive index ellipsoid the change in the refractive index due to the electro-optic effect is given as

$$\Delta\left(\frac{1}{n^2}\right)_i = \sum_{j=1}^3 r_{ij} E_j \quad (i=1, \dots, 6) \quad 1.10$$

where i represents axes on the refractive index ellipsoid and j represents Cartesian directions (x, y and z) of the electric fields. In the summation over j 1,2,3 represents x, y and z , respectively. The linear EO coefficient r_{ijk} is a third rank tensor, but in equation 1.10 a reduced notation may be used where symmetry permits [3].

1.2 Use of NLO in Device Applications

Non-linear optics plays an important role in photonics technology. In this technology photons are used to transmit information. The use of photons offers the prospect of increasing the speed of signal transmission by many orders of magnitude compared to electronic processes. For instance photonic switching can take place with femtosecond timescales. In the field of optical information storage the SHG process can provide for the conversion of near-infrared laser light from diode lasers into the blue. Using NLO phenomena one can build sources, light modulators [4,5], devices to control the phase or amplitude of a light beam, optical switches [5-7], optical logic gates [8], and optical power limiters [9]. There have also been other devices, based on $\chi^{(3)}$ effects such as the non-linear directional coupler [10-12]. The non-linear effects can be enhanced when

the optical power is confined into waveguides. In addition, the waveguide geometry offers long interaction lengths thus further reducing the power requirements.

1.3 Material Requirements

There are variety of different type of material classes used in NLO. These include semiconductors, non-linear glasses, inorganic crystals and organic materials.

Semiconductors (especially II-VI and III-V inorganic semiconductors) are extensively employed in electronic and opto-electronic applications. Semiconductors are generally used for third order non-linear optical properties for use in optical switching, optical gates etc. Group II-VI and III-V semiconductors, which have a zinc blende structure, lack a centre of symmetry therefore they show second order nonlinearity. The usefulness of second order nonlinearities in semiconductors is limited, however, by their limited range of transparency and by a lack of sufficient birefringence for phase matching.

Non-linear glasses are mostly centrosymmetric materials and do not show any $\chi^{(2)}$ effects. For this reason non-linear glasses are mostly studied for $\chi^{(3)}$ effects. However, recent experimental results have shown the presence of a second-order nonlinearity in silica glasses [13,14].

Inorganic crystals such as LiNbO_3 , KDP and KTP are used as electro-optic modulators [15]. The same materials are also used for second harmonic generation purposes [16,17].

Recently organic polymeric materials were developed as new NLO materials for NLO applications. Organic NLO materials can generally be either in single crystal form, in amorphous polymer form or as molecular layer LB films. Organic NLO materials can also be in the form of liquid crystals and crystalline polymers. Crystals can give higher NLO responses but crystal growth is a time consuming and difficult process. It is also difficult to fabricate crystals from a device applications point of view. Preparation of

LB films is easier when compared to crystals but can suffer from slow deposition and non-ideal alignment. By contrast amorphous polymers are easy to handle and easy to make into thin films for device applications.

Organic NLO materials have a number of specific characteristics which make them potentially superior to inorganic materials. Some of these characteristics are

- Ease of fabrication,
- Suitable for inexpensive mass production,
- Chemically-tailored control of physical and optical properties,
- Low relative permittivity,
- Wide bandwidth,
- Large nonlinearities.

Table 1.1 shows the electro-optic properties of some of the organic and inorganic materials.

Material,	r (10^{-12} mV ⁻¹) (at $\lambda = 632.8$ nm)
Inorganic crystal	
LiNbO ₃	$r_{33} = 30.8$
semiconductors	
GaAs	$r_{yzx} = 1.2$ ($\lambda = 1\mu\text{m}$)
Organic crystal	
MNA	$r_{xxx} = 67$
Polymers	
guest-host [1]	$r_{33} = 3.4$ (830 nm)
side-chain [2]	$r_{33} = 40$
main-chain [3]	$r_{33} = 40$

Table 1.1: Electro-optic properties of some organic and inorganic materials (MNA represent 2-methyl-4-nitroaniline, [1] Ermer S., J.F. Valley, R. Lytel, G.F. Lipscomb, T.E. Van Eck, and D.G. Girton, Appl. Phys. Lett. 61, (1992), 2272-2274, [2] : Shuto Y., M. Amano, and T. Kaino, IEEE, Transactions photonics technology lett., 3, (1991), 1003, [3] : Xu C., B. Wu, L.R. Dalton, P.M. R., Y Shi, and W.H. Steier, Macromolecules, 25, (1992), 6716-6718)

1.4 Origin of Nonlinearity in Organic Materials

In general, molecules for second order non-linear optics are composed of three functional groups. These are the electron donor group (ED), NH_2 , $\text{N}(\text{CH}_3)_2$ etc., the electron acceptor group (EA), NO_2 , CN etc., and conjugated single and double bond alternation. Figure 1.1 shows a schematic diagram of an organic NLO molecule.

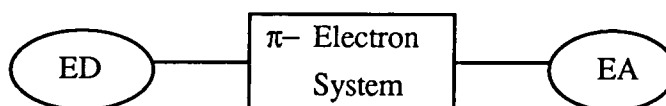


Figure 1.1: The basic molecular structure required for 2nd order NLO

The π - system connects the ED to the EA group. In the π - bonds electrons can move freely over the entire length of the molecule and the structure is said to be delocalised. It is this behaviour of the π - electrons that makes the π - electron distribution highly deformable and also gives rise to large optical nonlinearities. In inorganic crystals the SHG coefficient (high frequency) is much smaller than the linear EO coefficient (low frequency). This is due to the fact that at low frequency there are contributions from ions as well as from the electrons. At higher frequencies the only contribution to the nonlinearity arises out of electronic displacements. Electrons can follow the alterations in electric field at higher frequencies. For organic materials the relative permittivities at low frequency are comparable to those at optical frequencies, which leads to minimisation of phase mismatch between electrical and optical pulses in high-speed travelling wave devices.

1.4.1 Relationship Between $\chi^{(2)}$ and Electro-optic Coefficient

The electro-optic tensor, r_{ij} may be associated with the bulk second order non-linear coefficient through;

$$\chi_{\text{DK}}^{(2)}(-\omega; \omega, 0) = \frac{1}{2} n^4 r_{\text{D}} \quad 1.11$$

the derivation of which is in Appendix I.

The equation above may be related to the SH coefficient, $\chi^{(2)}(-2\omega; \omega, \omega)$, provided that the electro-optic effects are purely electronic in origin. This approximation is usually valid for polymers down to frequencies of a few kHz and thus at the frequencies at which the measurements were done in this work.

1.4.2 Different Types of Polymeric Systems

Organic NLO molecules can be incorporated into a polymeric host as guest molecules (guest-host system). Alternatively NLO molecules can be covalently bonded to the polymeric backbone (side-chain system), or they can be introduced into the polymers main-chain (main-chain system).

Guest-host systems are easy to prepare (i.e. do not necessitate complicated chemical synthesis), but poled guest-host systems suffer mainly in the thermal relaxation of polar species. For side-chain systems more effort is needed in synthesis but these systems have increased thermal stability of poling compared to guest-host systems. In the main-chain type materials the nonlinearity may increase due to an ability to increase the number density of NLO units. Thermal stability of poling induced alignment may be enhanced compared to both guest-host and side-chain systems.

As far as the low optical scattering properties are concerned, amorphous polymers have superiority over semicrystalline and crystalline polymers. Amorphous materials, however, possess no long range polar order and therefore are centrosymmetric. To utilise the second order NLO processes in these systems, the materials must be processed to remove the centre of inversion. This is done using electrical poling.

Electrical poling of polymer films is not new since 20 years ago Kawai et al. [18] found that electrical polarisation can arise in certain crystalline polymers of polyvinylidene fluoride (PVDF) and related polymers.

The poling induced alignment represents a non-equilibrium state and the alignment tends to relax back to the original position. The thermal stability of poling induced alignment is of vital importance for device applications. The relaxation of the alignment is a very common problem in polymeric systems. Increasingly the thermal stability of poled polymers has become the subject of much work.

Part of the aim of the work detailed in this thesis was to search for an improvement of the thermal stability of polar alignment in guest-host, side-chain and main-chain polymeric systems. In addition an aim was to study the optimum poling conditions for higher polar alignment in these material systems.

Chapter 2 thus describes the electrical poling process and introduces the theory and principles involved, along with the effect of poling on the macroscopic properties of materials. The relationship between macroscopic second order coefficient and microscopic parameters is described. This chapter also describes generally the relaxation process in polymers and some of the chemical and physical processes used to increase the thermal stability of poling induced alignment.

Sample preparation, characterisation and the experimental techniques used in this work is outlined in chapter 3. Thin film fabrication methods (dipping and spin coating) and prism coupled waveguiding methods are considered. Both parallel plate poling and corona discharge poling techniques were used. Also in this chapter the linear electro-optic and the SHG measurement techniques are discussed in detail. Chapter 4 reports on the results of $\chi^{(2)}$ properties of guest-host materials under various poling conditions. The effect of field, temperature and time on polar alignment of the guest molecules was investigated. In this chapter a successful attempt to increase the thermal stability of a poled guest-host system is also reported.

Chapter 5 and chapter 6 report poling studies of side-chain and main-chain type polymers respectively. In chapter 5 the effect of drying of poly(4-vinyl pyridine) solutions on the polar alignment and thermal stability of the alignment is discussed. Chapter 6 reports the poling and $\chi^{(2)}$ studies of the first in a serie of thermally stable

silicon containing polymers where a non-linear optical dipolar group is held in a rigid 'V' segment.

Finally in chapter 7 this work is concluded with recommendations for future studies.

1.5 References

- 1- Maiman T.H., *Nature*, **187**, (1960), 493
- 2- Franken P.A., A.E. Hill, C.W. Peters, and G.Weinreich "Generation of Optical Harmonics", *Phys. Rev. Letters*, **7**, (1961), 118
- 3- Nye J.F., "Physical Properties of Crystals", Oxford Univ. Press., London, 1977.
- 4- G.H. Cross A. Donaldson, R.W. Gymer, S. Mann, and N.J. Parsons, D.R. Haas, H.T. Man, H.N. Yoon, *SPIE*, **1177**, (1989), 77-91
- 5- Mohlmann, G.R., W.H.G. Horsthuis, A. Mc. Donach, M.J. Copeland, C. Duchet, P. Fabre, M.B.J. Diemeer, E.S. Trommel and F.M.M. Suyten, E.Van Tomme, P Baquero and P.Van Daele, *SPIE proc.* **1337**, (1990), 215-225.
- 6- Doran N.J. and D. Wood, *J. Opt. Soc. Am. B*, **11**, (1987), 1843-1846.
- 7- Stegeman G.I. and E.M. Wright, *Opt. Quant. Elect.*, **22**, (1990), 95-122.
- 8- Gibbs H.M., *Optical Bistability: Controlling Light with Light*, Academic Press, (1985).
- 9- Saukwan L., S.A. Jenekhe, and S.T. Wellinghoff, *SPIE proc.*, **824**, (1987), 162-169
- 10- Jensen S.M., *IEEE, J. Quant. Elect. QE-18*, (1982), 1580-1583
- 11- Aitchison J.S., A.H. Kean, C.N. Ironside, A. Villeneuve, and G.I. Stegeman, *Electronic Lett.*, **27**, 1709-1710
- 12- Frieberg S.R., A.M. Weiner, Y. Silberberg, B.G. Sfez, and Smith, P.W., *Opt. Lett.*, **13**, (1988), 904-906
- 13- Osterberg U. and W. Margulis, *Opt. Lett.*, **11**, (1986), 516
- 14- Kashyap R., B.J. Ainslie and G.D. Maxwell, *Elect. Lett.*, **24**, (1989), 206-207
- 15- Sasahi H., *Elect. Lett.*, **13**, (1977), 683

16- Lim E.J., M.M. Fejer, R.L. Byer and W.J. Kozlovky, *Elect. Lett.*, **25**, (1989),
731-732

17- Van der Poel C.J., J.D. Brown, and S. Colak, *Appl. Phys. Lett.*, **57**, (1990), 2074-
2076

18- Kawai H., *Jap. J. Appl. Phys.*, **8**, (1969), 975.

2.1 Electrical Poling

Polymer glasses are amorphous materials which do not possess three dimensional order. Such materials are centrosymmetric and do not show $\chi^{(2)}$ effects. To induce non-centrosymmetric order in these materials an electrical poling process must be used. This process of orienting guest molecules in host amorphous polymers was first investigated by Havinga and Van Pelt [1-3]. Williams [4] had also suggested the possibility of the second order processes in orientationally ordered glasses.

Electrical poling consists of heating the sample to about the glass transition temperature, T_g , of the polymer and then applying a very high dc electric field of the order 10^7 Vm^{-1} for some time. The dipole moments align in the field direction; then while the field is on, the sample is cooled down to room temperature, and the dipole alignment in the field direction frozen in.

It is easier to align the dipoles either at or above the glass transition temperature of the polymer. At this temperature the polymer glass becomes a rubbery substance and the molecular mobility increases. Especially in guest-host systems alignment of guest molecules is easier above the T_g of the host, due to an increase in the free volume in the host polymer. The free volume concept will be discussed in relation to relaxation in Section 2.6.

In order to see the effect of poling on the macroscopic properties of the materials, we need to understand the relationship between the bulk second order coefficient and the microscopic parameters.

The bulk second order coefficient $\chi^{(2)}$ is represented by a vectorial sum over the distribution of molecular tensor components of β in the medium thus

$$\chi_{ijk}^{(2)} = NF \langle \beta_{ijk} \rangle \quad 2.1$$

where N is the number density of the NLO moieties, F is the local field correction factor and $\langle \beta_{ijk} \rangle$ represents an orientational average value of β_{ijk} .

In the case of cylindrical polar symmetry there are only two independent non-linear optical coefficients; one perpendicular $\chi_{ZXX}^{(2)}$ and the other parallel $\chi_{ZZZ}^{(2)}$ to the polar axis (z). In this case the orientational averaging of one-dimensional molecules, where β_{zz} is taken to be the only significant tensor component is represented through

$$\chi_{ZZZ}^{(2)} = NF\beta_{zz} \langle \cos^3 \theta \rangle \quad 2.2$$

$$\chi_{ZXX}^{(2)} = NF\beta_{zz} \langle \cos \theta \sin^2 \theta \cos^2 \delta \rangle \quad 2.3$$

where θ is the angle of the molecule with respect to the z axis, and δ is the angle between the molecule and the x axis (figure 2.1).

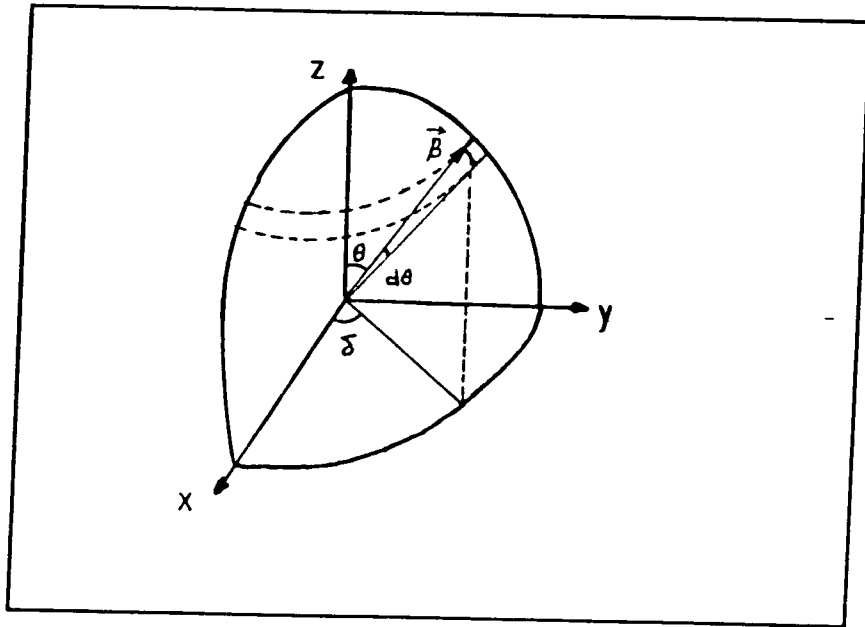


Figure 2.1: Position of a dipole moment in spherical coordinates

To calculate the angle terms in equation 2.2 and 2.3 one needs the probability of finding a molecule at a given angle θ , which is given as;

$$F(\theta) \sin \theta d\theta \quad 2.4$$

where $F(\theta)$ is the orientation distribution function defined as

$$F(\theta) = e^{\frac{-U(\theta)}{kT}} \quad 2.5$$

where $U(\theta) = -\mu \cdot E$ is the potential energy of the molecule in the presence of the poling field and kT is the thermal energy of the molecule.

If we consider $F(\theta) \sin \theta d\theta$ integrated over all the molecules in the system, we will end up with the integrals below for the orientational average of the molecules [5];

$$\langle \cos^3 \theta \rangle = \frac{\int_0^\pi F(\theta) \cos^3 \theta \sin \theta d\theta}{\int_0^\pi F(\theta) \sin \theta d\theta} \quad 2.6$$

and

$$\langle \cos \theta \sin^2 \theta \cos^2 \delta \rangle = \frac{\int_0^\pi F(\theta) \cos \theta \sin^3 \theta d\theta}{\int_0^\pi F(\theta) \sin^3 \theta d\theta} \int_0^\pi \cos^2 \delta d\delta \quad 2.7$$

The solution of the integrals are higher order Langevin functions.

$$\langle \cos^3 \theta \rangle = \left(1 + \frac{6}{p^2}\right) L_1(p) - \frac{2}{p} = L_3(p) \quad 2.8$$

$$\langle \cos \theta \sin^2 \theta \cos \delta \rangle = \frac{1}{2} [L_1(p) - L_3(p)] \quad 2.9$$

where $p = \frac{\mu E}{kT}$ and $L_1(p)$ is the first order Langevin function; $L_1(p) = \frac{1}{3} p - \frac{1}{45} p^3 + \dots$

In the limit of low poling fields and low dipole moments i.e. $\mu E \ll kT$ these two equations 2.2 and 2.3 take a simpler form

$$\chi_{ZZZ}^{(2)} = \frac{NF\mu\beta_{zz} E_p}{5kT} \quad 2.10$$

$$\chi_{ZXX}^{(2)} = \frac{NF\mu\beta_{zz} E_p}{15kT} \quad 2.11$$

From the above equations it is clear that in the low poling field and low dipole moment limit and with the additional approximation of no axial order prior to poling $\chi_{ZZZ}^{(2)}$ is three times that of $\chi_{ZXX}^{(2)}$.

2.2 Local Field Correction Factor

The local field factors relate the externally applied field $E(\omega)$ to the field $e(\omega)$ actually felt by a molecule in the condensed phase. The relationship between $e(\omega)$ $E(\omega)$ and is given by Zyss and Chemla [6] as:

$$e(\omega) = E(\omega) + 4\pi LP(\omega) \quad 2.12$$

where L is a tensor whose value is related to the geometry of the local environment surrounding the molecule of interest (L here should not be confused with the Langevin function). $P(\omega)$ is the polarisation of the medium (Equation 1.3)

For a spherical cavity $L_x = L_y = L_z = 1/3$. The subscripts denote x, y, z coordinates. The local field factor $f(\omega) = \frac{e(\omega)}{E(\omega)}$ can be expressed in terms of the dielectric constant

$$\epsilon(\omega) = n^2$$

$$f(\omega) = 1 + (n^2 - 1)L \quad 2.13$$

For media with spherical symmetry the above equation reduces to

$$f(\omega) = \frac{(n^2 + 2)}{3} \quad 2.14$$

which is the Lorentz correction factor. This factor results from the effects of induced dipoles in the medium via electronic polarisation. However, external fields and fields associated with neighbouring dipoles can induce orientation of permanent dipoles, which requires further correction through the Onsager correction factor, $f(0)$, where

$$f(0) = \frac{\epsilon(0)(n^2 + 2)}{(2\epsilon(0) + n^2)} \quad 2.15$$

2.3 Free Gas Model

A 'free gas' model is generally used to predict a theoretical electro-optic coefficient which can be compared with the measured value. This model describes the orientational distribution of independent dipoles under the influence of an applied field E_p [7]. It is assumed that prior to poling, the non-linear groups adopt an isotropic distribution both in space and in orientation. The direction of the dipole moment is assigned to μ_z and the largest tensor component to β_{zzz} where z denotes the molecular dipolar axis. The expressions used for the local field correction factors are those of Onsager and Lorentz, both of which apply to isotropic and homogeneous media. By substituting Equation 2.14 and 2.15 in Equation 2.10 and using Equation 1.19, the theoretical electro-optic coefficient r_{33} is given below

$$r_{33} = \frac{2N\beta_{zzz}f(0)f^2(\omega)\mu_z E_p f'(0)}{5n^2\epsilon(0)kT_p} \quad 2.16$$

An additional Onsager term, $f(0)$, is included to account for the local poling field at the poling temperature.

2.4 Optimisation of $\chi^{(2)}$

Equation 2.16 illustrates the interrelationships between experimental conditions and material properties and the second order coefficient, $\chi_{ZZZ}^{(2)}$ (i.e. the EO coefficient, r_{33}). $\chi^{(2)}$ is linearly related to the poling field, the number density of the NLO molecules [8,9], the ground state dipole moment, μ , the hyperpolarisability of the NLO molecules, β , and inversely related to kT (thermal energy). To increase $\chi^{(2)}$, for fixed poling conditions, one either needs to use a molecule with a high $\mu\beta$ or the number density of the NLO molecules should be increased. Alternatively, for the same molecule (fixed $\mu\beta$) the poling field should be increased.

2.4.1 Increasing N

The number density of NLO molecules in the polymeric structure is limited. The studies in the past have indicated that, in guest-host systems, doping of NLO molecules into the polymer host is limited to 15-30% (w/w), due to either phase segregation [10] or pairing of the guest molecules [11]. It has also been reported that doping of guest molecules reduces the T_g of the host polymer in proportion to the doping level due to the plasticizing effect. The depression in T_g of guest-host polymers is well documented [12-16]. For example, Boyd et al. [14] report an 85 °C depression in the T_g of 30% (w/w) DR1 doped bisphenol-A polycarbonate, BPA-PC. The T_g of BPA-PC is around 150 °C but after doping with 30% (w/w) DR1, it is reduced to 65 °C.

Incorporating the NLO moiety as a side-chain on a polymer backbone allows an increase in the number density by preventing the phase separation of the NLO moiety. Singer et al. [17] increased the number density of dicyanovinylazo dye, DCV, moieties from $2.3 \times 10^{20} \text{ cm}^{-3}$ to $8 \times 10^{20} \text{ cm}^{-3}$, by incorporating the DCV molecules as a

side-chain on a methacrylate random copolymer. By doing this Singer et al. [17] could overcome the adverse loading effect seen in the DCV/PMMA guest-host system.

2.4.2 Molecular Design

To produce a molecule with a high $\mu\beta$ is a problem of molecular design and synthesis. A great deal has been achieved by the molecular design of NLO molecules to increase the second order non-linearities. By using strong electron donor and electron acceptor groups and a long π -conjugated unit, the $\mu\beta$ of the molecules has been increased. Table 2.1 shows the $\mu\beta$ of some of the molecules whose chemical structures are shown in figure 2.2.

Compound	$\mu\beta$
I	271
II	846
III	358
IV	1090
V	2650
VI	4110

Table 2.1: Value of the product $\mu\beta$ determined from EFISH measurements for a series of molecules (β in 10^{-30} esu, μ in Debyes, $\lambda = 1.356 \mu\text{m}$) Katz et al. in "Introduction to Non-linear Optical Effects in Molecules and Polymers", Eds. Prasad and Williams, (1991), John Wiley & Sons, New York [5].

Replacement of H by an electron acceptor group (CN) in I increases the $\mu\beta$ three times. Compared to I and II, in IV the conjugated π bond length was increased, and this caused the $\mu\beta$ of IV to increase at least four times. In V the conjugation length was increased in comparison to IV and also the N=N group was replaced by a C=C group, this change caused $\mu\beta$ to increase more than twice. A similar change was seen in VI as

in II, and also with the C=C group replaced by N=N, the $\mu\beta$ of the molecule increased from 2650 to 4110×10^{-30} esu.

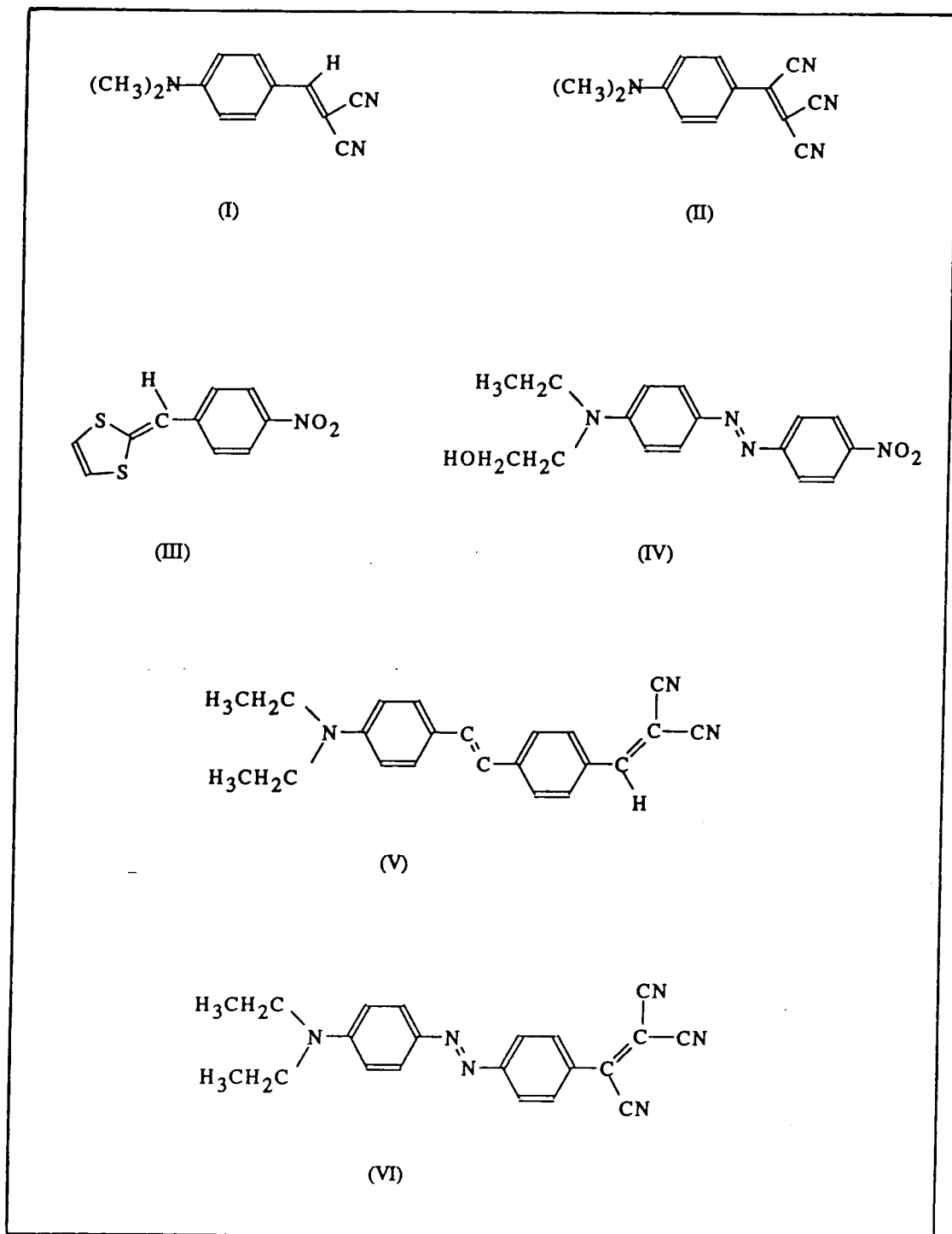


Figure 2.2 Structure formulae of the materials used in table 2.1

2.4.3 Increasing Poling Field

The poling field is limited due to the electrical breakdown of the polymers. When a guest-host system is poled above the glass transition temperature the increase in molecular mobility assists the current density increase. Increase in current at high temperature leads to breakdown in polymer films. A high level of impurities in the material reduces the breakdown field, because impurities cause a further increase in current density.

2.5 Thermal Stability

2.5.1 Introduction

There are different types of molecular motions in amorphous polymers. These motions can be characterised through the frequency dependence of the dynamical mechanical properties (dynamical mechanical analysis, DMA). A major resonance in the DMA spectrum occurs at the glass transition when the applied test frequency equals the natural frequency for main-chain rotations. There are other types of motions such as the rotation of side-groups which give rise to so called 'secondary transitions'. These motions have different resonance frequencies and resonances which are smaller in magnitude than those obtained at T_g . The peak which occurs at the highest temperature is normally labelled α , the subsequent ones β, γ etc. In an amorphous polymer the α -relaxation corresponds to the glass transition. For example, β -relaxation in atactic polystyrene has been assigned to rotations of phenyl groups around the main-chain. Two other secondary transitions γ and δ (related to other relaxations) were also seen in this polymer.

Identifying the existence of these motions helps in understanding the relaxation behaviour.

2.5.2 Thermal relaxation in Poled Polymers

Relaxation in poled polymers arises from thermal re-orientational effects whose rates are governed by the mobility of the molecules. The mobility is governed by free volume and by the proximity of the ambient temperature to characteristic transitions (α , β , γ etc.) in the polymer.

At T_g a polymer undergoes a transformation from the glassy state to the rubbery state. The molecular mobility increases near the T_g of the polymer. This increase can be explained in detail by using the concept of free volume. The free volume is the space in a solid or liquid sample which is not occupied by polymer molecules i.e. the 'empty-space' between molecules. The total sample volume V is defined as;

$$V = V_o + V_f \quad 2.17$$

where V_o is the volume occupied by the molecules and V_f is the free volume.

The free volume is dependent on temperature so that most of the thermal expansion of a polymer rubber or melt can be accounted for by a change in the free volume. As the temperature of the melt is lowered the free volume will be reduced until, eventually, there will not be enough free volume to allow free molecular rotation or translation to take place. The effects of free volume have been experimentally observed through some experimental techniques such as small-angle X-ray scattering [18-20] and diffusion of gases of different molecular sizes in strained polymer films [21,22]. The results of the above observations show that free volume elements have dimensions typically in the range of hundreds of \AA^3 .

From figure 2.3 one can see the effect of ambient temperature on the relaxation of the poled polymers. At temperatures close to T_g , due to the increase in free volume, the relaxation would be fast. If the ambient temperature is well below the glass transition temperature the relaxation will be slower. Thus, an increase in T_g will effect the stability of poled polymers. Changes in the physical and chemical nature of polymer molecules can effect the value of T_g . It has been reported [23] that the incorporation of

units which either hinder the rotation or stiffen the chain, causes a large increase in T_g . For example, the presence of a p-phenylene ring in the polyethylene chain produces a change in T_g of polyethylene from $-30\text{ }^\circ\text{C}$ up to $80\text{ }^\circ\text{C}$. The presence of side groups on the main-chain has the effect of increasing T_g through a restriction of bond rotation. Large and bulky side-groups tend to cause the greatest stiffening. However it has also been reported [31] that the presence of more side groups reduces the T_g due to an increase in the free volume. The presence of polar groups, however, such as $-\text{Cl}$, $-\text{OH}$ or $-\text{CN}$ tends to raise T_g more than non-polar groups of equivalent size. This is because the polar interactions will restrict the rotation further. This explains why the T_g of poly(vinyl chloride) $(-\text{CH}_2-\text{CHCl})_n$ is higher than the T_g of polypropylene $(-\text{CH}_2-\text{CHCH}_3)_n$ [23]. The physical characteristics of polymers such as branching and cross-linking also affect T_g . Branching increases T_g because of the steric hindrance i.e. restricted bond rotation. Chemical cross-linking in a polymer sample has the effect of increasing T_g . Physical ageing and annealing also tend to increase the stability of poling because of the reduction in the free volume. Each of these effects will be discussed later.

2.6 Models of Relaxation Phenomena

Relaxation of poling induced alignment in polymers often can be characterised by the Kohlrausch-Williams-Watts (KWW), or stretched exponential, function.

$$y = \exp\left[\left(-\frac{t}{\tau}\right)^\beta\right] \quad 2.18$$

where y is a quantity characterising the decay process (SHG for instance), τ is the characteristic relaxation time, and β (the stretch exponential coefficient) measures the width of the distribution of relaxation times ($0 < \beta < 1$).

The KWW equation has been used to fit the observed decay in some main-chain polymers [24] and recently it was used to fit the data of guest-host polyimide systems [25]. It was reported that in some of the guest-host and side-chain polymers the KWW fit is not adequate [26-29]. The decay characteristics of the SHG intensity in these polymers does not fit either a stretched or a single exponential which suggests that extrinsic factors, such as stored surface charge may be influential. In some of the guest-host [26] and especially side-chain polymers [27-30] a biexponential model has been used to fit the decay of the polar alignment.

$$y = \theta_1 \exp\left(-\frac{t}{\tau_1}\right) + \theta_2 \exp\left(-\frac{t}{\tau_2}\right) \quad 2.19$$

Where y again represents a quantity characterising the degree of alignment, t is time, τ_1 is the short-term relaxation time and τ_2 is the long-term relaxation time, θ_1 and θ_2 are coefficients where $\theta_1 + \theta_2 = 1$.

This model gives reasonable fits to relaxation data of the SHG coefficient in some of side-chain type polymers.

2.6.1 Temperature Dependence of Relaxation

The free volume in polymer glasses is composed of local free-volume elements of different sizes. There are thus several relaxation rates in a polymer, which can be associated with different size free-volume elements. The Williams-Landel-Ferry (WLF) equation (which is based on the free-volume theory) describes the temperature dependence of relaxation time in polymer glasses.

The WLF equation is given below;

$$\log \frac{\tau(T)}{\tau(T_0)} = \frac{-C_1 [T - T_0]}{C_2 + [T - T_0]} \quad 2.20$$

where τ is the relaxation time, T_0 is an arbitrary reference temperature, and C_1 and C_2 are constants that have values of 17 and 52 respectively. C_1 and C_2 are more or less independent of the polymer.

This model is found to be valid in many polymer systems above T_g . However, below T_g , the WLF equation in its original form breaks down as the non-equilibrium state of the glass is not accounted for. The validity of the WLF model was extended to include the low-temperature region [31]. According to this extended model in the glassy state, the total free volume content, $v(T)$ can be considered to consist of two parts, an equilibrium part $v_f(T)$, and a non-equilibrium part $w_f(T)$ (figure 2.3).

$$v(T) = v_f(T) + w_f(T) \quad 2.21$$

The non-equilibrium free volume is related to the cooling rate of a polymer. If a polymer is cooled infinitely slowly, the non-equilibrium free volume is zero and a break would occur in the volume/temperature curve at T_∞ (figure 2.3). When the polymer is cooled at a finite rate the non-equilibrium free volume increases and the break in the volume/temperature curve occurs at a higher temperature. Man and Yoon used the modified WLF theory to study the long-term relaxation behaviour of certain types of poled side-chain polymer [31].

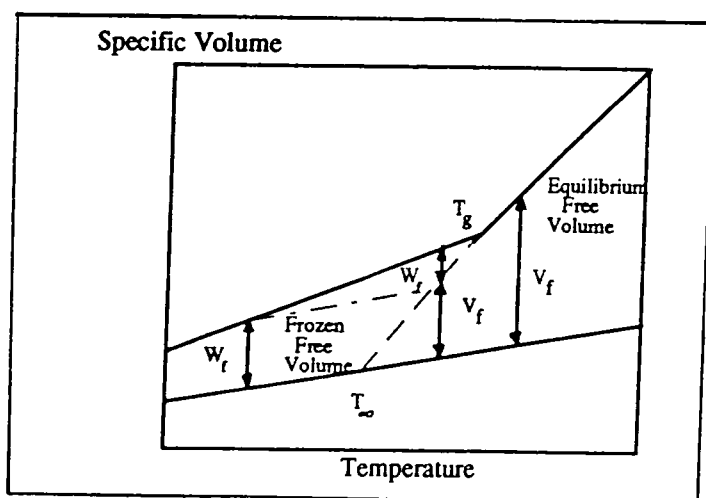


Figure 2.3: Temperature dependence of the specific free volume of typical glassy polymers (after Man and Yoon [31])

2.7 Attempts to Increase The Thermal Stability of Poled Polymer Films

Methods to improve the thermal stability of poled polymer films have been made through physical ageing [32,33], annealing [27,31], chemical cross-linking [34-41], and also hydrogen bonding [14,27,29,32].

2.7.1 Physical ageing

Physical ageing is known to be accompanied by a decrease in the free volume as a function of time at constant temperature. To explain the physical ageing Curro et al. [43] have proposed a diffusion model. This model describes the change in the free volume during annealing as a vacancy diffusion process. Physical ageing brings the polymer matrix closer to an equilibrium configuration due to the expected decrease in segment mobility. Hampsch et al. [32] have physically aged 4% (w/w) DANS doped BPA-PC at 25 °C for 10 hours. There was no detectable decrease in the SHG response from a poled and aged sample, while unaged samples gave 40% relaxation within the same time interval (8-10 hours).

2.7.2 Annealing

Annealing involves cooling the polymer very slowly from temperatures below the poling temperature to ambient temperature while the poling field is still on. Ye et al. [28] have reported that an unannealed and poled (PS)O-NPP film with 25% functionalization at room temperature had a relaxation in the SHG response of 50% after 800 hours. The SHG response of a poled and annealed sample relaxed to 80% of its initial value at room temperature within the same time interval. It was reported that the short-term relaxation was reduced as a result of annealing but the long-term relaxation was not affected [27,31].

2.7.3 Chemical Cross-linking

Cross-linking introduces branches and links between polymer chains which reduces the specific volume of the polymer. This means a reduction of the free volume, therefore, an increase of T_g . Good temporal stability of the SHG response has been obtained by Eich and coworkers at IBM by the cross-linking of a side-chain polymer [34]. Their poled and cured epoxy showed no detectable decay in SHG for over 550 hours under ambient conditions and no tendency to relaxation even at 85 °C. Mandal et al. [35] have studied photochemical cross-linking by irradiation after corona poling. The sample they used was a cross-linkable guest host pair, 3-cinnamoyloxy-4-[4-(N,N-diethylamino)-2-cinnamoyloxy phenylazo] nitrobenzene, CNNB-R, guest and polyvinyl-cinnamate, PVCN, host. The SHG response in the poled but not cross-linked sample decreased by 28% in 205 minutes, but the poled and cross-linked one did not show any measurable relaxation during this time. Jungbauer et al. [36] did not observe any sign of relaxation at 80 °C of the SHG response from the poled and cross-linked mixture of the bifunctional monomer N,N-(diglycidyl)-4-nitroaniline, NNDN, and the trifunctional monomer N-(2-aminophenyl)-4-nitroaniline, NAN, poled and cured at 110 °C for 16 hours over the short period of 30 minutes. Yu et al. [37] have reported a long term stability at 90 °C over at least 500 hours, for a newly synthesised, thermally cross-linkable polymer containing ethynyl groups. At room temperature, there was no relaxation in the SH intensity for more than 1000 hours. At 90 °C the SH intensity relaxed to 75% of its initial value over the same time interval. Wu et al. reported [41] that poled and cured (i.e. crosslinked) polyimide guest-host systems show a thermally stable EO response at 200 °C for 80 hours. A double end cross-linkable main-chain polymer [42] poled at 165 °C gives a second order susceptibility as high as 100 pmV⁻¹ (likely to be resonance enhanced). The thermal stability of this poled and cross-linked sample is very high. After 100 hours annealing at 90 °C, only 5% relaxation is observed.

2.7.4 Hydrogen Bonding

Hydrogen bonding occurs between two functional groups in the same or different molecules. The hydrogen is usually attached to an acidic group (a proton donor), typically, hydroxyl, carboxyl, amine, or amide group. The other group must be basic, usually oxygen as in carbonyls, ethers, or hydroxyls; nitrogen as in amines and amides and occasionally halogens. In the case of guest-host systems the hydrogen bond may occur between the guest NLO molecules and the host polymer. Hampsch et al. [32] reported that the decay rates of disperse orange-25, DO25, and DR1 in BPA-PC are slower than in PMMA. These two dyes have an OH group which forms a hydrogen bond with the carbonyl group in BPA-PC. Boyd et al. [14] have also reported hydrogen bonding in a similar guest-host system. Ye et al. [27] have reported an increase of the chromophore densities and an increase in the stability of poling induced chromophore alignment through a hydrogen bonding network. Recently Lindsay et al. [29] reported a very high stability in their poled (poly(methyl methacrylate-co-coumaromethacrylate) side-chain polymer. Over 400 hours only a 7% relaxation occurred in the SH intensity of this sample. They have attributed this high stability to the hydrogen bonding of the amide group.

Thermal relaxation of different guest molecules of different sizes in the same polymer host was studied [32]. The volume of the guest molecules was in the order DO25>DR1>DANS and the rates of decay of the SHG signals observed follows the order DO25<DR1<DANS. Through this observation Hampsch and coworkers have shown that the largest guest molecules have the slower decay rates in the host polymer. This observation goes hand in hand with free volume theory.

2.8 References

- 1- Havinga, E.E., and P. van Pelt, *Ber. Bunsenges. Phys. Chem.*, **83**, (1979), 816-821
- 2- Havinga, E.E., and P. van Pelt, *Mol. Cryst. Liq. Cryst.*, **52**, (1979), 145-156
- 3- Havinga, E.E. and P. van Pelt, B.R. Jennings (Ed.). Plenum Press, New York and London (1979), 89-97
- 4- Williams D.J., *Angew. Chem. Int. Ed. Engl.* **23** (1984), 690-703
- 5- Prasad P.D., D.J. Williams, *Introduction to Non-linear Optical Effects in Molecules and Polymers*, John Wiley & Sons Ltd., New York (1991), 67-70
- 6- Zyss J. and D.S. Chemla, in *Non-linear Optical Properties of Organic Molecules and Crystals*, Vol. 1, D.S. Chemla and J. Zyss (Eds.), Academic, New York, (1987), 97-98
- 7- Singer K.D., M.G. Kuzyk and J.E. Sohn, *J. Opt. Soc. Am. B*, **4**, (1987), 968-976
- 8- Singer K.D., J.E. Sohn and S.J. Lalama, *Appl. Phys. Lett.*, **49**, (1986), 248-250
- 9- Wu J.W., J.F. Valley, S. Ermer, E.S. Binkley, J.T. Kenney, G.F. Lipscomb and R. Lytel, *Appl. Phys. Lett.*, **58**, (1991), 225-227
- 10- Lei Du, J. Runt, A. Savari and R.E. Newman, *Macromolecules*, **20**, (1987)
- 11- Kuzyk M.G., J.E. Sohn and C.W. Dirk, *J. Opt. Soc Am B*, **7**, (1990), 842-858
- 12- Broussoux D., E. Chastaing, S. Esselin, P. Le Barny, R. Robin, Y. Bourbin, J.P. Pochelle and J. Raffy, *Organic Materials For Non-linear Optics*, *Revue Technique Thomson-CSF*, **20-21**, (1989), 151-190
- 13- Broussoux D., S. Esselin, P. L. Barny, J.P. Pochelle, and P. Robin, *Non-linear optics in doped amorphous polymers*. In *Non-linear Optics of Organics and Semiconductors*, T Kobayashi (Ed.), Springer- Verlag, Berlin (1989), 126-139.
- 14- Boyd G.T., C.V. Francis, J.E. Trend and D.A. Ender, *J. Opt. Soc. Am. B*, **8**, (1991), 887-894
- 15- Stahelin, D.M. Burland, M. Ebert, R.D. Miller, B.A. Smith, R.J. Tweek, W. Volksen and C.A. Walsh, *Appl. Phys. Lett.*, **61**, (1992), 1626-1628
- 16- Valley J., J.W. Wu, E.S. Binkley, J.T. Kenney, G.F. Lipscomb, and R. Lytel., *Appl.*

- Phys. Lett., **60**, (1992), 160
- 17- K.D. Singer, M.G. Kuzyk, W.R. Holland, J.E. Sohn, S.L. Lalama, R.B. Comizzoli, H.E. Katz and M.L. Schilling, *Appl. Phys. Lett.*, **53**, (1988), 1800-1802
- 18- Tanabe Y., N. Muller, E.W. Fischer, *Polym. J.*, **16**, (1984), 445
- 19- Roe R., J.J. Curro, *Macromolecules*, **16**, (1983), 428
- 20- Curro J.J., R. Roe, *Polymer*, **25**, (1984), 1424
- 21- Levita G., T.L. Smith, *Polym. Eng. Sci.*, **21**, (1981), 936
- 22- Smith T.L., W. Opperman, A.H. Chan, G. Levita, *Polym. Prepr.*, **24**, (1983), 83
- 23- Yang R.J., *Introduction to Polymers*, Chapman and Hall, London, New York (1981), 202-206
- 24- Teraoka I., D. Jungbauer, B. Reck, D.Y. Yoon, R. Twieg and C.G. Willson, *J. Appl. Phys.*, **69**, (1991), 2568
- 25- Stahelin M., D.M. Burland, M. Ebert, R.D. Miller, B.A. Smith, R.J. Twieg, W. Volksen and C.A. Walsh, *Appl. Phys. Lett.*, **61**, (1992), 1626-1628
- 26- Hampsch H.L., J. Yang, G.K. Wong, and J.M. Torkelson, *Macromolecules*, **23**, (1990), 3640-3647.
- 27- Ye C, N. Minami, T.J. Marks, J. Yang, G.K. Wong, *Macromolecules*, **21**, (1988), 2901-2904
- 28- Dai D.R., T.J. Marks, J. Yang, P.M. Lundquist, and G.K. Wong, *Macromolecules*, **23**, (1990), 1894-1896
- 29- Lindsay G.A. R.A. Henry, J.M. Hoover, A. Knosen, M.A. Mortazavi, *Macromolecules*, **25**, (1992), 4888-4894
- 30- Rusch R.C., and R.H. Bech, *J. Macromol. Sci. Phys.*, (1969), B3, 365.
- 31- Man H.T. and H.N. Yoon, *Adv. Mater.*, **4**, (1992), 159
- 32- Hampsch H.L., J. Yang, G.K. Wong and J.M. Torkelson, *Polym. Comm.*, **30**, (1989), 40-43
- 33- Hayden L.M., G.F. Sauter, F.R. Ore, P.L. Pasillas, *J. Appl. Phys.*, **68**, (1990), 456-465
- 34- Eich, M. B.Reck, D.Y. Yoon, C.G. Willson, G.C. Bjorklund, *J. Appli. Phys.*,

- 6,(1989), 3241-3247
- 35- Mandal B.K., Y.M. Chen, J.Y.Lee, J. Kumar and S. Tripathy, Appl. Phys. Lett., **58**, (1991), 2459
- 36- Jungbauer D., B. Reck, R. Tweig, D. Y. Yoon, C.G. Wilson, and J.D. Swalen, Appl. Phys. Lett., **56**, (1990), 2610-2612
- 37- Yu L., W. Chan and Z. Bao, Macromolecules, **25**, (1992), 5609-5612.
- 38- Chen M., L.P. Yu, L.R. Dalton, Y.Q. Shi, W.H. Steier, SPIE Proc., (1991), 1409-1426
- 39- Chen M., L.P. Yu, L.R. Dalton, Y.Q. Shi, W.H. Steier, Macromolecules, **24**, (1991), 5421
- 40- Shi, Y.Q., W.H.Steier, L.P. Yu, M. Chen, L.R. Dalton, Appl. Phys. Lett., **58**, (1991), 2459
- 41- Wu J., W. E.S. Binkley, J.T. Kenney and R. Lytel, A.F. Garito, J. Appl. Phys., **69**, (1991), 7366-7368
- 42- Xu C., B Wu, L.R. Dalton, Y. Shi, P.M. Ranon, and W.H. Steir, Macromolecules, **25**, (1992), 6714-6715
- 43- Curro G.J., R.R. Lagasse, R. Simha, "Diffusion Model for Volume Recovery in Glasses", Macromolecules, **15**, (1982), 1621-1626

3.1 Introduction

In this chapter the preparation and characterisation of thin polymer films are discussed. To induce a non-centrosymmetric structure the samples were dipole aligned using applied DC fields i.e. they were 'poled'. The poling techniques used, parallel plate poling and corona discharge poling, are described. The polar alignment is determined through measuring the EO response from the poled samples. For measuring the linear EO coefficient of the poled samples a simple reflection technique was used. This technique is described in detail and compared with the alternative, waveguiding technique. The second harmonic generation, SHG, properties of the corona poled samples were also studied. To measure the second harmonic, d , coefficient, the Maker Fringe method was used and is outlined here.

3.2 Sample Preparation

The thin films of the polymer were prepared by either spin or dip coating methods.

3.2.1 Spin Coating

Spin coating is a technique whereby a solution of the polymer is put on a substrate which is then spun around on an axis normal to its surface. This has the effect of spreading the solution in a thin film over the substrate and removing any excess solution. The viscosity of the solution and the number of revolutions per minute (rpm) are the critical factors determining the thickness of the film produced.

3.2.2 Dip Coating

In this technique a substrate is dipped into a polymer solution and when withdrawn from the solution a thin layer of polymer is deposited [1,2]. The apparatus used is shown in figure 3.1. The thickness of the resulting film is governed by

- (1) the concentration of the polymer solution
- (2) the volatility of solvent
- (3) the withdrawal velocity.

The relation between thickness and the above mentioned parameters is described by Yang et al [2] through

$$t_p = \left(\frac{\eta - \eta_s}{\eta_0} \right)^{0.84} \left(\frac{\eta U}{g \rho_s} \right)^{\frac{1}{2}} \quad 3.1$$

where t_p is the thickness, η_s is the viscosity of the solvent, ρ_s is density of the solution, η is the viscosity of the solution, η_0 and g are constants, and U is the withdrawal velocity. The validity of equation 3.1 has been shown experimentally [2,3].

For poling and electro-optic measurements a conductive and transparent indium tin oxide (ITO) layer coated glass slide was used as a substrate. The ITO served as a bottom electrode. To provide a second electrode for fixed electrode poling and EO measurement a silver electrode was evaporated on the polymer film. The evaporation of silver was done using an Edwards 634 evaporator.

The refractive index and thickness of the samples were measured by prism coupled waveguiding (section 3.3.1). Thickness measurements were also carried out by 'Tencor' surface profiler. The refractive index of the samples which were too absorptive for prism coupling were calculated from the spacing of interference fringes seen in transmission studies. Here the relation between thickness and refractive index is given by

$$t = \frac{1}{2n_f \Delta f}$$

3.2

where t is thickness, n_f is refractive index, and Δf is the interference maxima difference in wavenumber.

In this technique the accuracy in the measurement of thickness is $\pm 0.008 \mu\text{m}$ (by Tencor surface profiler) and the accuracy of the fringe separation is $\pm 1 \text{ nm}$. Hence the refractive index can be calculated to an accuracy of ± 0.01 . The prism coupling method is a much more accurate method, having an accuracy for the refractive index measurement of ± 0.001 .

3.3 Characterisation of Samples

3.3.1 Prism Coupling

Prism coupling is a technique to couple a light beam into a thin film optical waveguide [4]. A schematic diagram of the prism coupling set up is shown in figure 3.2. To be able to excite all the possible waveguide modes in the film, the refractive index of the prism, n_p , should be larger than that of the film, n_f . An incoming laser beam is totally reflected at the prism base and because of this a standing wave field, the evanescent field is formed which continues below the base of the prism. The boundary condition for the electromagnetic fields at the prism base is one of continuity, requiring that the fields above and below the interface have the same horizontal component. When this condition (phase matching) is achieved, the wave in the prism is coupled exclusively into a specific waveguide mode. Hence it is possible to couple the light wave to any waveguide mode by simply choosing an appropriate angle for the incoming laser beam.

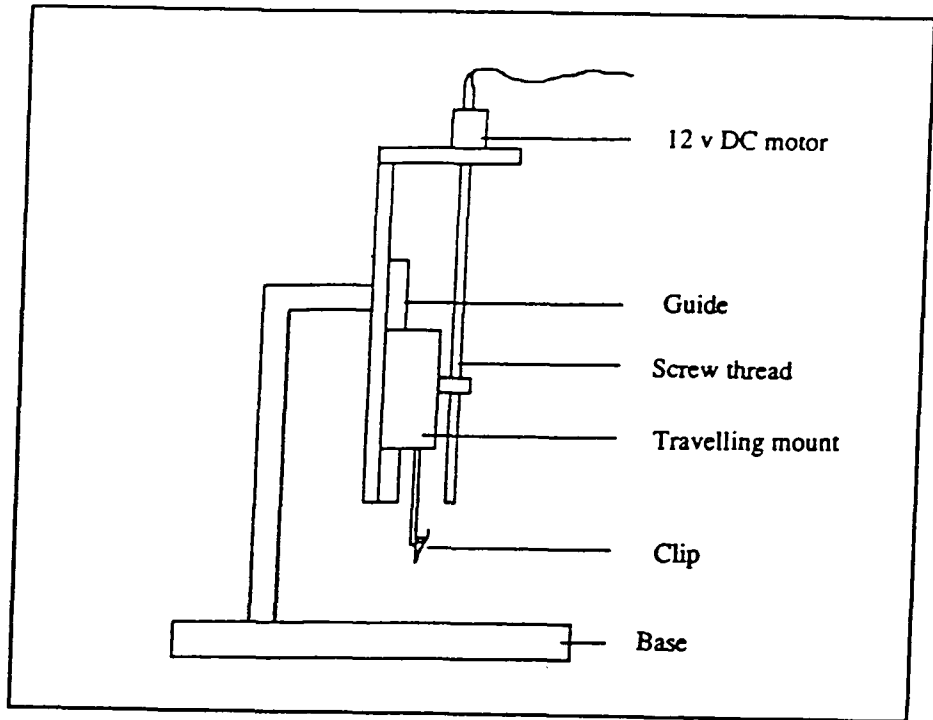


Figure 3.1: Dip coating apparatus

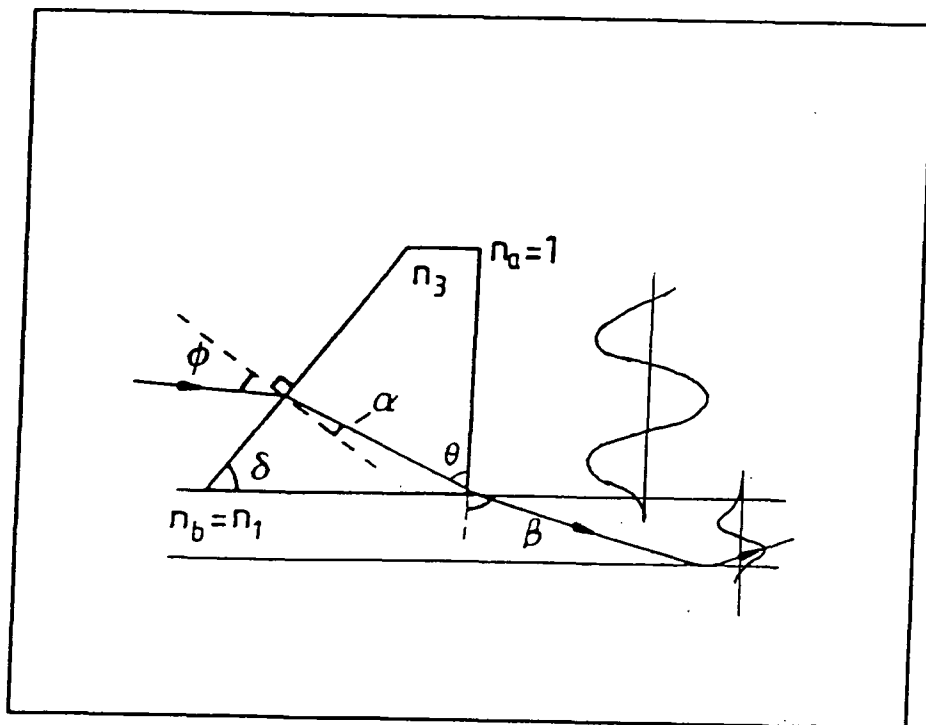


Figure 3.2: Schematic diagram of prism coupling set-up

As can be seen from figure 3.2 the coupling is due to the overlap, in the air gap, of the two evanescent fields from the prism and the film. Once light has been coupled into the film it will be seen as a streak across the film. This is because of the inhomogeneity and impurities in the film which scatter light. The number of modes in a film is related to the thickness. Thicker films give more modes. The coupling angle of a mode increases with an increase in its mode order. The coupling angle θ inside the prism is such that the following equation is satisfied

$$kn_p \sin \theta = \beta_x \quad 3.3$$

in which n_p is the prism index, and β_x is the mode propagation constant (x directed). The coupling angles measured experimentally, ϕ , are related by geometry and Snell's law through the following

$$\theta = \alpha + \delta \quad 3.4$$

where δ is the angle of the prism and α the refraction angle where α is determined via Snell's law.

The equations used to calculate the guide thickness and refractive index are those of Kogelnik and Ramaswamy [5]. The mode index and waveguide thickness for a given geometry of waveguide must have a single pair of values. These values for a typical film system are shown in figure 3.3. The crossing point of the modes gives the bulk refractive index and the thickness.

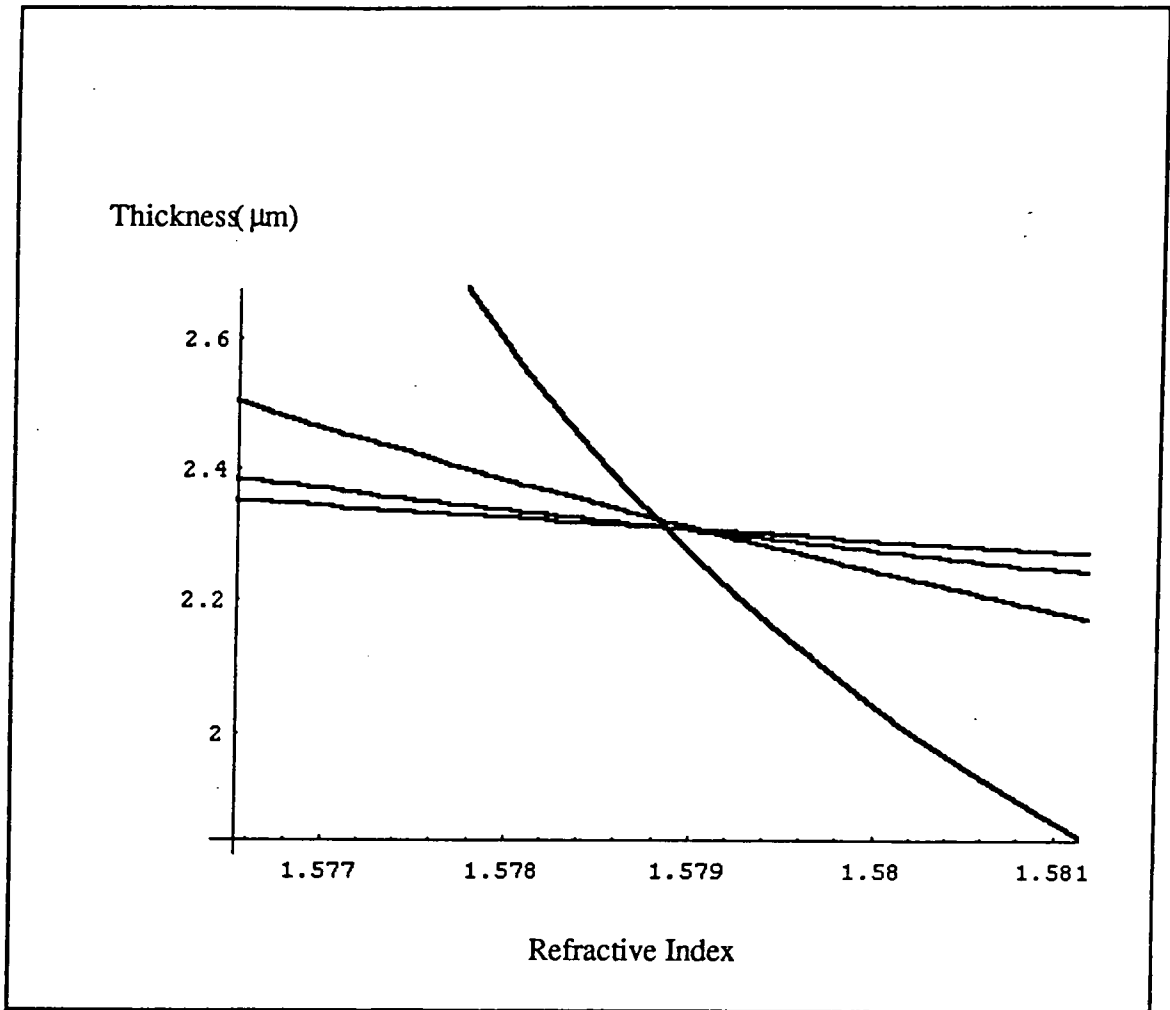


Figure 3.3: The bulk refractive index and the thickness of a 10% (w/w) DAN/BPA-PC film

3.3.2 Relative Permittivity Measurements

The relative permittivity of the films was obtained using a HP 4342A Q meter. The frequency of measurement was 40 kHz.

The relative permittivity of the samples was determined from the standard relation:

$$C = \frac{\epsilon_0 \epsilon_r A}{d} \quad 3.5$$

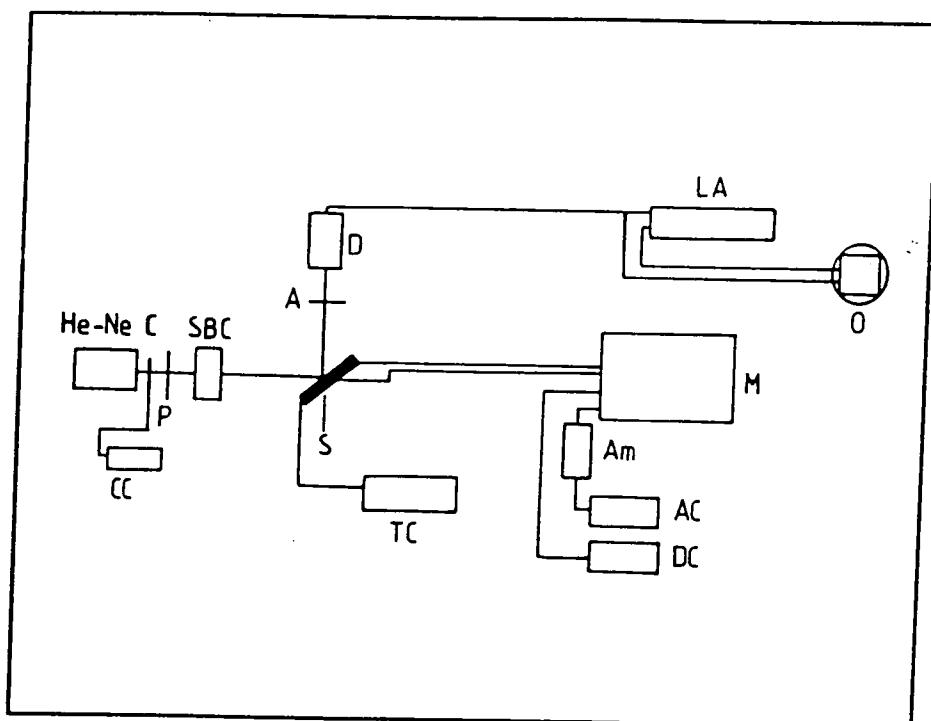
where ϵ_0 is the permittivity of free space ($8.85 \times 10^{-12} \text{ Fm}^{-1}$), ϵ_r the relative permittivity, A the area of the electrode ($4 \times 10^{-6} \text{ m}^2$) and d the thickness of the film.

3.4 Electrical poling

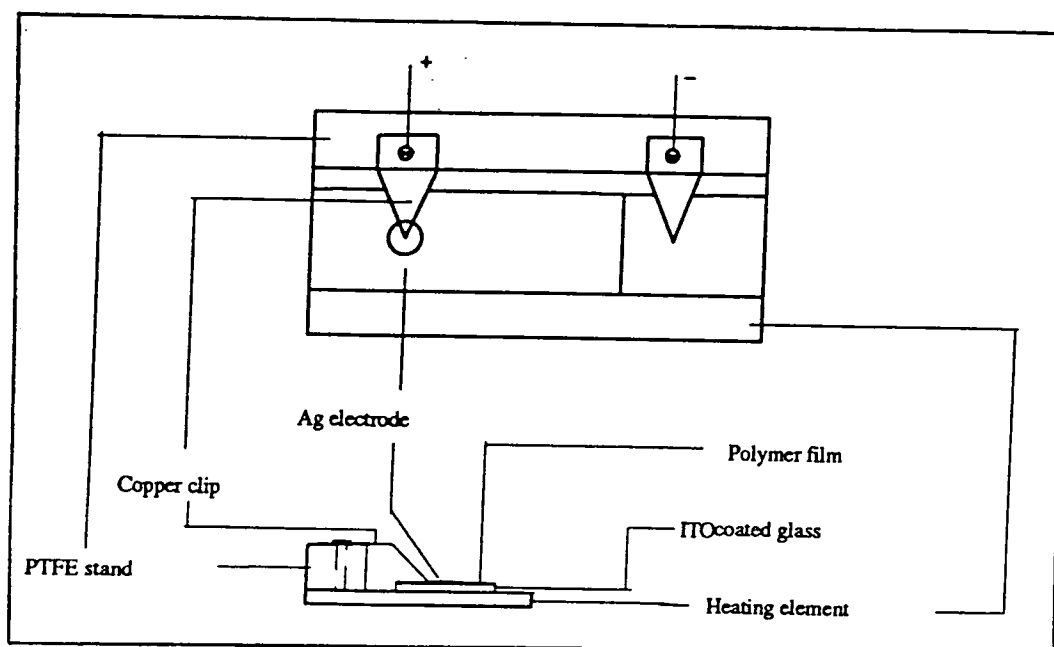
In this study two different poling techniques are used. These are the parallel plate or fixed electrode poling and the corona discharge poling. Each technique has its own advantages and disadvantages.

3.4.1 Parallel Plate Poling

In this technique the sample is placed on a temperature controlled hot stage and heated up to poling temperature. A d.c. field is applied through fixed contacts. The fixed electrode poling experimental set-up is shown in figure 3.4 (a). The electrical connections to the sample are made via the copper contacts on the ITO and the Ag electrodes, figure 3.4 (b).



(a)



(b)

Figure 3.4: (a) The parallel plate poling experimental set-up (C, chopper; CC, chopper controller, P, polarizer; SBC, Soleil-Babinet compensator; S, sample; TC, temperature controller; A, analyser; D, detector; LA, lock-in amplifier; O, oscilloscope; M, modulator; Am, amplifier; AC, AC signal generator; DC, DC power supply), (b) Electrical connections

The temperature of the sample stage was controlled by a CALL 9000 type temperature controller, using a resistive heating element. The d.c. electric field was supplied by a 350 V output Farnell instrument (type E350). Due to a temperature gradient, the temperature indicated on the controller was different to the temperature at the sample. A thermocouple in direct surface contact with the sample was used to measure temperatures at the sample. This set-up, which is an adaptation of that used in [7], allows the poling and EO measurements to be conducted with the sample in situ. This reduces the possibility of damaging the sample and the electrode through handling. The disadvantage of this technique is the limited poling field, since electrical breakdown events are catastrophic.

3.4.2 Corona Discharge Poling

The experimental arrangement for corona poling is shown in figure 3.5 [6]. A sharp steel needle at high static potential -5kV is positioned above a grounded ITO electrode. A copper block which is connected to the temperature controller allows for temperature variation. Onset of discharge occurs at a particular voltage, depending on the diameter of the needle tip and atmospheric conditions. Ions are created and deposited on top of the bare surface of the polymer film. This creates an electric field which is defined by the surface potential and the film thickness. The major advantage of this method is the fact that only a bare, low-conductivity polymer surface is charged. Impurities, defects, and pinholes, therefore cause only relatively small local currents and do not result in short circuiting the whole sample. As a consequence, much higher breakdown field strengths are typically achieved ($E > 1 \text{ MVcm}^{-1}$) compared to conventional poling with fixed electrodes.

The first disadvantage of corona poling over fixed electrode poling is that the poling field is not readily determined. But a rough value of the poling field can be estimated if the r_{33} versus poling field, E_p , characteristic of the sample and its EO coefficient are known. From fixed electrode poling it is possible to determine the relationship between r_{33} and E_p . After corona poling the EO coefficient of this sample can be measured and

an approximate value for the field obtained. The second disadvantage of corona poling is that the poling field is not uniform across the sample, see below.

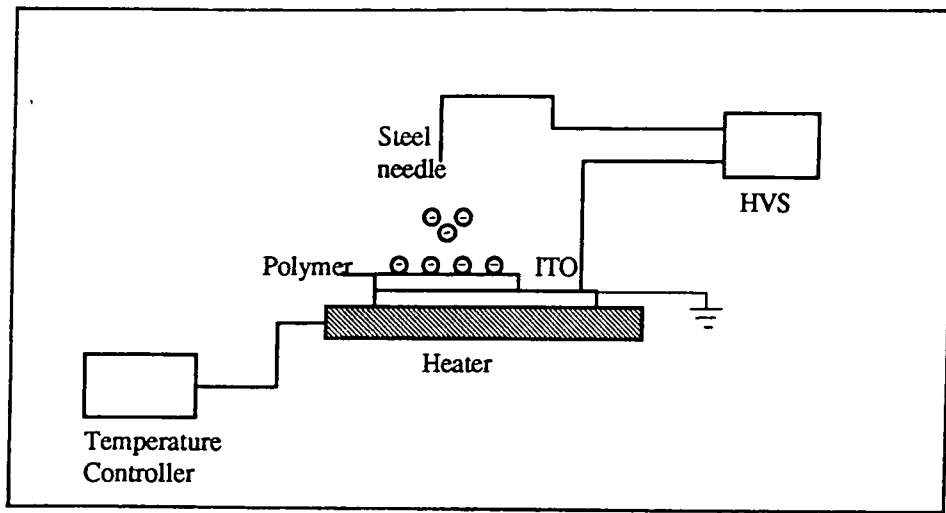


Figure 3.5: The experimental arrangement for corona poling (HVS stands for high voltage supplier)

3.5 Uniform Field Distribution of Corona Discharge Poling

In the corona poling experiment the ion flow from the needle is not ideally conical. So as stated above the electric field induced by ions generated in the discharge is not uniform across the surface of the sample. This was shown in two different experiments. In the first experiment two different electrodes were evaporated on the surface of a 20% DAN/BPA-PC sample corona poled at 84 °C for a needle voltage of -5 kV. The EO response was measured at each electrode. The measured EO response was 0.6 pmV⁻¹ from the first electrode, yet there was no EO response from the second. The area on which the first electrode was evaporated, was close to the needle tip during poling. The ion population, and thus the poling field, was highest in that area.

Secondly, a similar sample (20% DAN/BPA-PC) of the same thickness was corona poled under the same conditions. The SHG response was measured immediately after

poling. When the sample was tracked up and down in the fundamental beam, the detected SHG signal changed dramatically.

These two individual experiments showed that the poling field induced by the ions is not uniform. In order to measure the maximum SHG response for a particular needle voltage the area of the sample under the needle (ion discharge) was marked out. For SHG measurements the 1.064 μm beam was focused on the marked point on the sample. For EO measurements, after poling, a silver electrode was evaporated onto this marked point.

3.6 Electro-optic Reflection Technique

The optical configuration of this technique, which was developed by Teng and Man [7], is shown in figure 3.6.

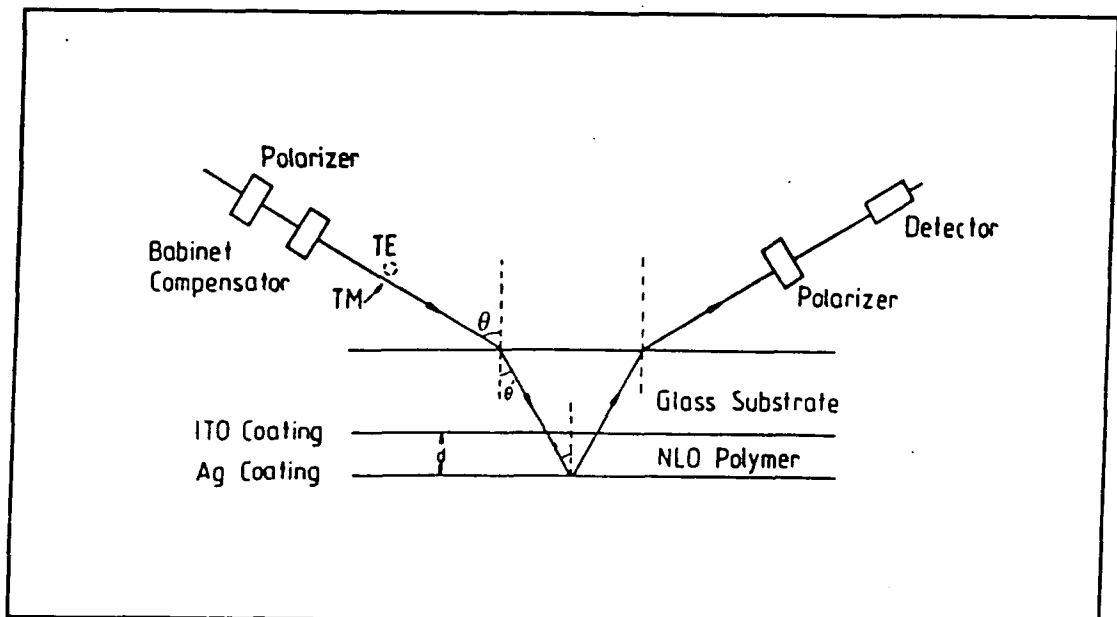


Figure 3.6: The optical configuration of the EO reflection technique

A 5 mW, HeNe (wavelength, $\lambda = 632.8 \text{ nm}$) was used as an optical source. HeNe radiation passes through a polariser which is set at an angle of 45 degrees from the

plane of incidence so that the parallel p, and perpendicular s components of the optical field are equal in intensity. Linearly polarised light passes through a Soleil-Babinet Compensator, SBC, causing a $\pi/2$ phase difference between s and p to give circularly polarised light. After the SBC, the light passes through the substrate, the ITO, and the film and is then reflected back from the silver electrode. The reflected beam is incident on a second polariser (analyser), and then a silicon detector. This set-up converts the field induced phase difference in the material into amplitude modulation. The modulation in the beam is measured using a lock-in amplifier.

In order to determine the field induced birefringence any other birefringence must be eliminated. If a natural birefringence exists in the sample, its effect on the beam can be removed by adjusting the SBC.

When modulation voltages, $V = V_m \sin(\omega_m t)$ are applied across the electrodes, a change in the phase angle $\Delta\psi$ in both the s and p waves is induced by the change in refractive index δn due to the electro-optic effect. There is also a change in path length δs due to the change in the refraction angle θ' but comparatively this is very small and was not taken into consideration in the calculations. Because of negligible index difference between film and the substrate, the latter can be ignored. The effect of index difference on the internal angle is also negligible.

The optical path length of the beam in the sample is given by;

$$l = 2 \frac{d}{\cos \theta'} \quad 3.6$$

where d is the film thickness, and $\theta' = \sin^{-1} \left(\frac{\sin \theta}{n} \right)$ (figure 3.6). The electro-optic change in the refractive index is given as [8];

$$\delta n = \frac{1}{2} n^3 r \frac{V}{d} \quad 3.7$$

The change in the optical path length of the beam will also change due to the change in the refractive index. These changes will effect the relative phase retardation between s and p waves. $\Delta\psi$ can be taken to represent the phase retardation, in which case

$$\Delta\psi = k l \delta n \quad 3.8$$

with $k = \frac{2\pi}{\lambda}$.

By substituting equations 3.7 and 3.8 in equation 3.9 the phase retardation becomes

$$\Delta\psi = \frac{2\pi n^3 r_{\text{eff}} V}{\lambda \cos \theta'} \quad 3.9$$

where r_{eff} is the effective linear electro-optic coefficient.

In uniaxial poled films, only two components of the electro-optic tensor are of interest, these are r_{33} and r_{13} . For s polarisation then the angle of incidence is inconsequential since there is azimuthal symmetry i.e. the material is symmetric around the 3 direction and $r_{13} = r_{23}$ thus;

$$\Delta\psi^o = \frac{2\pi n^3 V}{\lambda \cos \theta'} r_{13} \quad 3.10$$

where $\Delta\psi^o$ is the phase retardation of the 'ordinary' ray in the film.

For 'p' polarisation, the effective electro-optic coefficient, r_{eff} , a combination of r_{13} and r_{33} , is given by

$$r_{\text{eff}} = r_{33} \sin^2 \theta' + r_{13} \cos^2 \theta' \quad 3.11$$

thus

$$\Delta\psi^e = \frac{2\pi n^3 V}{\lambda \cos \theta'} (r_{33} \sin^2 \theta' + r_{13} \cos^2 \theta') \quad 3.12$$

where $\Delta\psi^e$ is the phase retardation of the 'extraordinary' ray in the film.

By using equations 3.11 and 3.13, the relative phase difference between the ordinary and extraordinary rays $\Delta\Psi = \Delta\psi^e - \Delta\psi^o$ can be given as

$$\Delta\Psi = \frac{2\pi n^3 V}{\lambda \cos \theta'} (r_{33} \sin^2 \theta' + r_{13} \cos^2 \theta' - r_{13}) \quad 3.13$$

The transmission factor of a cross-polarised EO modulator is then given by;

$$\frac{I_m}{I_o} = \sin^2(\Delta\Psi) \quad 3.14$$

where I_m is modulation intensity, and I_o is input intensity.

The modulator is usually biased with a fixed retardation $\Gamma = \pi/2$, to the 50% transmission point which corresponds to a linear region in the transmission curve [8].

The modulation field was applied at this point (figure 3.7).

By substituting Equation 3.14 into Equation 3.15 the EO coefficient, r_{33} , is expressed by

$$r_{33} = \frac{3\lambda I_m}{4\pi n^2 V_m I_o} \frac{(n^2 - \sin^2 \theta)^{\frac{1}{2}}}{\sin^2 \theta} \quad 3.15$$

A detailed derivation of r_{33} is shown in Appendix II.

The waveguiding technique [9] can also be used to measure the EO coefficient of a poled polymer film. In this technique the sample has to be prepared in a waveguide form. A non-linear polymer core is sandwiched between two polymer buffer layers, which have smaller refractive index compared to the core layer. The buffer-core-buffer layer system is sandwiched between two electrodes. The poling field is applied through

these electrodes. In this technique the Pockels coefficient of the poled polymer waveguide is obtained by a measurement scheme based on prism coupling. The electro-optic birefringence between two orthogonal modes of similar effective index is measured and the Pockels response can be obtained.

This technique is not applicable for materials which are absorptive. Furthermore the simple reflection technique places less demands on sample preparation than the waveguide method. Hence it was used in preference to the latter method.

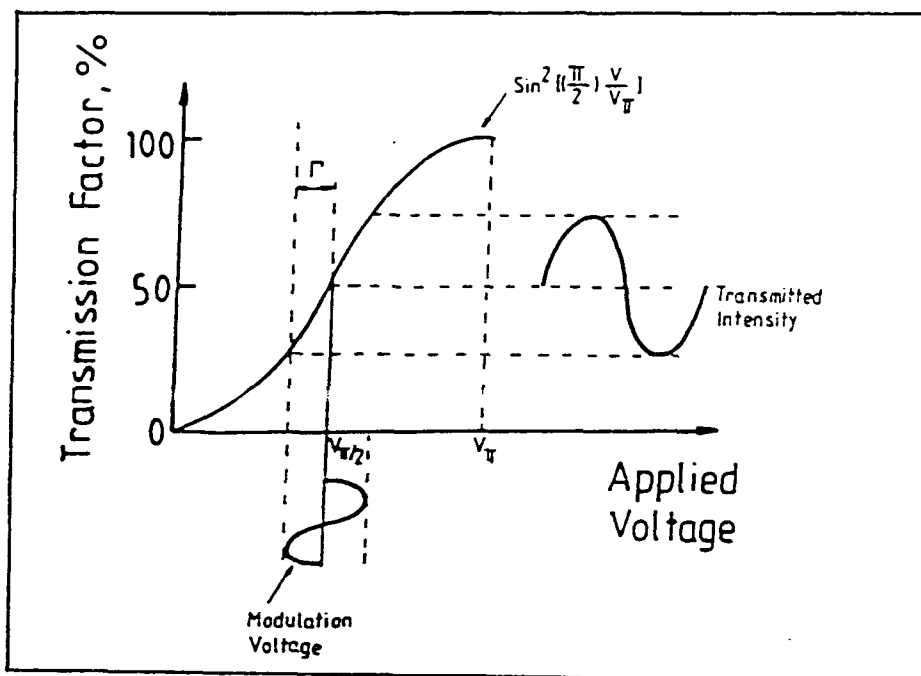


Figure 3.7: Transmission factor of a cross-polarised EO modulator as a function of an applied voltage (Yariv, Optical Electronics, New York, 1985, pp: 293)

3.7 Maker Fringe Analysis Technique for Second Harmonic Generation Measurements

The Maker fringe technique was used to measure the second harmonic generation intensity of corona poled samples. The experimental measurement set-up used is shown in figure 3.8. The accuracy of the measurement was dependent on the alignment of the fundamental beam over a relatively long distance (around 3m). A HeNe laser was used to maintain the alignment. A Nd:YAG laser with $\lambda = 1.064 \mu\text{m}$ was used as a fundamental beam. The second harmonic of the Nd:YAG is in the visible spectrum at a

To find the second harmonic, d , coefficient of a poled sample a quartz wedge which has a known d coefficient ($d_{31} = 0.5 \text{ pmV}^{-1}$) was used as a reference. For the same polarisation and intensity, the normalised second harmonic power was determined for both sample and reference.

The coherence length l_c is a measure of the maximum material length that is useful in producing the SHG power. The definition of coherence length is given by

$$l_c = \frac{\pi}{\Delta k} \quad 3.16$$

where $\Delta k (= k_{2\omega} - 2k_\omega)$ is the phase mismatch of the fundamental and the harmonic.

By using $k_\omega = \frac{2\pi n_\omega}{\lambda}$ and $k_{2\omega} = \frac{2\pi n_{2\omega}}{\lambda/2}$, l_c becomes

$$l_c = \frac{\pi}{k_{2\omega} - 2k_\omega} = \frac{\pi}{\frac{2\pi n_{2\omega}}{(\lambda/2)} - \frac{4\pi n_\omega}{\lambda}} = \frac{\lambda}{4(n_{2\omega} - n_\omega)} \quad 3.17$$

where λ is the free space wavelength of the fundamental beam.

In the thick sample approximation ($l \geq l_c$), the following relationship for the normalised second harmonic power, derived by Jerphagnon and Kurtz [10], was used to calculate the d coefficient

$$\frac{P_{2\omega}}{P_\omega} = \left[\frac{8\pi c}{(n_\omega^2 - n_{2\omega}^2)} \right] d^2 p(\theta)^2 T_{2\omega} t_\omega^4 P_\omega \sin^2 \left(\frac{\Delta k l}{2} \right) \quad 3.18$$

where $p(\theta)$ is the projection factor, $T_{2\omega}$ and t_ω are transmission factors, l is the film thickness, $n_{2\omega}$, n_ω are index of the film at 2ω , and ω , θ is incidence angle and Δk is

the phase mismatch between the incident fundamental and generated second harmonic waves.

The factor, $\sin^2(x)$, ($x = \left(\frac{\Delta k l}{2}\right)$), originates from the interference between the bound and free second harmonic waves and takes values of between zero and one. It becomes one if the phase matching condition ($\Delta k = 0$) is achieved.

The values for $n_{2\omega}$ and n_{ω} were obtained by interpolation, and extrapolation at short wavelength of the measured index at 543 nm using a green HeNe laser, at 1.3 μm using a semiconductor diode laser and at 633 nm using a conventional HeNe laser. The refractive index values are of particular significance with regard to quantitative SHG studies.

The size of the fundamental beam has special importance in this experiment. In order to resolve two adjacent SHG maxima in a quartz wedge, the beam diameter should be smaller than 2.45 mm.

3.8 References

- 1- Oldroyd A.R., G. Elliott, S. Mann and N.J. Parsons, "Highly Efficient Loading of Polymeric Optical Waveguides with Non-linear Organic Materials", Proc. SPIE, **800**,(1986), 193
- 2- Yang C.C., J.Y. Josefowicz and L. Alexandru, Thin Solid Films **74**, (1980), 117-127
- 3- Wells P.J., Ph.D. thesis,(1990), University of London Queen Mary and Westfield College
- 4- Tien P. K. Appl. Opt. **10**, (1971), 2395
- 5- Kogelnik H. and V. Ramaswamy Appl. Opt., **13**, (1974), 1857
- 6- Mortazavi M. A., A. Knoesen, S.T.Kowell, B.G.Higgins and A. Dienes, J. Opt. Soc. Am. B, **6**, (1989), 733-741

- 7- C.C. Teng and H.T.Man, Appl. Phys. Lett., **56**, (1990), 1734-1736
- 8- Amnon Yariv, "Optical Electronics", CBS College Publishing, California, (1985),
293
- 9- Horsthuis W.H.G., and Krijnen G.J.M. Appl. Phys. Lett. **55**, (1989), 616-618
- 10- J.Jerphagnon and S.K.Kurtz, J. Appl. Phys., **41**,(1970), 1667-1681.

4.1 Introduction

In this section the guest-host system is discussed as a second-order non-linear optical material. A brief summary of some physical and optical properties of the materials used as guest NLO molecules and host polymer glasses is given. Electrical poling of guest-host materials at various fields, temperatures and times is studied. Related to the plasticizing effect in doped polymer, differential scanning calorimetry, DSC measurements are carried out for undoped and doped polymer samples. Comparative poling studies and $\chi^{(2)}$ properties of various combinations of the guest-host mixtures are investigated and discussed. The electro-optic, EO, properties of these guest-host systems are compared with the free gas model and deviation from ideal behaviour is observed. The stability of poled guest-host polymers used in this study are investigated for their technological use. Second harmonic generation on corona poled samples is also studied. The SHG response is compared to the EO response in order to confirm the electronic origin of the EO effect in these systems.

4.2 Physical Properties of Materials Used

4.2.1 Guest Molecules

In this study 4-(N,N-dimethylamino)-3-acetamidonitrobenzene, DAN, and (4-methyl-n-((4-nitrophenyl)methylene)benzamine), NMBA, were used as guest NLO molecules. The structural formulae of the guest molecules are shown in figure 4.1 (a).

In DAN the dimethylamino group and the acetanilide side group combine to give electron donating character. The dimethylamino group was found to be among the strongest of electron donating groups in a study by EFISH of donor/acceptor model

molecules [1]. The nitro group is known to be a strong electron acceptor. DAN was first investigated for SHG by Tweig and Jain [2]. The ground state dipole moment μ and the second order molecular hyperpolarisability β of DAN were calculated using an AM1 molecular modelling package [3]. The largest vector component of the dipole moment is in the molecular x direction where $\mu_x = -8.928$ D. The y and z components are -3.077 and 1.059 D, respectively. The calculated total dipole moment, is 9.489 D and $\beta(0)$ is $41 \times 10^{-40} \text{ m}^4\text{V}^{-1}$. The measured value of DAN in 1,4-dioxane is 9.2 D [4]. Uemiya et al. [5] have measured the β value of DAN molecules by EFISH and obtained $76 \times 10^{-40} \text{ m}^4\text{V}^{-1}$ (at $\lambda = 1.064 \text{ }\mu\text{m}$). This value is in excellent agreement with recent measurements [4] which finds $\beta = 71 \times 10^{-40} \text{ m}^4\text{V}^{-1}$ at and also with the theoretical value. DAN has a strong absorption edge at 370 nm and in crystals [6] an effective quadratic non-linear optical susceptibility of $27 \pm 3 \text{ pmV}^{-1}$. DAN crystals were used in phasematched SHG studies where phase matched SHG efficiencies of 20-25% have been observed [7]. More recently, 30-35% efficiencies were measured by Kolinsky et al. [8] on a 1.5 mm thick sample.

NMBA is a rod-like molecule in which the electron donor and acceptor groups are separated by a fully conjugated π -orbital system. In this molecule the CH_3 group is electron donating and the NO_2 is the electron acceptor group. These two groups are bridged by two fully conjugated aromatic units. The μ and the $\beta(0)$ of this molecule were also calculated using the AM1 model and are 7.47 D and $10 \times 10^{-39} \text{ m}^4\text{V}^{-1}$ respectively. NMBA shows the highest dipole moment in the long axis x direction, $\mu_x = -7.439$ D. NMBA has a relatively small μ_y of -1.287 D and very small μ_z of 0.024 D. NMBA has a strong absorption edge at 380 nm . Cross et al. [9] reported a measured EO coefficient, $r = 27 \text{ pmV}^{-1}$, at 632.8 nm using a $42 \text{ }\mu\text{m}$ thick NMBA crystal (by using an estimated refractive index $n \cong 1.7$). Recently, Bailey et al. [10] reported Pockels measurements on an NMBA crystal (at 488.0 , 514.5 and 632.8 nm). They have calculated the EO coefficients through measuring the half-wave voltage

$(V_{\pi} = \frac{\lambda}{r_{11}n_x^3})$. The result found at 632.8 nm was similar to the one reported by Cross et al. [9]. DAN and NMBA were supplied by Merck Ltd. with a purity of 99.99%.

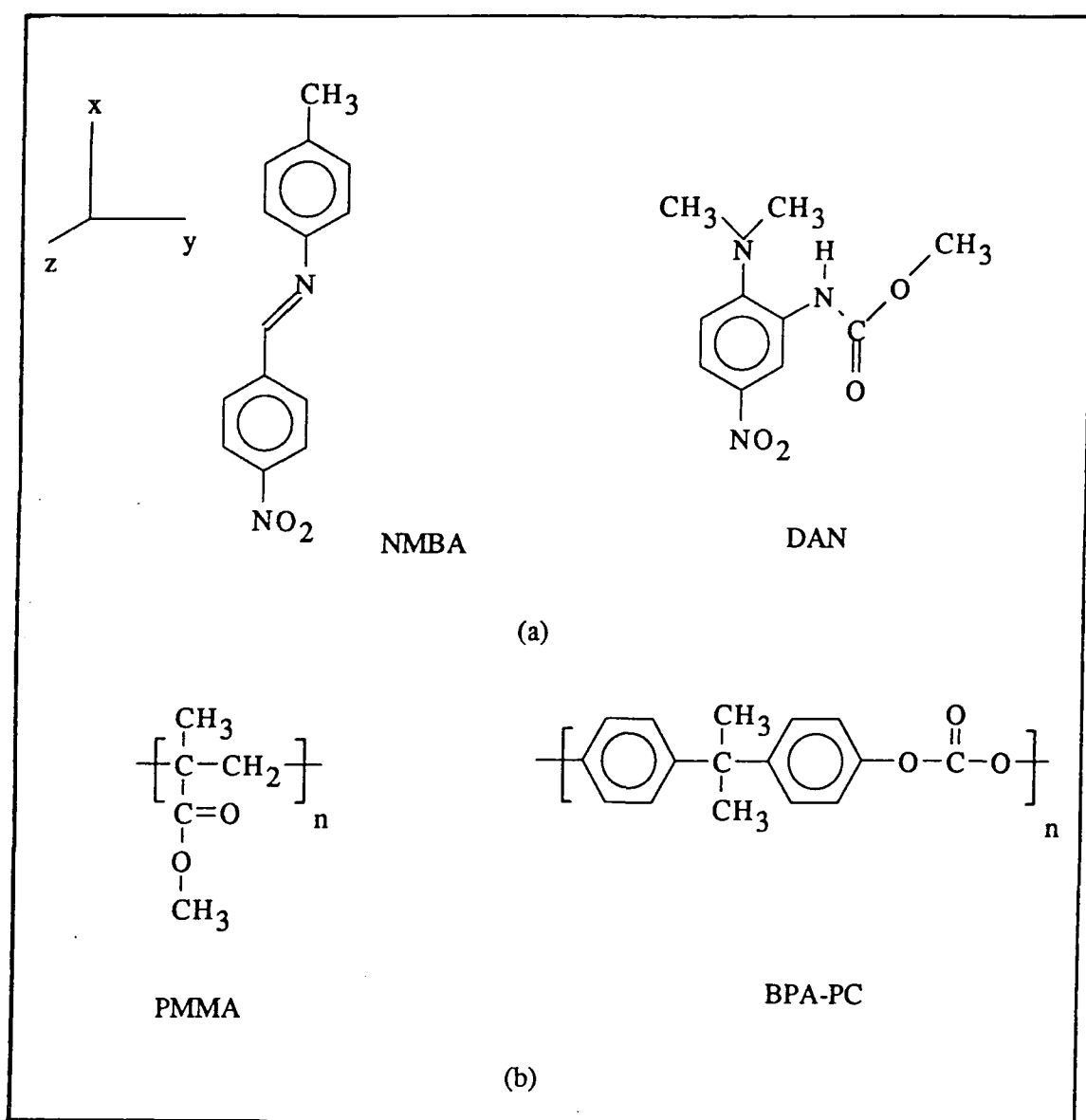


Figure 4.1: Structural formulae of materials used (a) guest molecules (b) host polymers

4.2.2 Host Polymers

Poly(methyl methacrylate) (PMMA) and bisphenol A-polycarbonate (BPA-PC) were used as host polymer glasses. The structural formulae of the host polymers are shown in figure 4.1(b). These two polymers were supplied by Aldrich Chemical Company.

Both PMMA and BPA-PC are amorphous i.e. optically homogenous to visible light and are characterised by an outstanding transparency (93% in PMMA and 89% in BPA-PC). The measured refractive index, n , of PMMA is 1.492 [11] and the refractive index of BPA-PC is 1.578 (at $\lambda = 632.8$ nm) [12]. The glass transition temperature, T_g of PMMA (110 °C) is low in comparison to the T_g of BPA-PC (150 °C). Because of the high T_g BPA-PC shows excellent high temperature resistance. These two polymers find applications in optical materials such as lenses and plastic fiber and can be used as a substrate for optical disks [13,14].

The mechanical properties of BPA-PC have been the subject of numerous investigations [15-17], because of its well-known toughness (i.e. high energy absorption capacity during impact). From dynamical mechanical studies of BPA-PC three relaxation peaks were observed at 155 °C, at 80 °C, and at -97 to -100 °C. These are the α , β and γ -relaxations, respectively (figure 4.2). The very prominent α -relaxation is undoubtedly due to the glass-rubber transition. The small and broad β -relaxation is attributed by Illers and Breuer [15] to the orientational stress in the specimen, to the motion of the phenyl (-CH₃) group by Reading et al. [16]. Investigators seem to agree that the carbonate group motion is responsible for the γ -relaxation. Yee and Smith [17] have reported that the effect of substituting the isopropylidene group by more flexible groups is to reduce T_g and by more rigid or bulky groups to raise T_g .

4.3 Sample Preparation and Characterisation

Solutions (in dichloromethane) of the host polymers (both BPA-PC and PMMA) and the NLO molecules, DAN and NMBA doped (for various concentration) polymers were made. The solutions were filtered through 0.5 μm pore size Millipore filters. Thin films were dipped from solution onto substrates at withdrawal speeds of 15-50 mm minute⁻¹. The samples were dried under vacuum at various temperatures (40-100 °C) for various times (2-16 hours). The linear optical properties of the samples were studied by

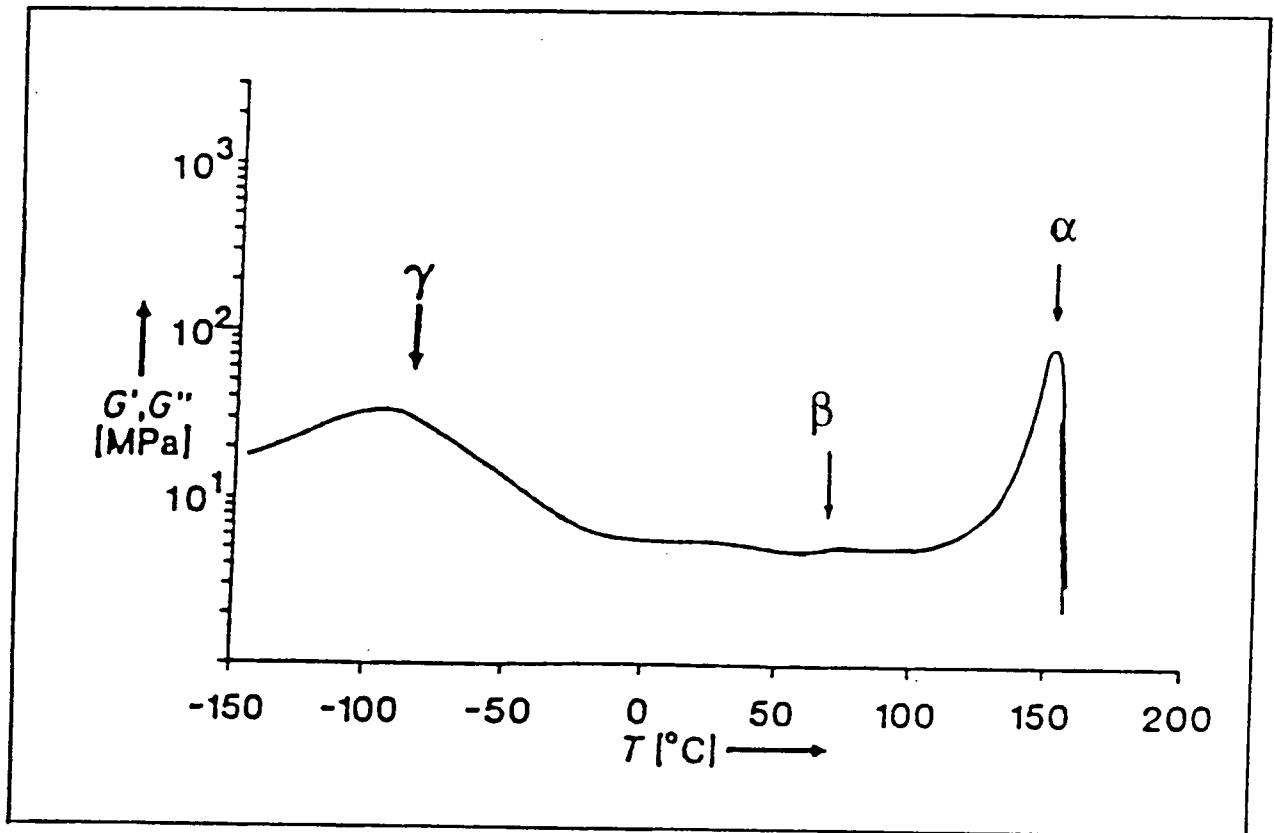


Figure 4.2: α , β , γ relaxations in bisphenol-A polycarbonate measured by dynamical mechanical analysis (G' = storage modulus, G'' = loss modulus) (adapted from [14])

prism-coupled waveguiding. A 60 degree prism of SF6-type glass with refractive index $n = 1.798$ at $\lambda = 632.8$ nm was used to couple the light beam into the film. Glass microscope slides which have a known refractive index $n = 1.507$ (at $\lambda = 632.8$ nm) were used as substrates. Table 4.1 shows the refractive index of doped and undoped BPA-PC. The absorption spectra of doped polymers were studied by a Perkin Elmer UV/VIS/NIR Lambda 19 Spectrometer. The glass transition temperature of undoped and doped polymers were measured by a Perkin Elmer DSC-7.

Sample	Doping con. (% w/w)	n (633 nm) ± 0.001
PC	-	1.578
DAN/BPA-PC	5	1.579
	10	1.579
	15	1.580
	20	1.580
NMBA/BPA-PC	5	1.579
	10	1.580
	20	1.580
	30	1.581

Table 4.1: Refractive index versus doping level for polycarbonate guest-host films

In the following sections the poling of DAN and NMBA guest molecules in BPA-PC and PMMA host polymers is presented. These guest-host materials were poled at various fields, temperatures and times in order to find the optimum poling conditions.

4.4 Linear and Quadratic Electro-optic Response

The linear EO response (Pockels response) and the quadratic EO response (Kerr response) of a film of 20% DAN/BPA-PC were measured before and after poling. These responses, when measured using the lock-in amplifier (see chapter 3, section 3.6) were sampled at the drive frequency of the experiment, ω , and at twice the drive frequency, 2ω , respectively. The relationship between the modulation intensity I_m and the drive voltage, V_m was also studied (figures 4.3 and 4.4). The linear dependence of I_m on V_m at the drive frequency and the quadratic dependence of I_m on V_m at twice the drive frequency can be seen clearly from the above mentioned figures. Table 4.2 shows the modulated intensity, I_m , (at ω and at 2ω) versus the angle of the analyser, θ .

Before poling				After poling			
ω		2ω		ω		2ω	
θ	I_m 10^{-5} V	θ	I_m 10^{-5} V	θ	I_m 10^{-4} V	θ	I_m 10^{-5} V
0	0.0	0	0.0	0	0.0	0	0.0
45	0.0	45	-1.8	45	8.0	45	-1.8
90	0.0	90	0.0	90	0.0	90	0.0
135	0.0	135	1.8	135	-8.0	135	1.8
180	0.0	180	0.0	180	0.0	180	0.0

Table 4.2 : ω and 2ω response of poled DAN/BPA-PC

As can be seen from table 4.2 the Kerr response was the same before and after poling. Being a third order, $\chi^{(3)}$, effect, the Kerr effect is independent of symmetry considerations unlike second order effects. Before poling there was no intensity modulation at the drive frequency (1.8 kHz. in these studies), in accordance with the centrosymmetric structure ($r = 0$). After poling, the material showed a finite ($r > 0$) EO response. Following the application of a 94 V rms field an intensity modulation, 44 times higher than the modulation obtained at twice the drive frequency, was observed.

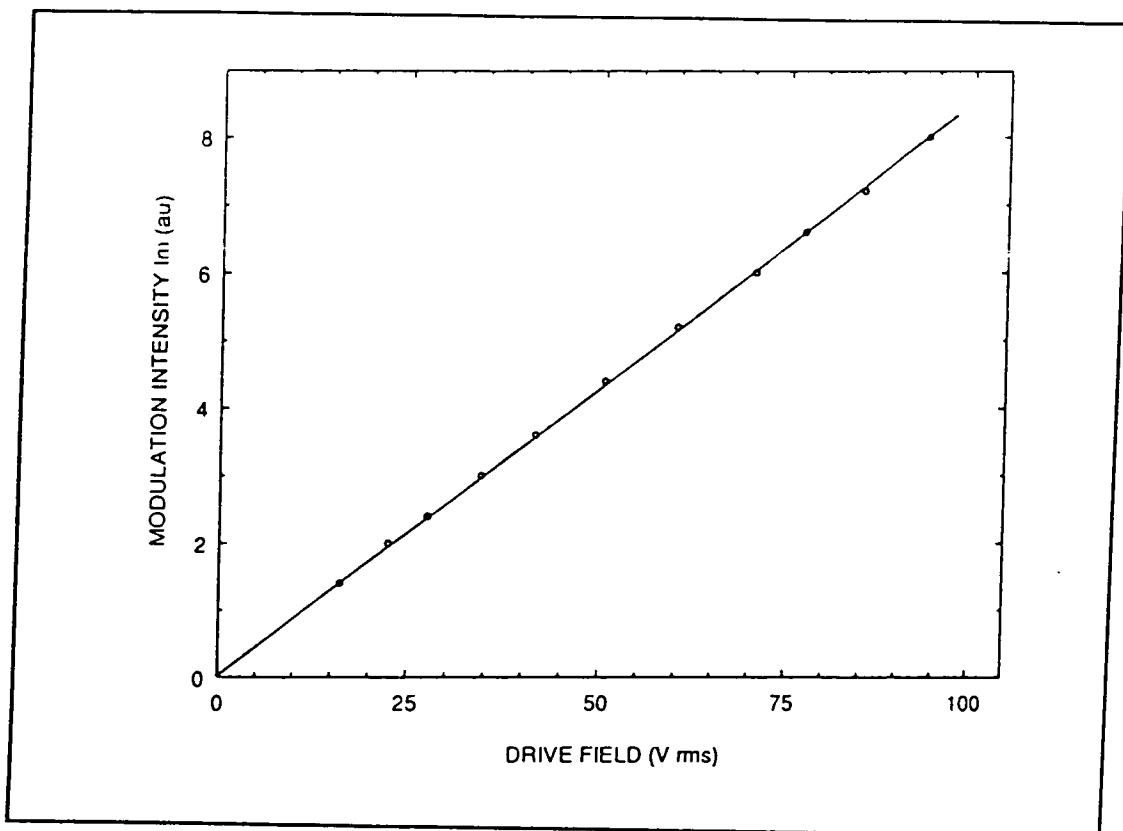


Figure 4.3: Modulation intensity (I_m) vs. drive field characteristic of DAN/BPA-PC film at ω .

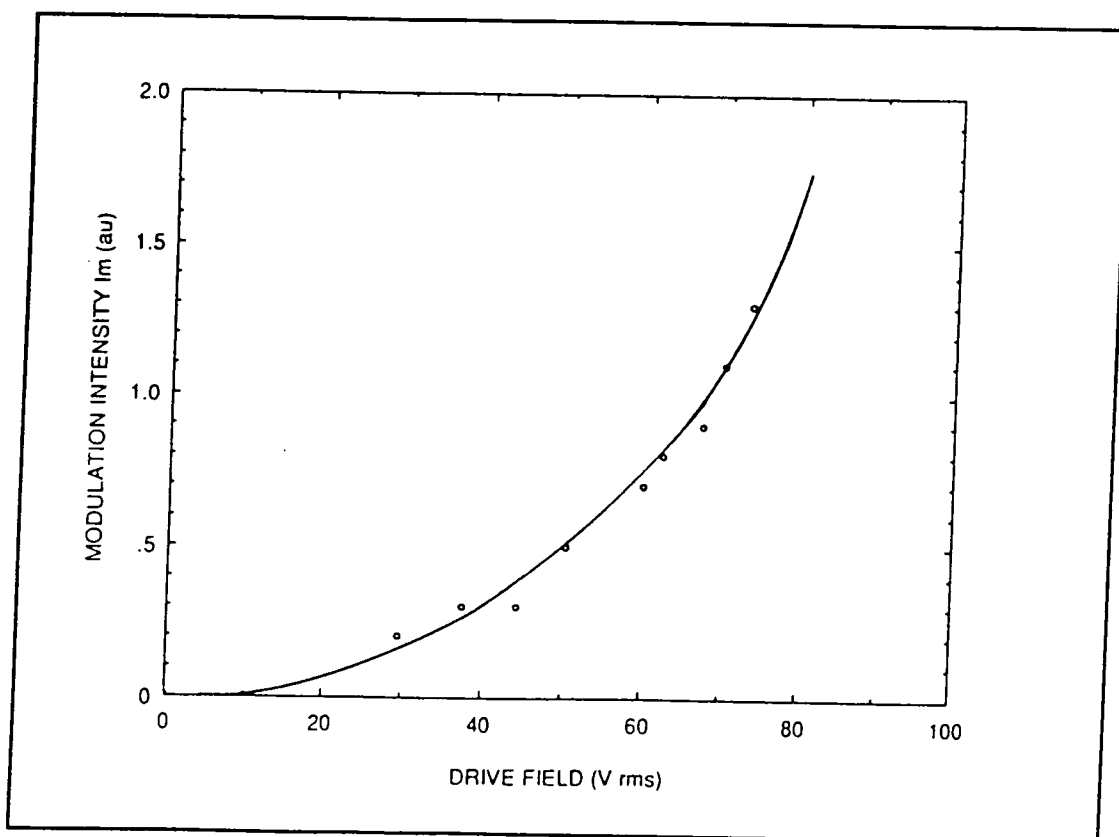


Figure 4.4: Modulation intensity (I_m) vs. drive field characteristic of DAN/BPA-PC film at 2ω

When a modulation field was applied to the sample, the circularly polarised light (figure 4.5 a) is partially converted into elliptical polarised light (figure 4.5 b), due to the linear EO effect. The electric field vector directed along the semi-major axis of the ellipse will then oscillate in a plane which is 45 degree to the horizontal and vertical axes (figure 4.5 b). Because of this fact the maximum modulation intensity (either (+) or (-)) occurs at odd multiples of $\pi/4$ ($n\pi/4$, $n = 1,3,5\dots$). At even multiples of $\pi/4$ ($n\pi/4$, $n = 0,2,4\dots$) zero modulation occurs.

As is shown in this experiment the quadratic EO response does not depend on poling, so from here onwards only the linear EO response will be considered.

4.5 Plasticizing Effects in DAN/BPA-PC and DAN/PMMA Films

The glass transition temperatures of these samples were measured using differential scanning calorimetry, DSC, and found to be 90 °C for 20% (w/w) DAN/BPA-PC and 55 °C for the 20% (w/w) DAN/PMMA. Figures 4.6-4.10 reveal the position of the T_g . This reduction of T_g is due to the plasticizing effect, which has been previously documented [chapter 2 references 9,11,12,14,15]. A peak which indicates the α transition (T_g) in BPA-PC occurs at a temperature of about 145 °C. The T_g of PMMA appears at 100 °C. Doping by DAN with weight fractions 5, 10, 15, and 20 % in BPA-PC reduces the T_g from 145 °C, down to 118, 100, 93 and 90 °C, respectively (figure 4.11). Doping of 20 % by weight into PMMA depressed the T_g by 45 °C. NMBA was doped into BPA-PC with a 20% weight fraction. The T_g of the host polymer decreased to 88 °C. Doping of BPA-PC with the same amount of different size guest molecules (DAN and NMBA) reduces the T_g of the host polymer to the same level.

Comparable results have been observed by Boyd et al. [Chapter 2 reference 14] who reported a plasticizing effect in dye doped BPA-PC. They have found that the doping of 30% DR1 into BPA-PC depresses the T_g of the host by 85 °C. Further strong evidence of the plasticizing effect in these guest-host systems is mentioned in the section 4.6.

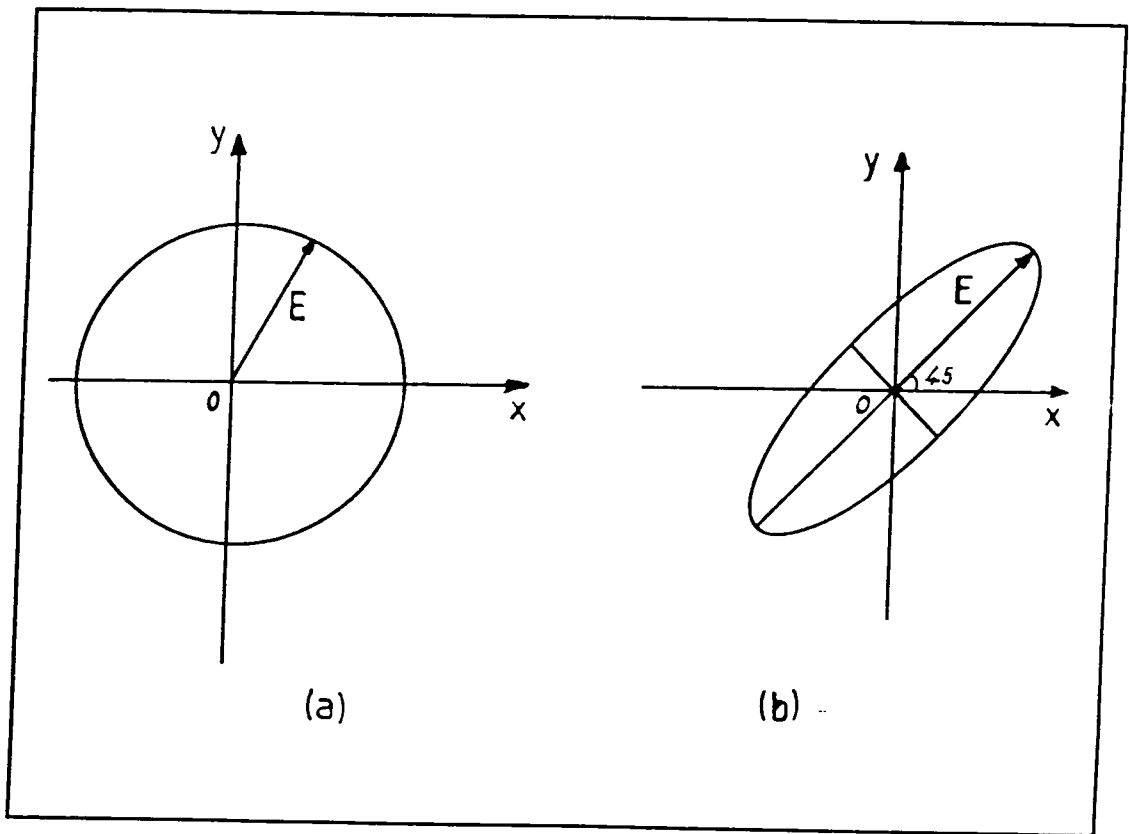


Figure 4.5: a) Circular polarisation ($V_m = 0$), b) Elliptical polarisation ($V_m > 0$)

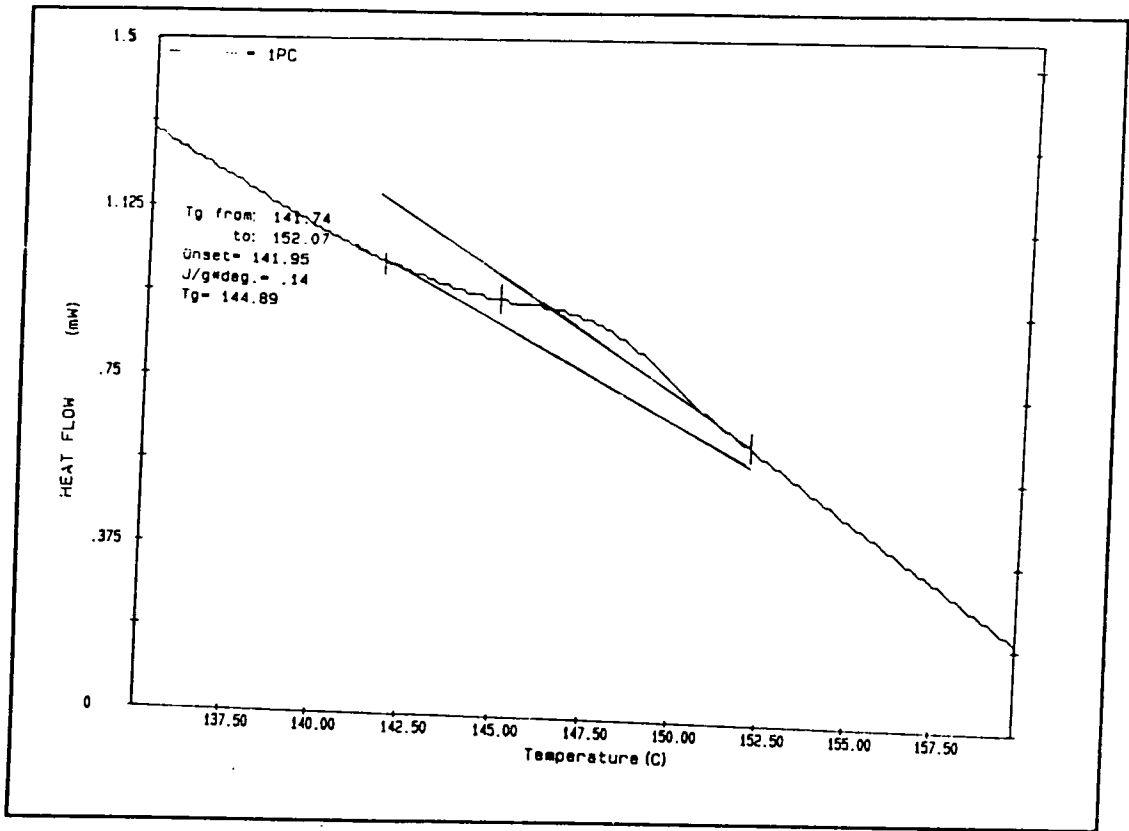


Figure 4.6: DSC of un-doped BPA-PC film

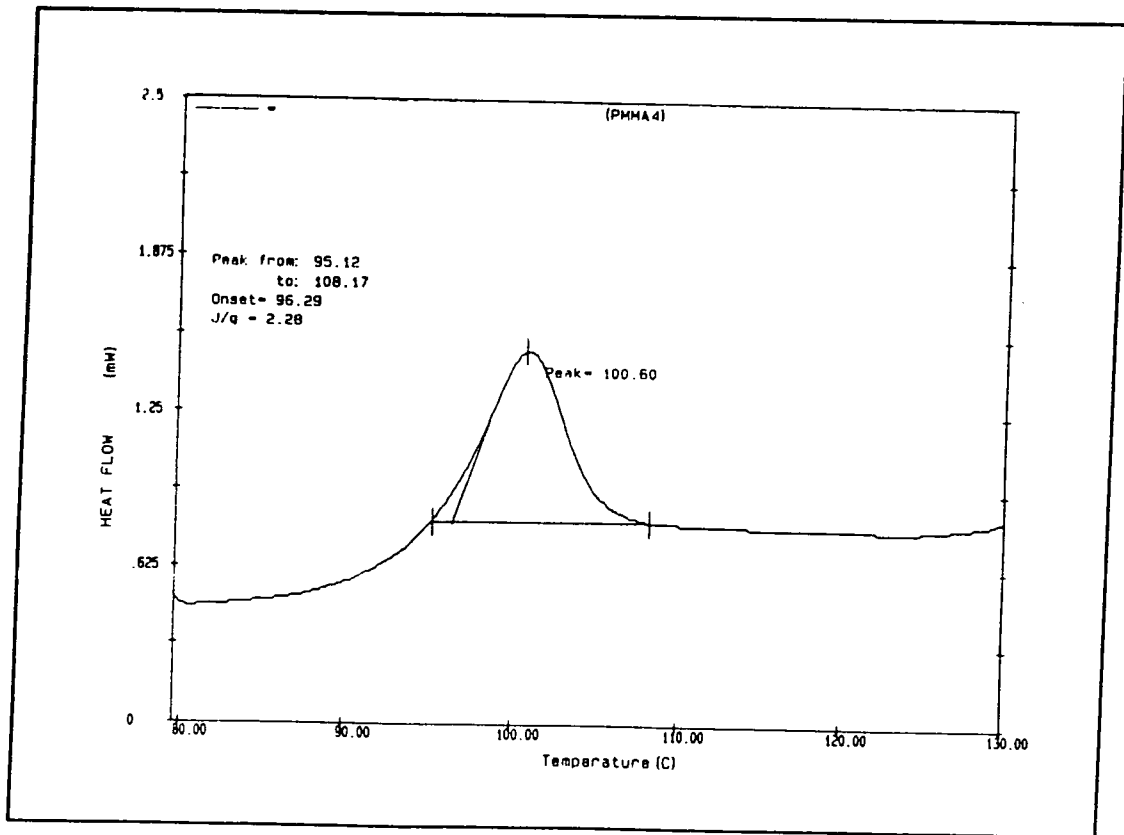


Figure 4.7: DSC of un-doped PMMA film

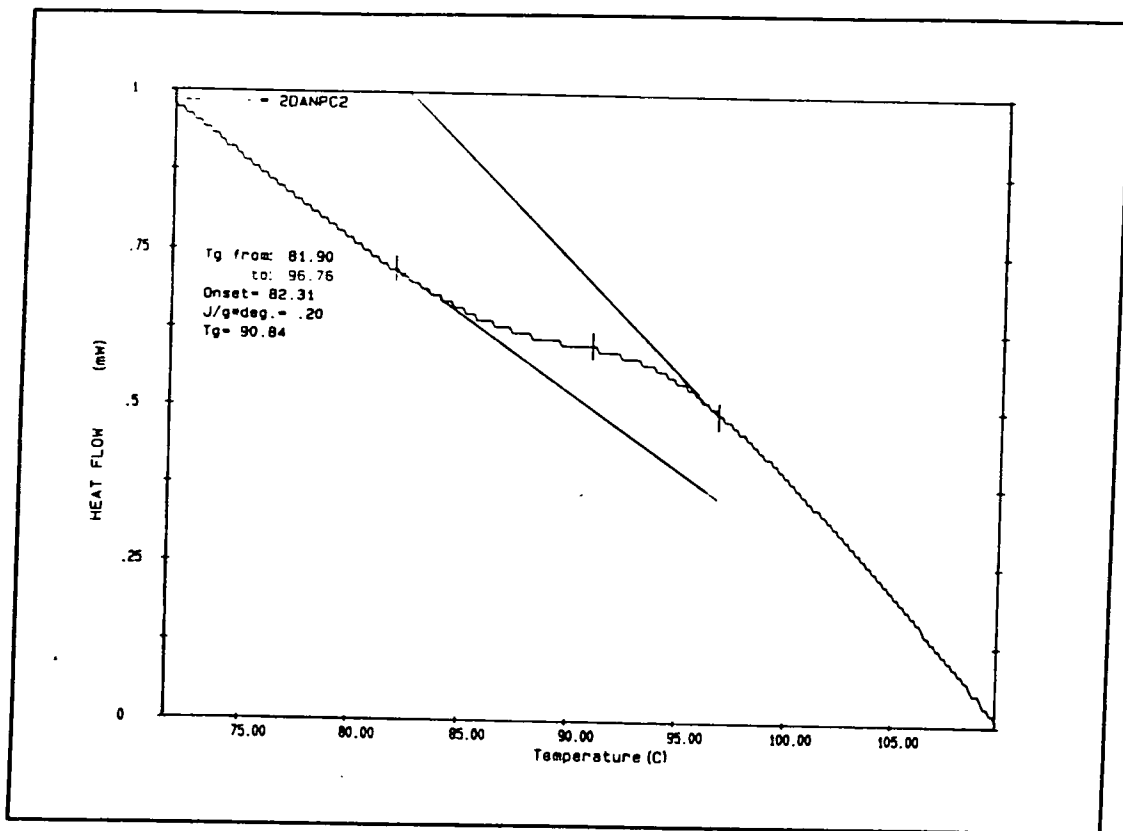


Figure 4.8: DSC of 20% DAN/BPA-PC film

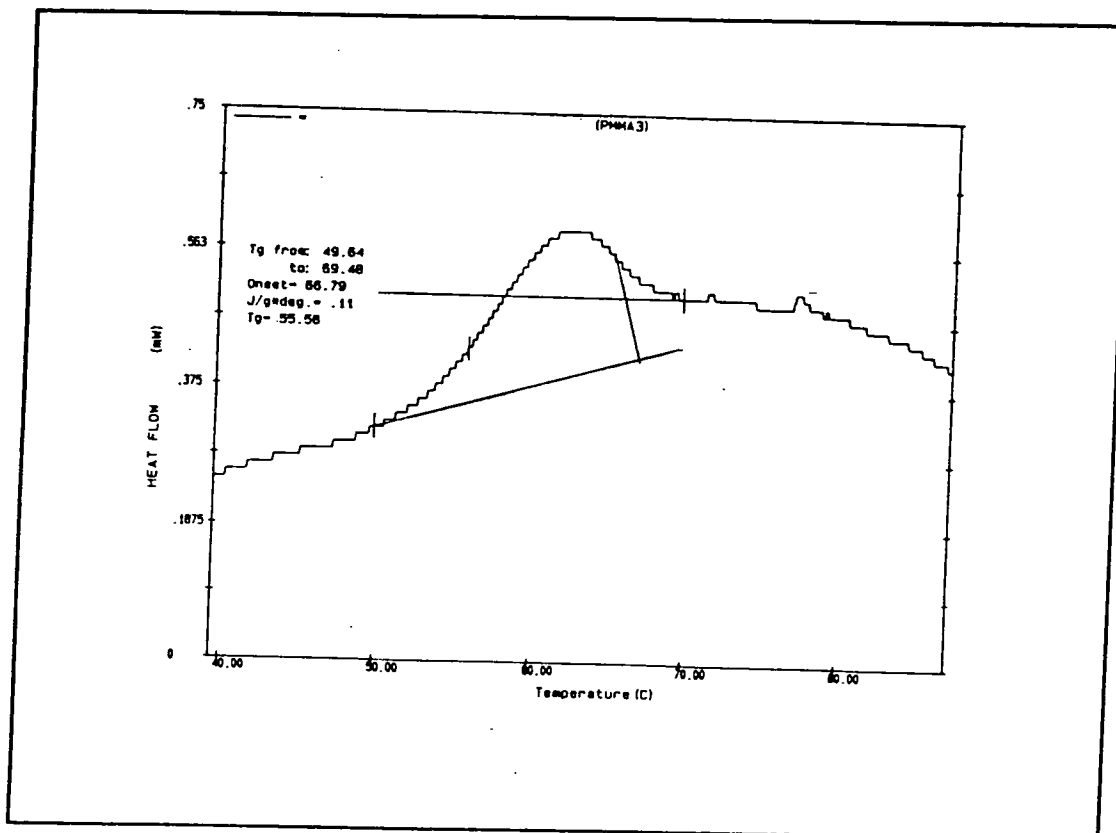


Figure 4.9: DSC of 20% DAN/PMMA film

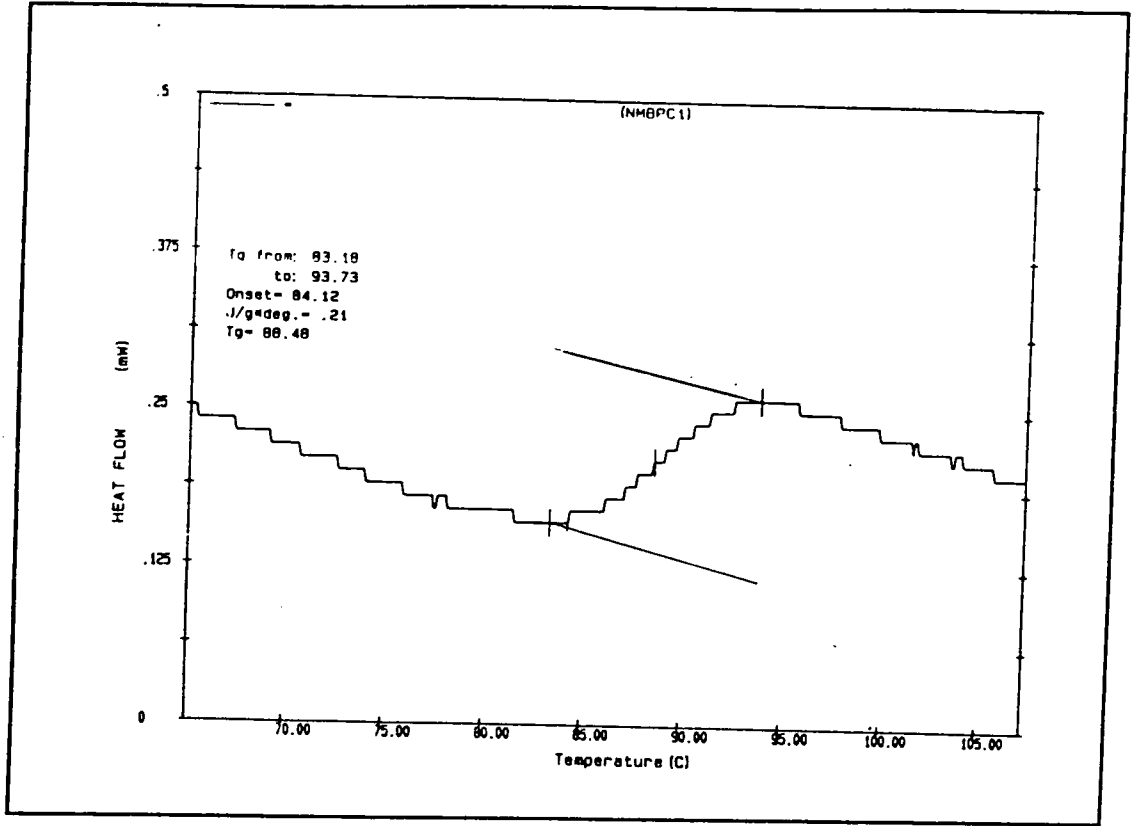


Figure 4.10: DSC of 20% NMBA/BPA-PC film

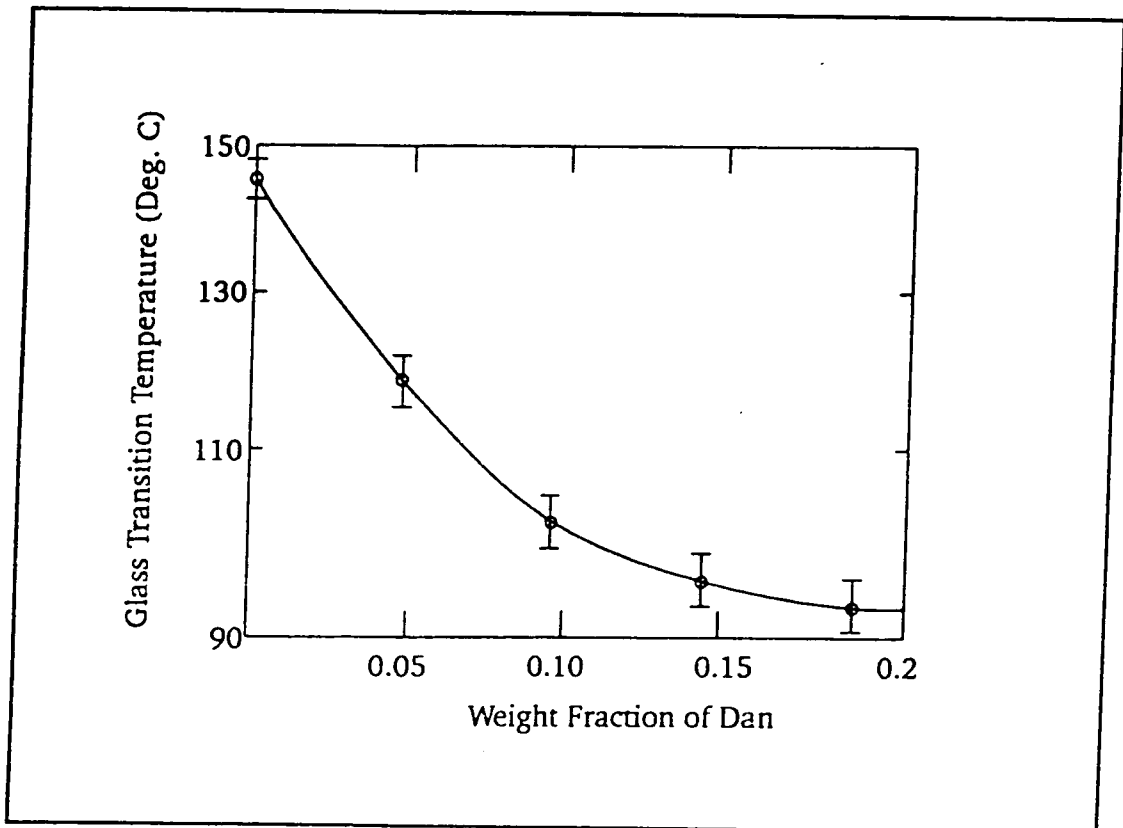


Figure 4.11: T_g of DAN/BPA-PC films vs. weight fraction of DAN

4.6 Thermal Relaxation in a Poled 20 % DAN/BPA-PC Sample

The thermal relaxation of a corona poled (-5 kV needle voltage at 80 °C for 30 minutes) 20% DAN/BPA-PC sample was examined. The aim of this experiment was to see the effect of temperature on poling induced alignment. The sample was heated gradually from room temperature up to 80 °C. At successive temperatures, after three minutes, the EO response was monitored in-situ. In figure 4.12 the measured EO response is shown with respect to temperature.

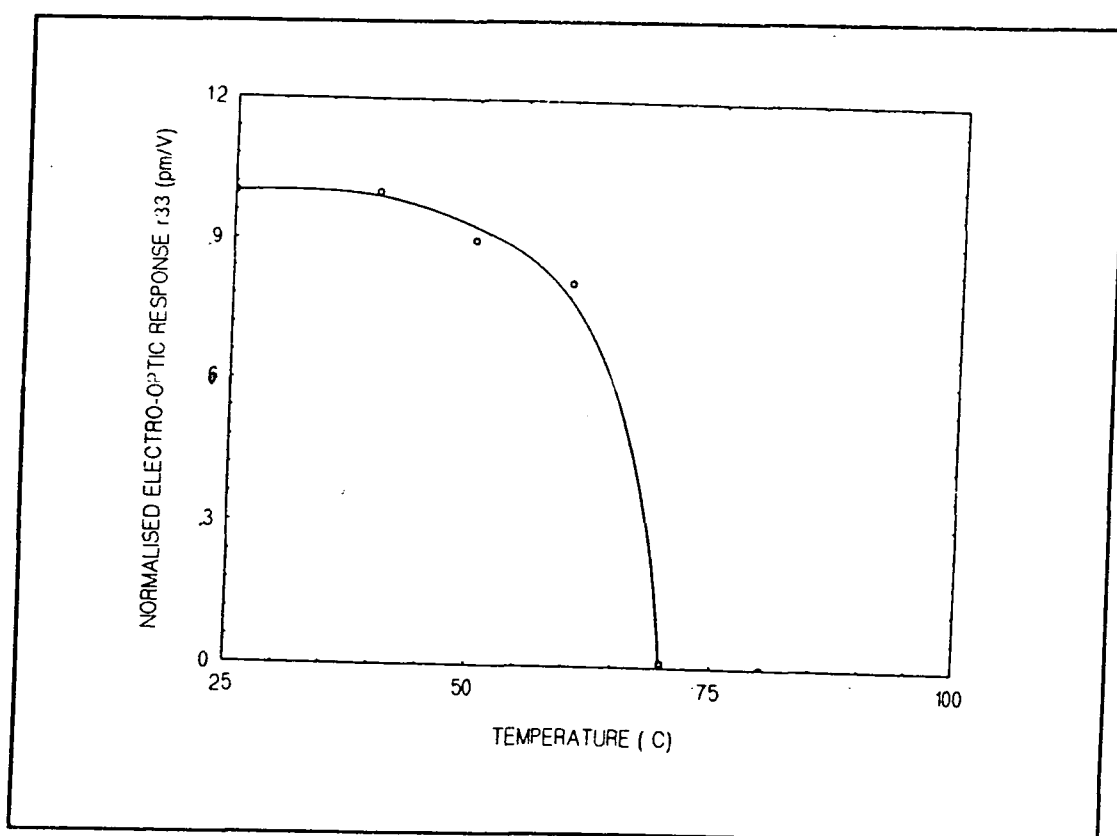


Figure 4.12: Normalised EO response (r_{33}) vs. temperature for 20% DAN/BPA-PC thin film

By increasing the temperature the thermal energy of dipoles is increased. At 80 °C the energy gained by these dipoles is enough to eliminate the poling induced alignment and the rapid relaxation is associated with the glass transition temperature. Similar experiments were performed by Kohler et al. [18], with a different experimental technique. These authors measured the relaxation of electric field-induced polar orientation in some polymeric materials by simultaneously measuring second harmonic

generation and the thermally stimulated discharge current. They have shown that the decay of the second harmonic signal with increasing temperature follows the α -relaxation peak.

The reorientation of dipoles in the poled 20% DAN/BPA-PC sample above 70 °C can be explained using the free volume concept. An increase in the free volume allows the dipoles to reorient. Free volume increase occurs at temperatures higher than the glass transition temperature. Man and Yoon [Chapter 2 reference 31] have observed similar behaviour in their poled side-chain polymer P2ANS/BMA 25/75 with a T_g of 68 °C. They have seen a 40% decrease at 30 °C and an 80% decrease at 40 °C in the SHG response. At 60 °C the SHG response fell to zero over a few minutes.

4.7 Electrical Poling of DAN Doped BPA-PC and PMMA Thin Films

To see the relationship between the EO response and the poling parameters (field, temperature, and time) 20% DAN doped BPA-PC and PMMA samples were poled at various temperatures, fields, and times.

4.7.1 Poling at Different Temperatures

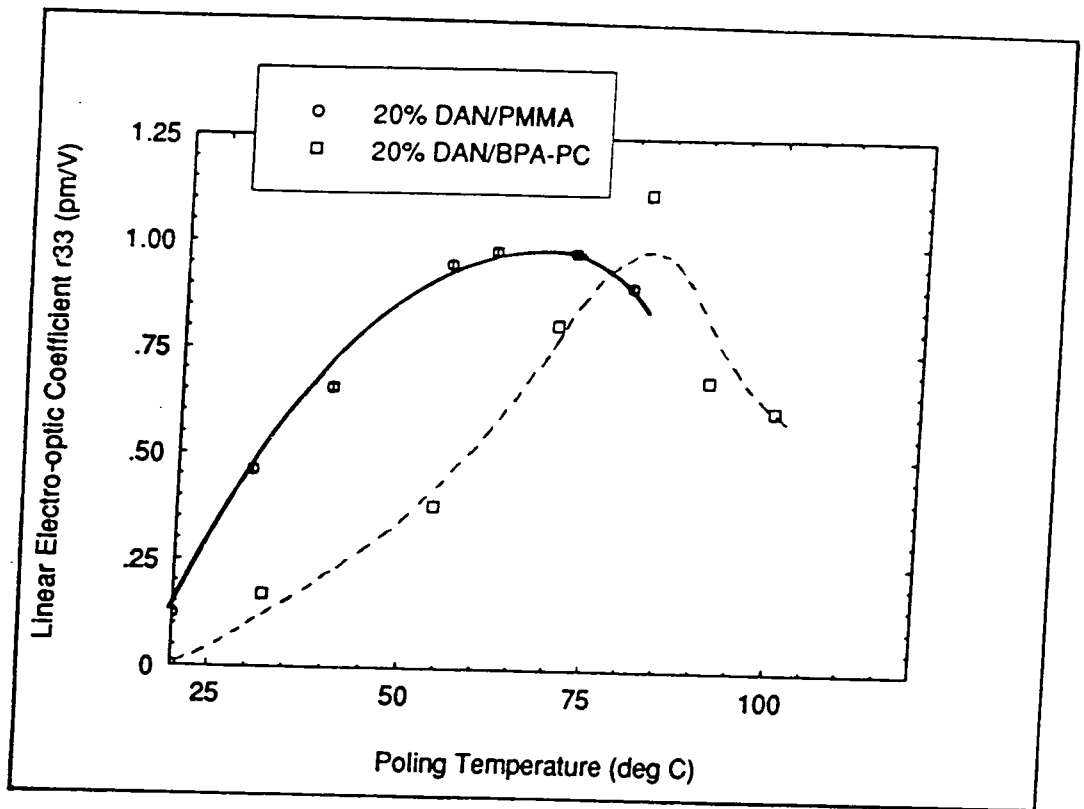
To determine the relationship between r_{33} and poling temperature, 20% w/w DAN/PMMA and 20% w/w DAN/BPA-PC samples were poled at various temperatures. The poling field ($50 \text{ V}\mu\text{m}^{-1}$ in the first sample and $27 \text{ V}\mu\text{m}^{-1}$ in the second) and the poling time (5 minutes in DAN/PMMA and 10 minutes in DAN/BPA-PC) were kept constant. The poling characteristics of these samples are shown in figure 4.13. At room temperature the EO response of the DAN/BPA-PC sample was zero and the r_{33} of DAN/PMMA was 0.12 pmV^{-1} . The reason why there was no EO response in 20% DAN/BPA-PC at room temperature is that the T_g (90 °C) of this sample is well above room temperature. In the 20% DAN/PMMA sample, however, the T_g is closer to room

temperature. This allows poling at such a low temperature. In both samples the EO response increases with the increase in temperature. It reaches a maximum value at 80 °C in DAN/BPA-PC and between 50 and 60 °C in DAN/PMMA. Singer et al. [19] have shown that a 10% DR1 doped PMMA sample gave electric field induced SHG at temperatures close to room temperature. These authors have also shown that the maximum polar alignment occurs at temperatures around 75 °C. In the 20% DAN/PMMA sample the maximum alignment was achieved 20 °C lower. This is due to the fact that doping to 20% with guest DAN molecules reduces further the T_g of PMMA. To confirm the results found in the case of DAN/BPA-PC, another sample was poled at a higher field ($27 \text{ V}\mu\text{m}^{-1}$) for the same temperature range. The results obtained are shown in figure 4.13 (b) and compared to the first sample. The same temperature/EO response characteristic was seen. The highest EO response again occurred at around 80 °C which confirms the previous results.

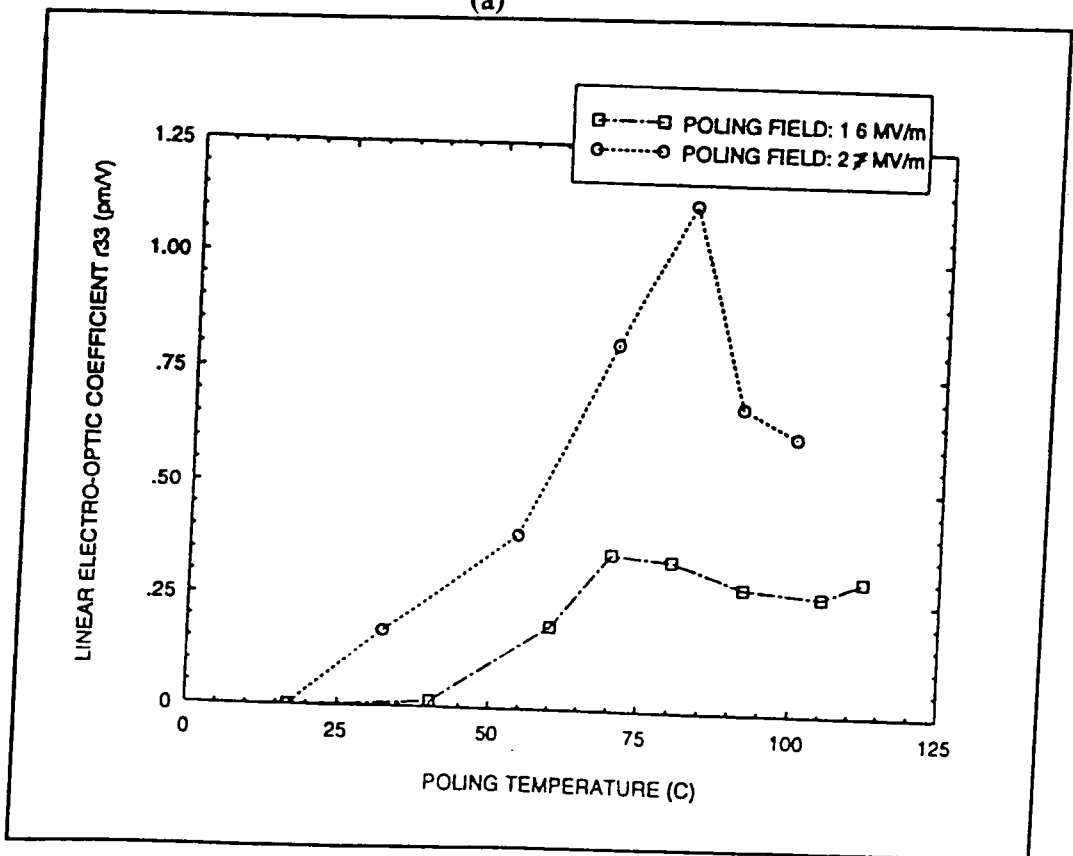
4.7.2 Poling at Different Fields

To see the relationship between the poling field and the polar alignment a 10 μm thick DAN/BPA-PC and a 12 μm thick DAN/PMMA sample (with 20% weight fraction) were poled at 100 °C for 10 minutes, for a poling field varying from 10 to 70 $\text{V}\mu\text{m}^{-1}$. Figure 4.14 shows the relationship between the poling field and the EO coefficient of these samples.

The expected linear relationship, appropriate for 'low' field poling, is seen between the poling field and the electro-optic response. The EO response is higher in DAN/BPA-PC compare to DAN/PMMA. The reasons behind this will be discussed in sections 4.8.



(a)



(b)

Figure 4.13: (a) EO coefficient (r_{33}) vs. poling temperature of 20% DAN/BPA-PC and 20% DAN/PMMA films (b) r_{33} vs. T_p of two different 20% DAN/BPA-PC samples

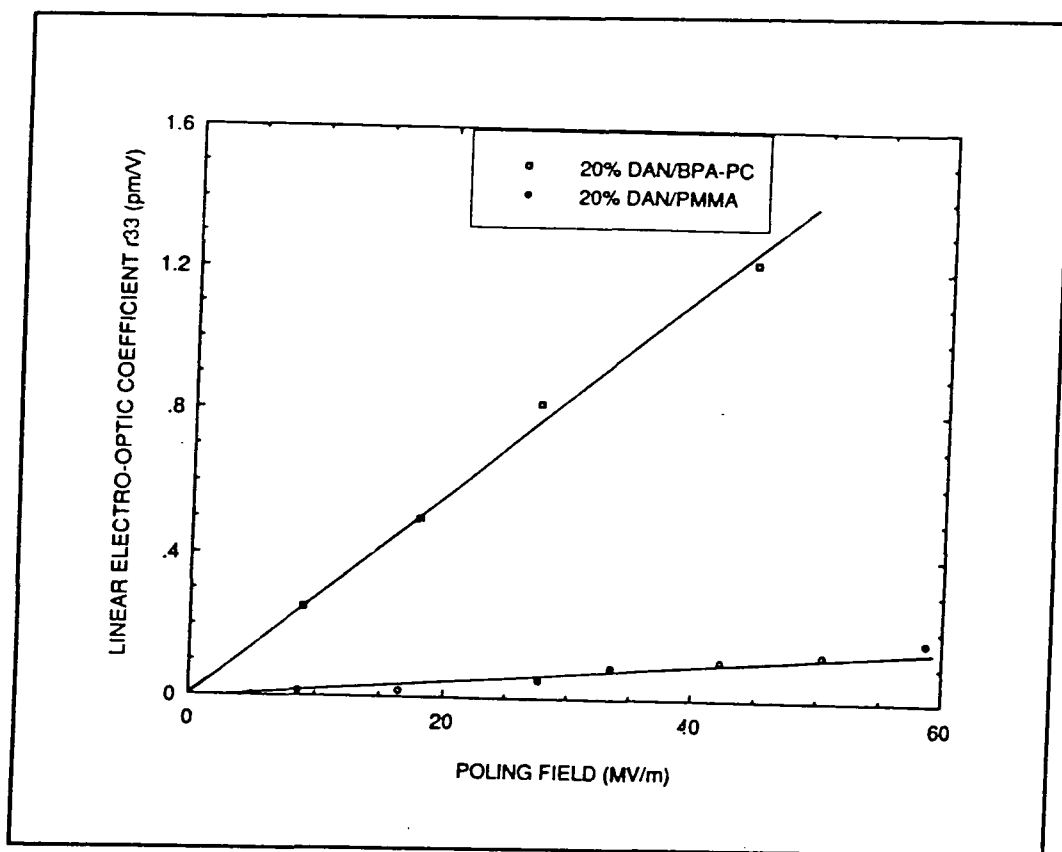


Figure 4.14: EO coefficient (r_{33}) vs. poling field for 20% DAN doped BPA-PC and PMMA

4.7.3 Effect of varying Poling Time

A 10 μm thick 20% w/w DAN/BPA-PC sample was poled with a poling field of 11 $\text{V}\mu\text{m}^{-1}$ at 80 $^{\circ}\text{C}$ for a poling time varying from 1 to 15 minutes in order to see the effect of time on the polar alignment. The other parameters were kept constant. The EO coefficient increased from 0.24 pmV^{-1} up to 0.33 pmV^{-1} when the poling time was increased from 1 to 5 minutes. Over 5 minutes the increase in the EO response was negligible which proves that alignment of guest molecules occurs in less than 5 minutes at 80 $^{\circ}\text{C}$.

A 2 μm thick 20% w/w DAN/PMMA sample was also studied. This sample was poled with a poling field of 50 $\text{V}\mu\text{m}^{-1}$ at 51 $^{\circ}\text{C}$ for a poling time varying from 10 to 900 seconds. The resulting EO coefficients are shown in table 4.3.

Poling time (second)	r_{33} (10^{-12} mV^{-1})
10	0.78
22	0.74
60	0.99
240	1.15
480	0.76
600	0.50
900	0.46

Table 4.3 : r_{33} \poling time relationship of 20% DAN/PMMA sample

The table shows that an increase in the poling time from 10 to 240 seconds causes only a small increase in the EO response. Above 240 seconds, the EO response decreases with the increase in poling time. This decrease is probably due to the loss of dopant which occurs in this sample at this temperature. Obviously the amount of loss would increase with the increase in poling time as shown by Kobayashi et al. [20].

Poling at different fields, temperatures and times has shown that the polar alignment strongly depends on the poling temperature and the poling field, but depends less importantly on the poling time.

4.8 Current Density versus Temperature

The poling field was limited to $70 \text{ V}\mu\text{m}^{-1}$ in DAN/BPA-PC and to $68 \text{ V}\mu\text{m}^{-1}$ in DAN/PMMA because of the breakdown effect. A high doping level, 20 weight % of NLO molecules into polymer, causes an increase in current density. Higher temperatures and correspondingly higher currents lead to break down in the film. The current density versus temperature relationship of these samples is therefore important in determining the values of poling field and temperature range at which they can be poled without electrical breakdown.

The current density/temperature, J/T , relationship of DAN doped BPA-PC and PMMA samples were studied. The general trend of current density is that it initially increases with the increase in temperature (figure 4.15). At the poling temperature a 10-15% decrease occurs over the few minutes of poling time. Finally, it decreases to values close to the initial value at room temperature. During heating of the sample some contribution to the total current density derives from impurities and/or surface currents. Once these impurities are swept out of the sample the surface currents decay and the total current decreases.

The J/T characteristics of BPA-PC were also studied and compared to a 20% DAN doped BPA-PC film (figure 4.16). A slow current increase, beginning around 70-80 °C, is seen in the undoped BPA-PC sample. In DAN/BPA-PC films the current density increase occurs in the same temperature range i.e. just below T_g , but is sharper and rises over two orders of magnitude.

4.9 Comparative Poling Study of DAN Doped BPA-PC and PMMA

In order to compare the EO response between samples where the host material only is different, a comparative poling study of films of 20% DAN/BPA-PC and 20% DAN/PMMA was carried out. Both samples were poled at similar temperatures and for the same time (15 minutes). The poling conditions and the EO responses obtained are shown in table 4.4

Material	N 10^{20} cm^{-3}	E_p $\text{V}\mu\text{m}^{-1}$	T_p $^{\circ}\text{C}$	r_{33} 10^{-12} mV^{-1}	r_{33} (theor.) 10^{-12} mV^{-1}
DAN/PMMA	6.4	50	75	0.14 ± 0.05	0.27
DAN/BPA-PC	6.0	27	70	0.81 ± 0.1	0.11

Table 4.4: Poling conditions and electro-optic response obtained at 633 nm for DAN-doped polymers

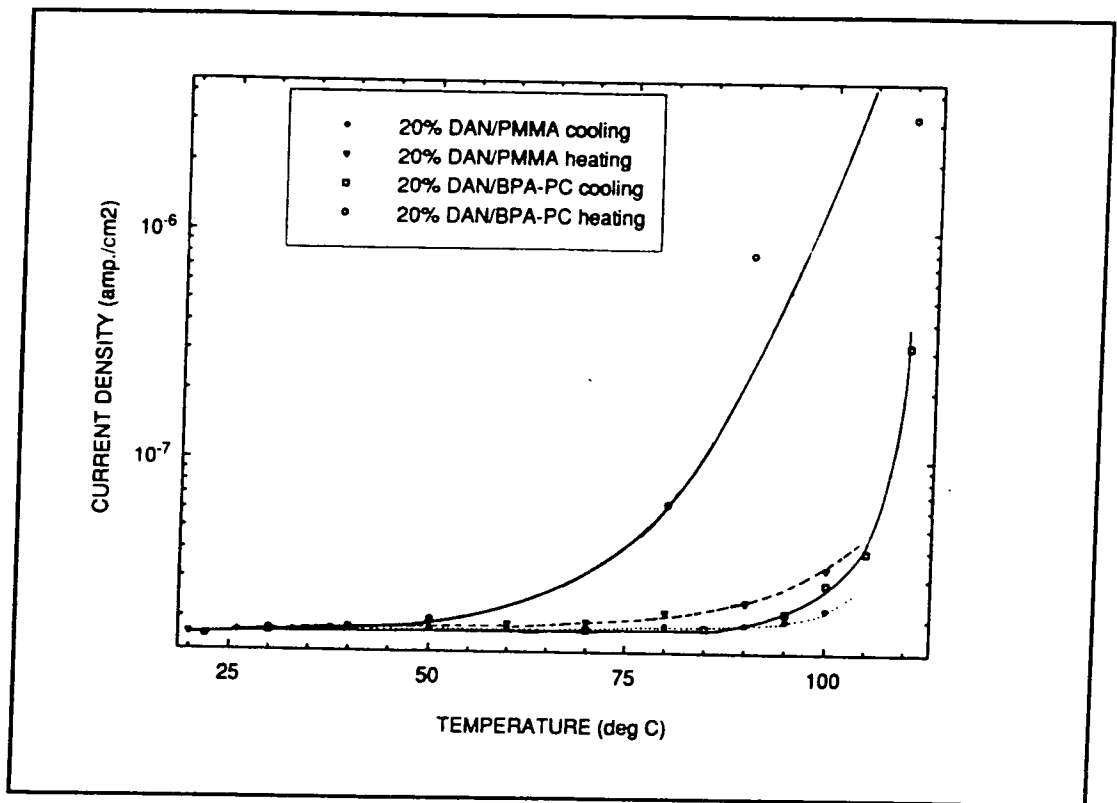


Figure 4.15: Current density/ temperature relationships for guest/ host polymers. Note that the decrease in current density between cycles occurs over the poling time of 15 minutes.

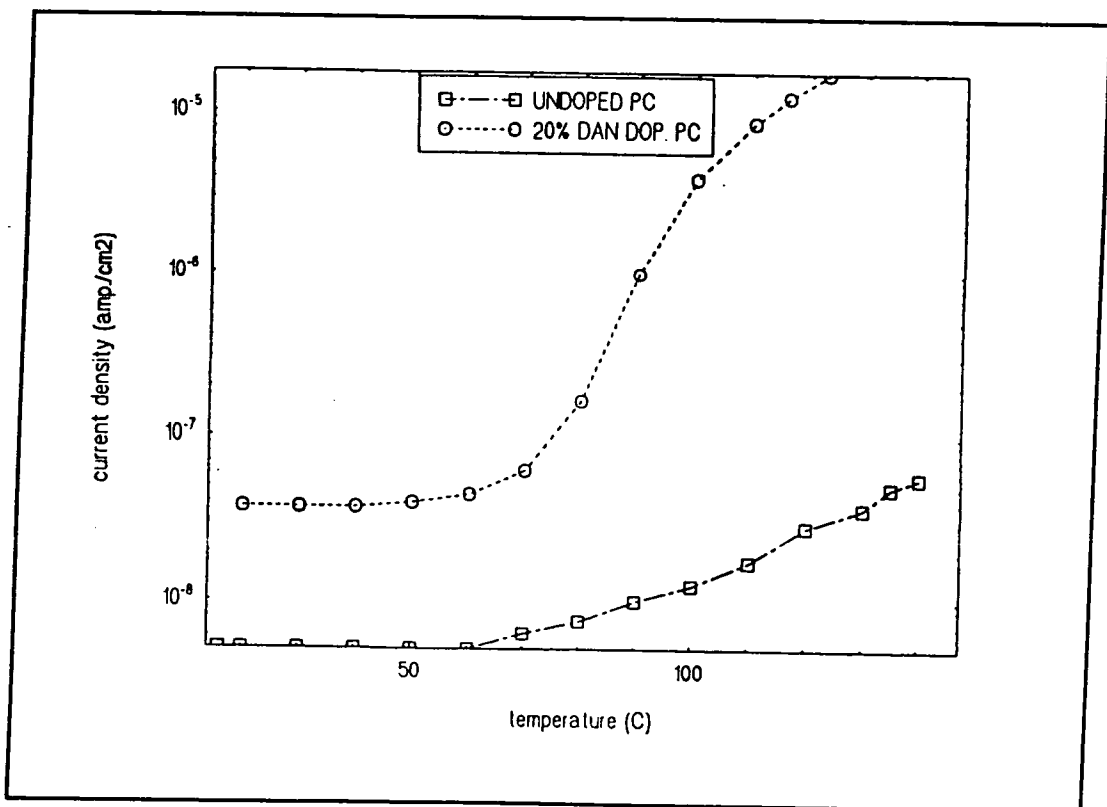


Figure 4.16: J/T of BPA-PC and 20% DAN doped BPA-PC sample

It is clear from the above table that the theoretical r_{33} of DAN/PMMA is eight times higher than the experimental r_{33} . However, the experimental r_{33} of DAN/BPA-PC is seven times higher than the theoretical r_{33} . The most significant result is that the figure of merit, taken to be $\frac{r_{33}}{E_p}$, for DAN/BPA-PC, is ten times higher than that of

DAN/PMMA. This difference in the EO coefficient may originate from the following:

- contribution of BPA-PC to the EO response of the DAN/BPA-PC,
- the loss of DAN guest molecules in PMMA host polymers,
- a possible guest-host interaction in DAN/BPA-PC.

These are discussed in turn.

4.9.1 Contribution of BPA-PC

Undoped BPA-PC exhibits an EO response following poling. This is due to the alignment of the carbonyl groups by rotation around the polymer main-chain [21].

A 10 μm thick BPA-PC sample was poled at 127 °C for a poling field of 85 $\text{V}\mu\text{m}^{-1}$ for 10 minutes. Immediately after poling the measured EO response was 0.03 pmV^{-1} . The value obtained here for r_{33} is in agreement with the value published by Gulloty et al. [21].

These authors' second harmonic generation measurement gave a $d_{33} = 0.03 \text{ pmV}^{-1}$ for $E_p = 42 \text{ V}\mu\text{m}^{-1}$ which we relate to r_{33} simply by using,

$$\chi_{ZZZ}^{(2)}(-\omega; \omega, 0) = \frac{1}{2} n^4 r_{33} = 2d_{33} \quad 4.1$$

The r_{33} obtained is 0.02 pmV^{-1} .

The contribution of BPA-PC is thus too small on its own to account for the difference seen.

4.9.2 Loss of Dopant

During the poling of these samples some loss of guest molecules occurred. The loss was due to the evaporation of guest molecules from the host polymer at elevated temperatures. Since this reduces the number density of guest NLO molecules, the EO response of the system is consequently reduced. The amount of the loss was quantified through the absorption spectrum of these two DAN doped polymers. The absorption spectrum between 300 - 500 nm of DAN/BPA-PC and DAN/PMMA films were taken by a Perkin Elmer UV/VIS/NIR Lambda 19 spectrometer. In 20% DAN doped BPA-PC and PMMA samples a loss of dopant was seen both during drying and poling of the thin films. Figures 4.17 and 4.18 show the absorption spectra of these two samples before and after drying.

During 1 hour drying of the films at 110 °C under vacuum, 46% of the dopant molecules were lost from DAN/PMMA and 15% dopant were lost from DAN/BPA-PC. The higher T_g of DAN/BPA-PC films could possibly account for the lower loss of dopant.

In order to quantify the loss which occurs during poling, two separate samples were taken. One of them was poled and the other one used as a control. Both samples were treated under the same conditions (temperature and time, 15 minutes). Figures 4.19-4.20 show the absorption spectra of 20% DAN doped BPA-PC and PMMA samples. In DAN/BPA-PC the absorption was constant up to 90 °C. Above this temperature it started to decrease. At 110 °C the absorption decreased to 92% and at 135 °C it decreased to 51% and finally at 150 °C, it decreased to 32%, of its initial value. The absorption decrease in the DAN/PMMA sample is larger than in DAN/BPA-PC. The absorption decrease started at comparatively lower temperatures in DAN/PMMA. At 60 °C the absorption decreased to 88% and at 110 °C it decreased to 25% of its initial value.

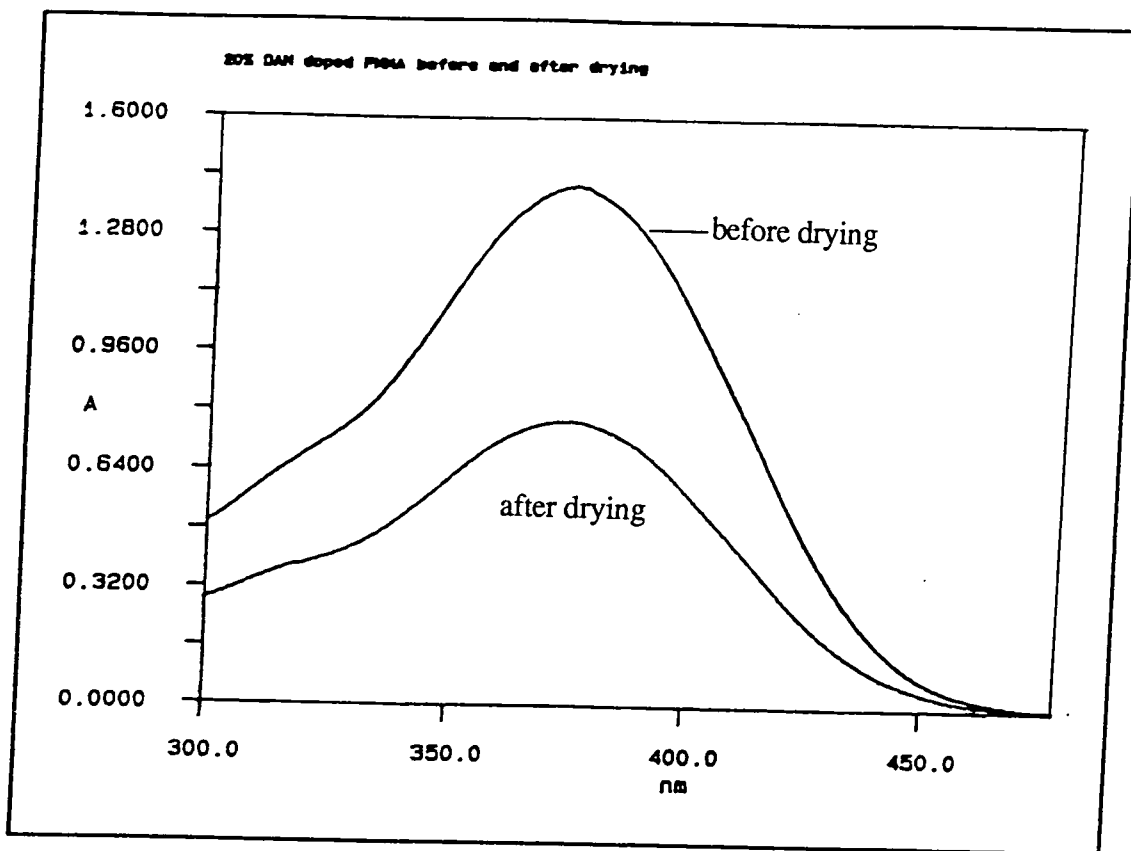


Figure 4.17: Absorption spectrum of 20% DAN/PMMA films (before and after drying)

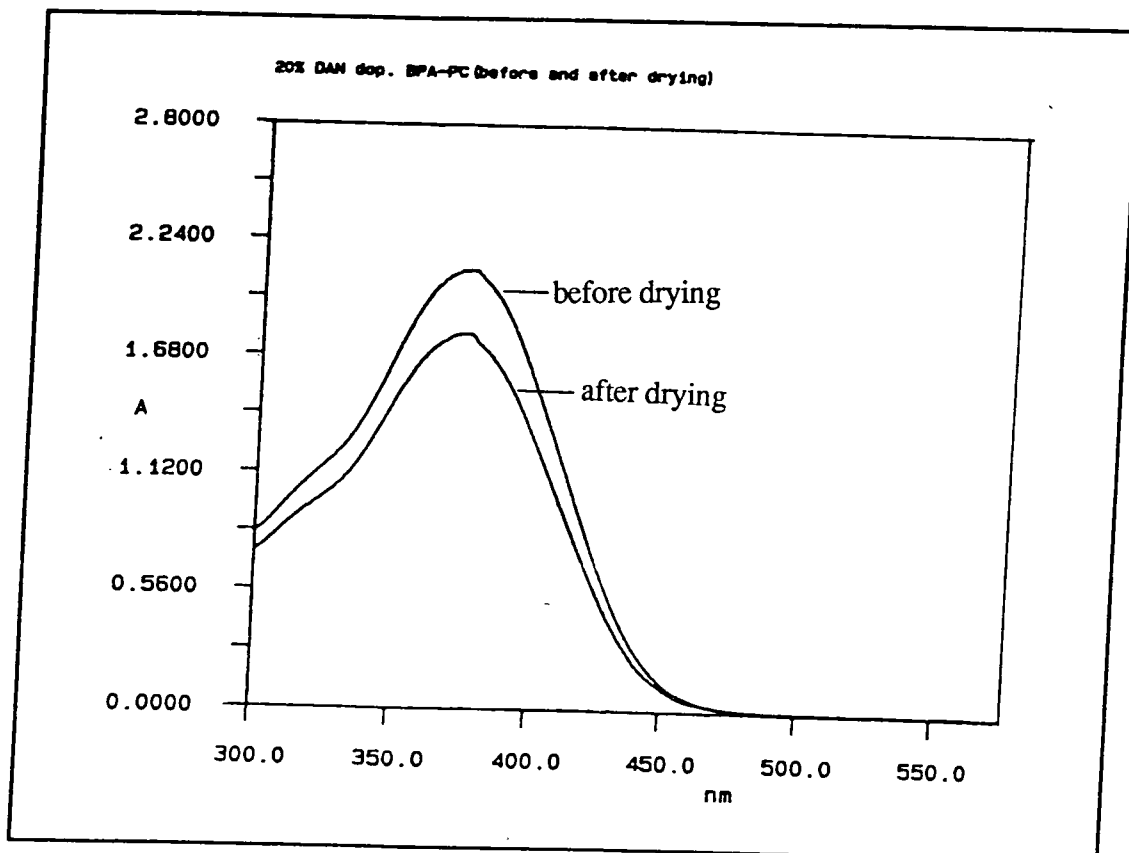


Figure 4.18: Absorption spectrum of 20% DAN/BPA-PC films (before and after drying)

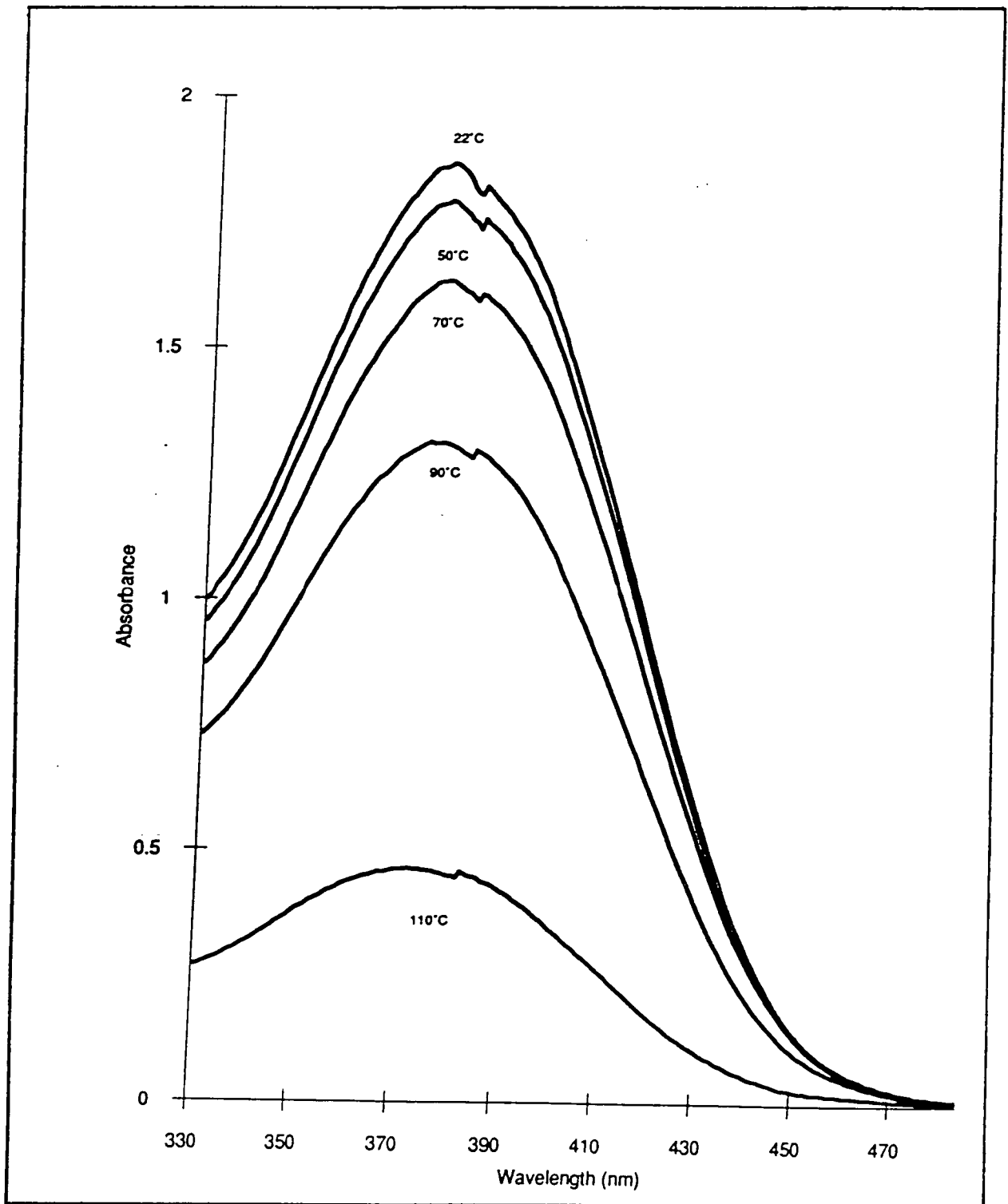


Figure 4.19: Absorption spectrum of 20% DAN/PMMA film at different temperatures

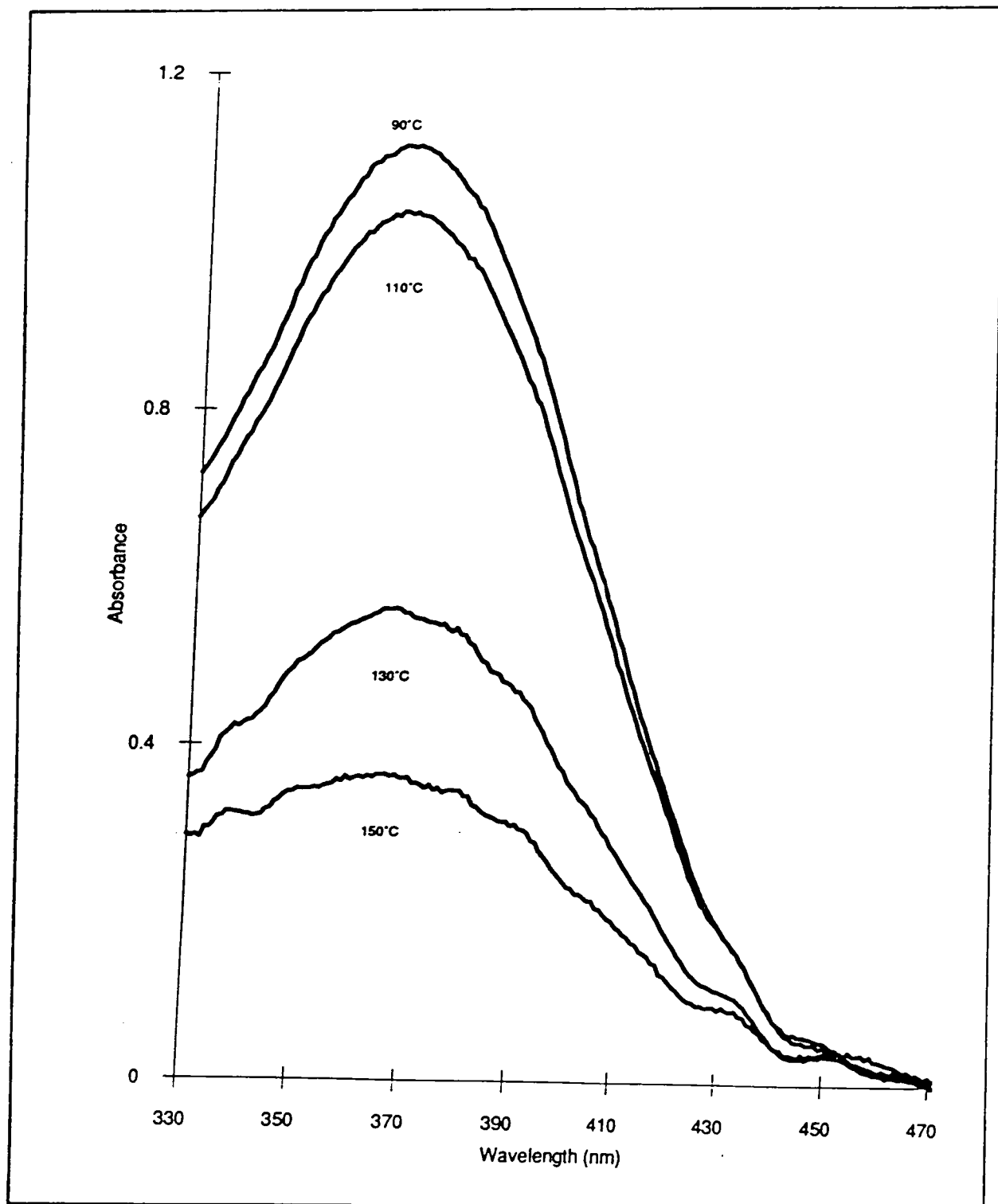


Figure 4.20: Absorption spectrum of 20% DAN/BPA-PC film at different temperatures

The absorption of doped polymer is related to the number density of NLO molecules as shown below;

$$I_t = I_0 e^{-\sigma NL} \quad 4.2$$

where I_t is the transmitted intensity, I_0 is the incident intensity, σ is the absorption cross section of the dopant (cm^2), N is the number density of NLO molecules (cm^{-3}), and L is the thickness of the sample.

Taking logs, equation 4.3 becomes;

$$\ln\left(\frac{I_t}{I_0}\right) = -\sigma NL \quad 4.3$$

where $\ln\left(\frac{I_t}{I_0}\right)$ is the absorbance.

From the above equation it can be seen that the absorbance is directly proportional to the number density of doped NLO molecules.

The effect of losing DAN guest molecules on the EO response can be clearly seen in the following two different 20% DAN/PMMA samples. The sample preparation differs between these two samples. The first sample was dried quickly (for 1 hour at 110 °C under vacuum) and the second one was dried slowly (at 40 °C for 16 hours, at 60 °C for 30 minutes and at 90 °C for 1 hour). These temperatures and times were chosen arbitrarily with the intention of slowing the drying rate. The poling of these two samples was carried out at various temperatures. Poling field was $50 \text{ V}\mu\text{m}^{-1}$ for both samples. Poling time was 15 minutes in the first case and 5 minutes in the second. The r_{33} vs. poling temperature relationship of these samples is shown in figure 4.21.

As may be seen in figure 4.21 the EO response in the quickly dried sample is much smaller than found in the slowly dried sample. The reason behind this difference is the dopant loss. In the quickly dried sample a 46% loss of guest molecules occurred during the drying process (figure 4.17). In addition, further losses of guest molecules occurred

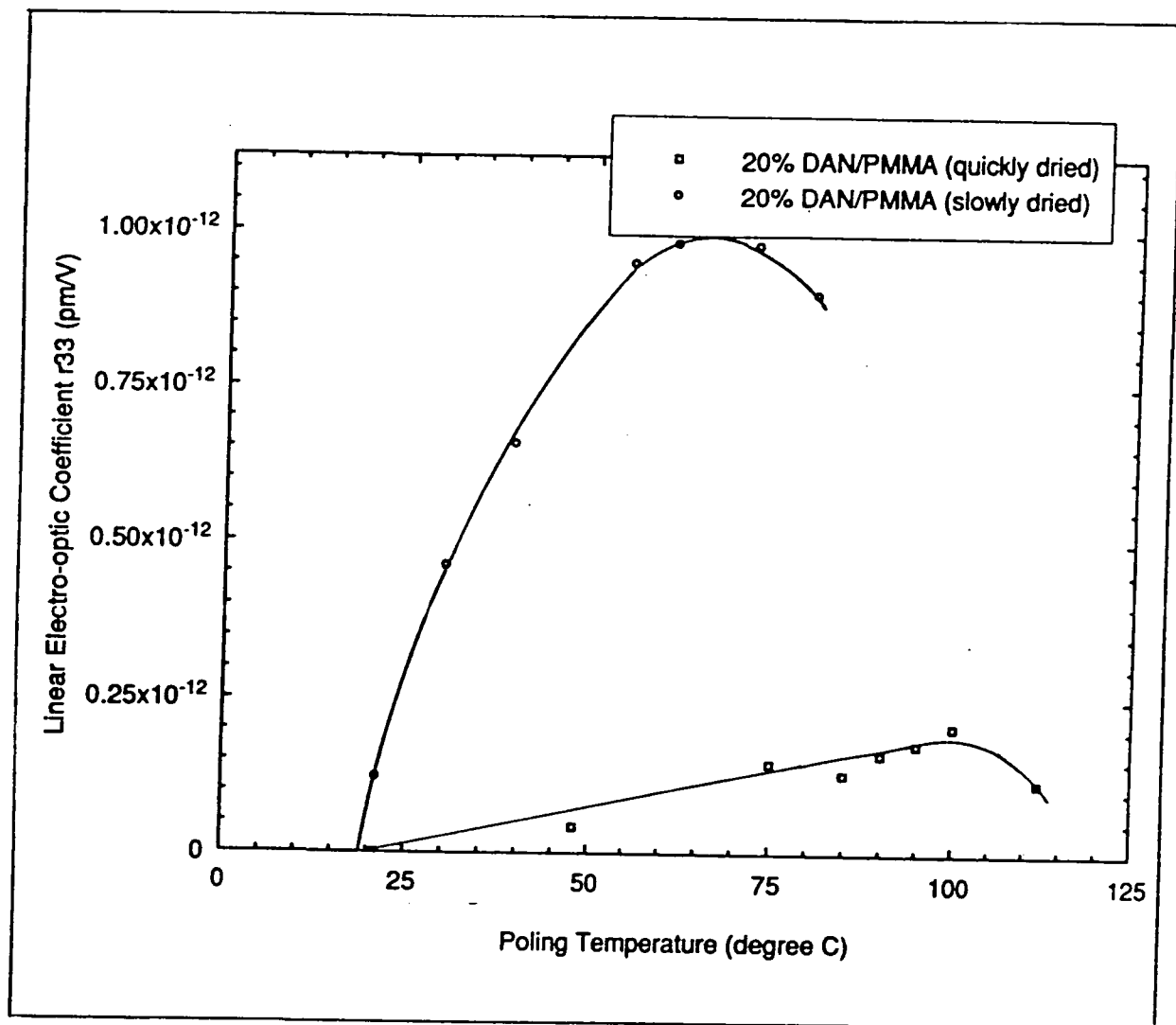


Figure 4.21: r_{33} vs. poling temperature for two different 20% DAN doped PMMA samples

during the poling of this sample (figure 4.19). By contrast, the loss of guest molecules in the slowly dried sample was negligible. Figure 4.21 also shows that the maximum EO response occurs around 60 °C (which is close to T_g of this material) whereas the T_g of the quickly dried sample shifted towards 100 °C (the T_g of PMMA). This proves that most of the guest molecules were lost in this case.

4.9.3 Guest-host Interaction

It is of interest to compare the poling characteristics of BPA-PC when doped with both NMBA and DAN. A summary of the poling conditions and measured EO responses (at 633 nm) is shown in table 4.5.

Material	N 10^{20} cm^{-3}	E_n $\text{V}\mu\text{m}^{-1}$	T_n °C	r_{33} 10^{-12} mV^{-1}	r_{33} (theory) 10^{-12} mV^{-1}
NMBA/BPA-PC	5.3	27	82	0.16 ± 0.07	0.19
DAN/BPA-PC	6.0	27	82	1.12 ± 0.1	0.11

Table 4.5: Poling conditions and the measured EO responses of NMBA and DAN doped BPA-PC thin films [12]

In the case of NMBA/BPA-PC the theoretical r_{33} is close to the experimental r_{33} . This shows that the theoretical gas model is realistic in this case. The small difference ($\pm 0.03 \text{ pmV}^{-1}$) between theoretical and experimental r_{33} may be due to the 15% dopant loss which occurs during drying of the film. The theoretical r_{33} of NMBA/BPA-PC is twice that of the theoretical r_{33} of DAN/BPA-PC. Despite this difference the experimental r_{33} of DAN/BPA-PC is seven times higher than that of NMBA/BPA-PC. In addition the experimental r_{33} of DAN/BPA-PC is about ten times higher than the theoretical r_{33} .

The difference in the degree of alignment between DAN and NMBA doped BPA-PC measured directly through the EO response, and the large difference between the theoretical and experimental EO coefficient of DAN doped BPA-PC, are both indications

of a guest-host interaction between DAN guest molecules and BPA-PC host polymer. A number of other facts indirectly indicate this interaction. No phase segregation occurs at 20% w/w loading of DAN and the DAN content of films remains stable during drying and poling at the temperatures up to 80-100 °C.

4.10 Poling Stability

Further evidence of a guest-host interaction is obtained from a comparison of thermal relaxation between the two materials. The short and the long term stability of fixed electrode poled DAN and NMBA doped BPA-PC and PMMA samples was thus carried out. Figures 4.22 and 4.23 show the relaxation of the EO coefficient of DAN/BPA-PC compared to DAN/PMMA, NMBA/PMMA and NMBA/BPA-PC, respectively. The short term relaxation of DAN/BPA-PC shows that after 30 hours only 9% relaxation occurs. Over six weeks the EO response relaxed by only 25%. This long term stability is unexpectedly good for a guest-host system. Typical guest-host systems return to an isotropic state within a few days at room temperature. In DAN/PMMA the EO response relaxed to 25% of its initial value in 24 hours. In the case of NMBA/BPA-PC a very sharp relaxation was seen in the 10-15 minutes following poling. After this initial relaxation the EO coefficient decreased to the level of undoped BPA-PC. It is thus assumed that more or less all the guest NMBA molecules are relaxed over a few minutes.

The long term stability must be associated with the characteristics of the host material. The rapid initial relaxation in NMBA/BPA-PC is very similar to that seen in films of DAN/PMMA and NMBA/PMMA whose EO coefficient rapidly falls within a few hours. In very long term studies it has been found that DAN/BPA-PC stored at room temperature retains an EO response 70% of its original value after nine months. This extended lifetime of the polar orientation is comparable to that obtained in studies of the annealing of either guest-host [22] or side-chain polymers [Chapter 2 ref. 31], and yet no annealing is included in this work. Presumably annealing will further stabilise the polar

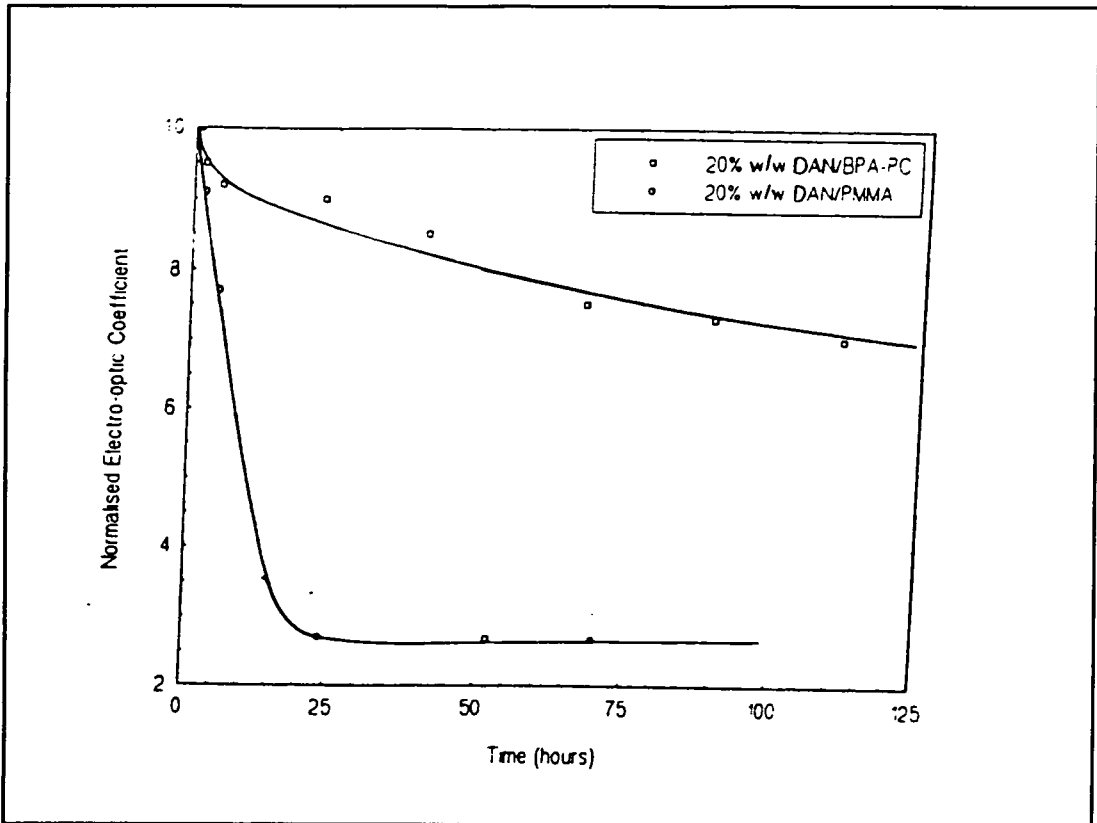


Figure 4.22: Normalised EO coefficient (r_{33}) vs. time for poled 20% DAN doped PMMA and BPA-PC samples

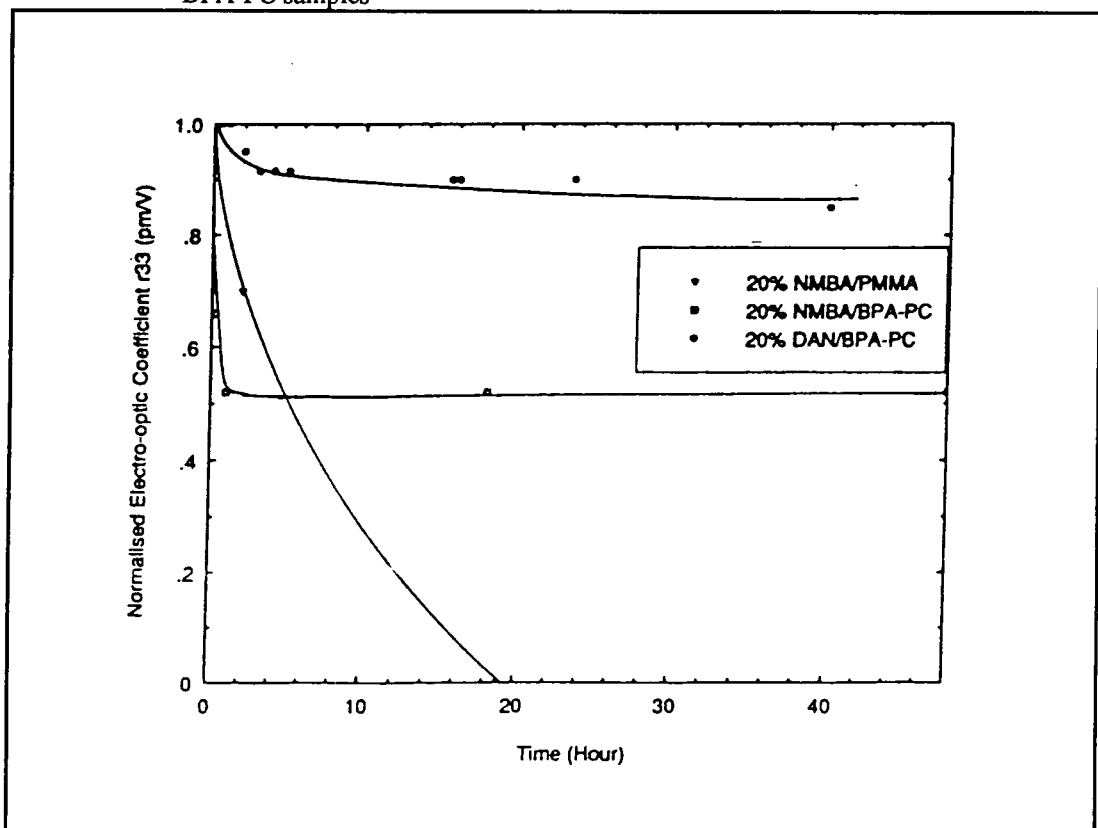


Figure 4.23: Normalised r_{33} of poled 20% DAN/BPA-PC, NMBA/PMMA and NMBA/BPA-PC films

order. In figure 4.24 a KWW plot of this guest-host system is shown in comparison with a side-chain polymer which has been annealed to minimise the free volume [chapter 2 ref. 31]. The decay rates are seen to be comparable. This is surprising since BPA-PC has a large free volume radius [23] which is increased by the addition of the DAN as evidenced by the decrease in T_g . This is then further strong evidence for a cooperative interaction.

4.11 Hydrogen Bonding in DAN/BPA-PC Films

This strikingly different behaviour between the two polycarbonate doped systems may be attributed to hydrogen bonding interactions. Hydrogen bonding must be very weak in the case of NMBA-doped polymer since there are no strongly acidic protons in the dopant. This is clearly not the case in DAN where there is a hydrogen atom on the acetanilide group and the attachment to the adjacent phenyl ring should make the proton highly electro-positive. Hydrogen bonds may be formed to the carbonyl groups on the polycarbonate chain and perhaps also to carbonyls between DAN molecules themselves. Hydrogen bonding and a consequent cooperative dipole re-orientation on poling may account for the enhanced stability in DAN/BPA-PC films. Kumar et al. [24] have shown that at around 150 °C in certain ferroelectric liquid crystal polymers hydrogen bonds break down. This may explain the dramatic loss of DAN molecules around 130 °C in 20% DAN/BPA-PC film (figure 4.20). By contrast in 20% DAN/PMMA films the loss of guest molecules starts at very low temperature (40 °C). This suggests that hydrogen bonding in DAN/PMMA is either very weak or unfavourable. Further evidence for hydrogen bonding in DAN/BPA-PC films was found in infra red studies (figure 4.25). The broad resonance at 3350 cm^{-1} is not evident in the spectra of the isolated constituents. Such a hydrogen bonding system is at least hinted at in previous studies. Boyd et al. [Chapter 2 ref.14] have reported the possible mechanism of a

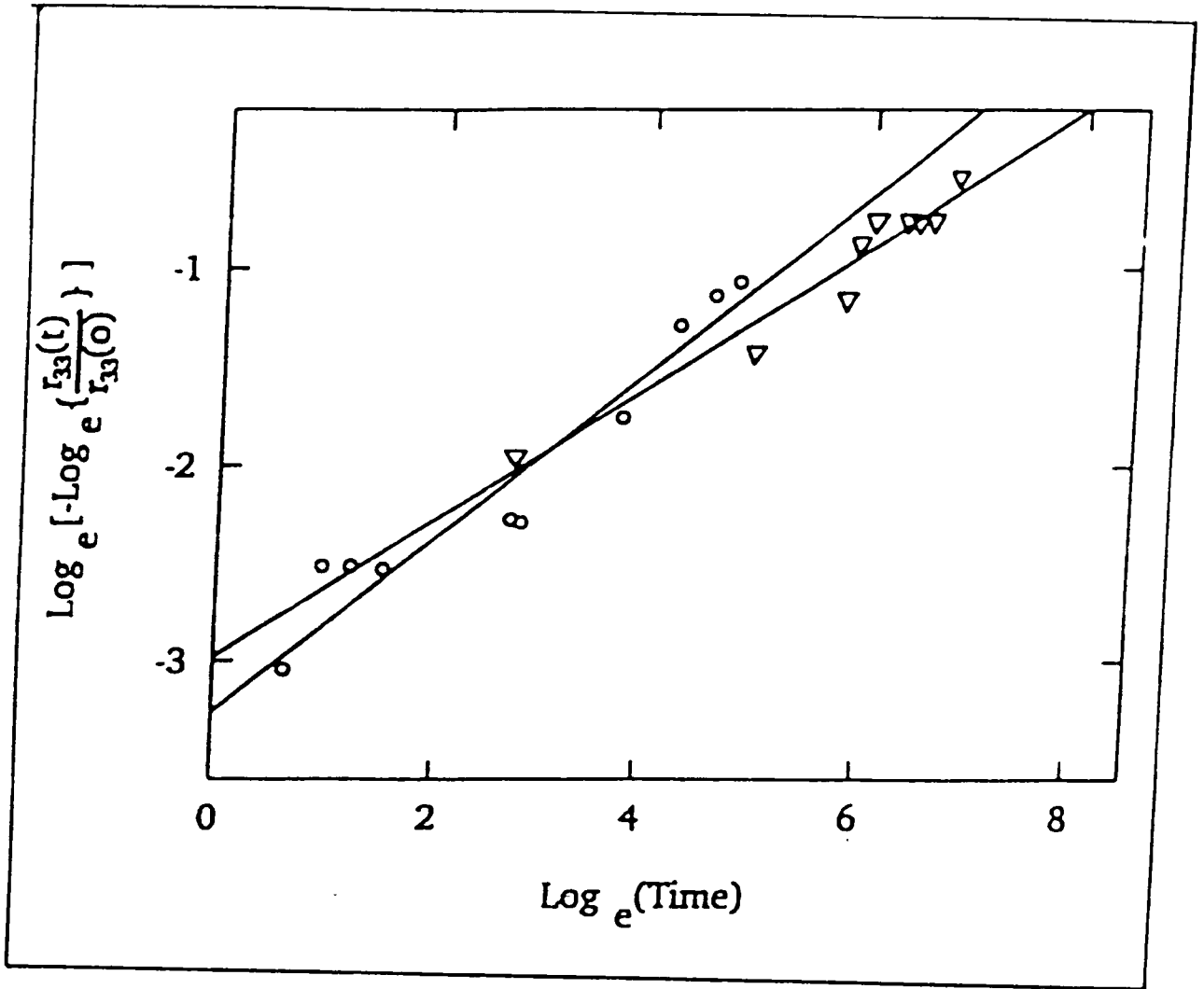


Figure 4.24: KWW plot of 20% DAN/BPA-PC (circles) and an annealed side-chain polymer (triangles, [Chapter 2 ref. 31])

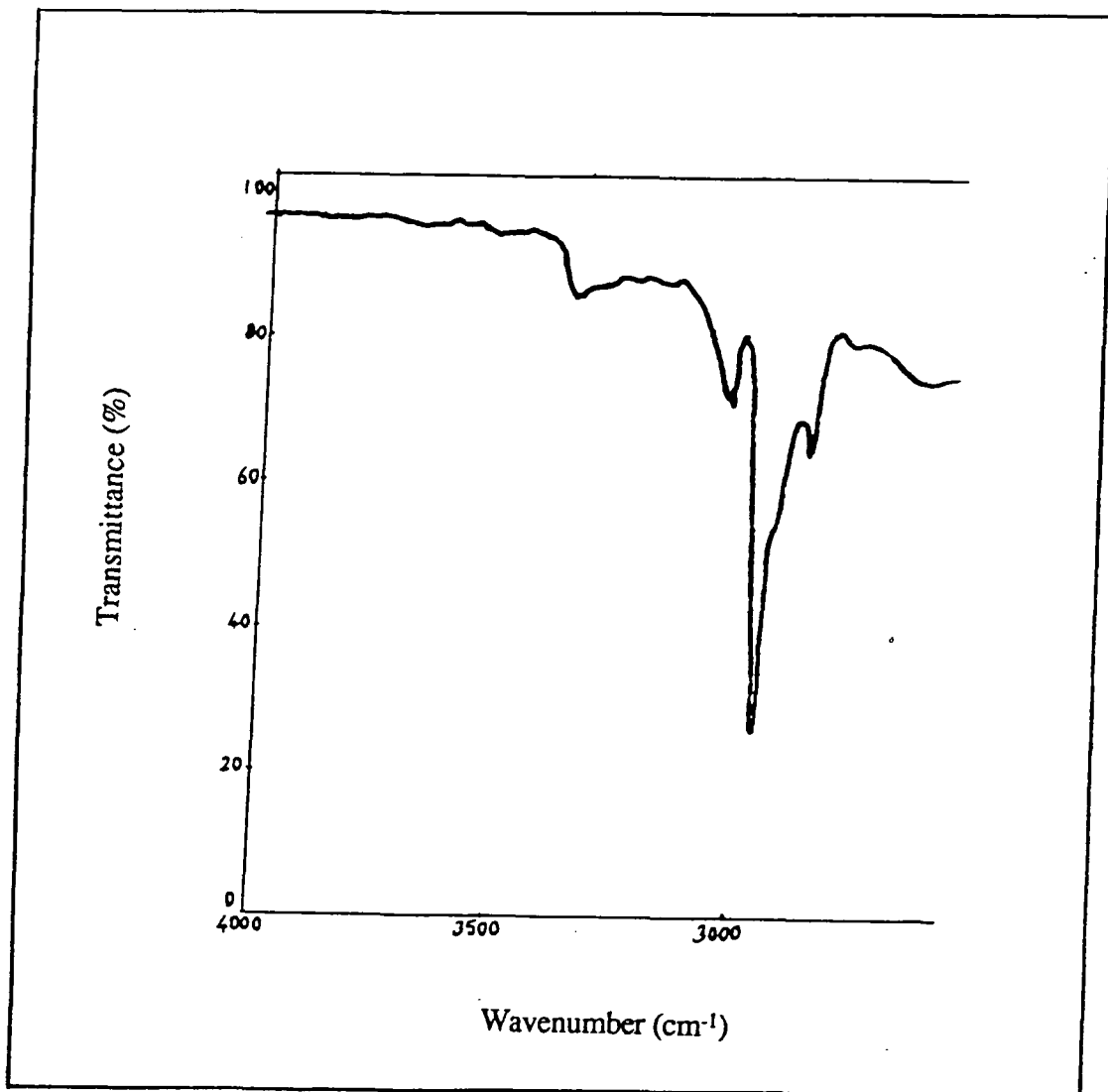


Figure 4.25: Infrared spectrum of a 20% (w/w) DAN/BPA-PC thin film

hydrogen bond fixing DR1 at one end in BPA-PC. The hydrogen bonding occurs between the hydroxyl group in DR1 and carbonate group in BPA-PC.

4.12 Second Harmonic Generation Measurements

There is often an assumption made that the high frequency non-linearity of organic materials is of the same magnitude as that at low frequency. To test the validity of this, SHG measurements were compared with EO measurements.

A 5 μm DAN/BPA-PC sample was corona poled using a -5 kV needle potential at a poling temperature of 80 °C for 30 minutes. The measured poling current was less than 1×10^{-7} amp. Immediately after poling the normalised second harmonic intensity in transmission through the film was measured. Figure 4.26 shows the normalised SH intensity of p- polarised fundamental and second harmonic light versus θ . The normalised SH intensity is zero at 0 degree. For p-polarised input fields, at normal incidence the direction of non-linear polarisation, is orthogonal to the field vector. Thus no SHG is possible. The maximum is reached at a position at which the increasingly favourable interaction between the fields and d_{eff} , the effective second harmonic coefficient, is cancelled by the increase in reflectance. Seven days after poling, the measured SHG coefficient, d_{33} , was 2.25 pmV^{-1} and the calculated r_{33} using Equation 4.1 was thus 1.43 pmV^{-1} . Immediately after the SHG measurements on this sample, a silver electrode was evaporated on the poled film, and the EO coefficient was measured using the reflection technique. The measured r_{33} was found to be 1.24 pmV^{-1} . This value is in excellent agreement with the SHG result, particularly if it is considered that the pump and probe wavelengths differ between the experiments.

It has been shown that at low frequencies the molecular reorientation can contribute strongly to the observed EO response [25]. Such effects could not be involved in second harmonic generation at optical frequencies. It is shown here that in DAN/BPA-PC sample this is not the case. The measured EO response at higher

(optical) frequency and at lower frequency (1.8 kHz.) are very close to one another. This indicates that the non-linearities are electronic in origin, and justifies the use of equation 4.11.

Nine months after this measurement, the measured EO response was 1.12 pmV^{-1} . Hence over nine months only a further 10% relaxation occurred in the EO response of the poled DAN/BPA-PC sample. This incredibly high stability is due to the hydrogen bonding as mentioned above. This sort of long term stability -which is as good as poled and cross linked polymers- may satisfy the needs for EO device applications. It would, however, be advantages to have higher T_g and non-linearity.

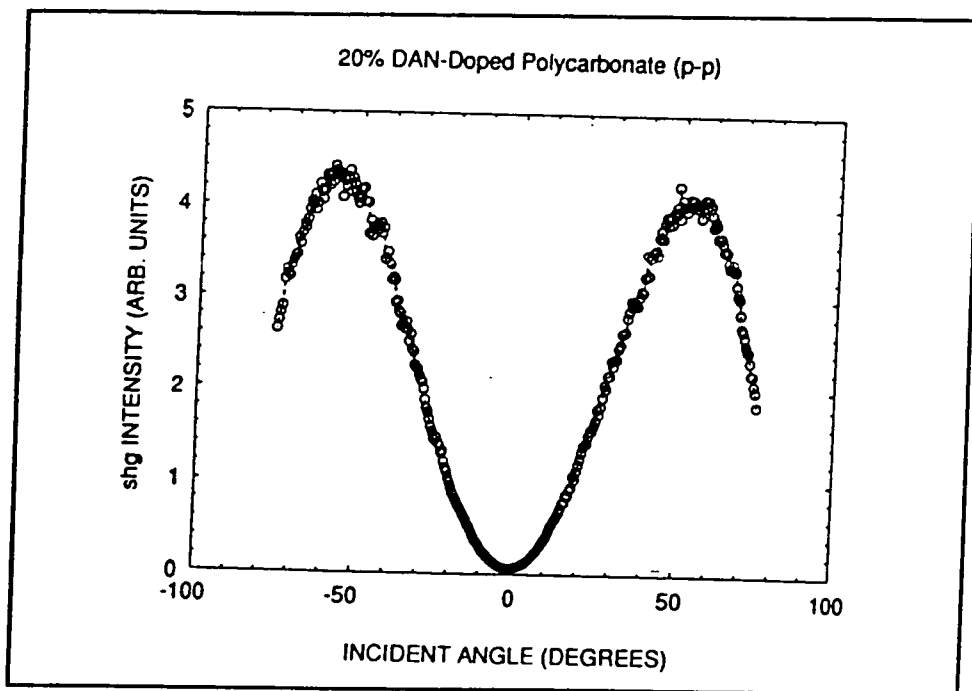


Figure 4.26: The normalised SH intensity of p-polarised fundamental and second harmonic light versus θ

4.13 Conclusions

Poling of DAN and NMBA doped BPA-PC and PMMA samples was carried out at various poling conditions, in order to find the optimum poling conditions. The highest polar order was achieved at $80 \text{ }^\circ\text{C}$ in 20% DAN/BPA-PC and at $55 \text{ }^\circ\text{C}$ in 20%

DAN/PMMA films. These temperatures are the glass transition temperatures of these samples after doping. The T_g of host polymers is depressed by 55 °C in 20% (w/w) DAN/BPA-PC and 45 °C in 20% (w/w) DAN/PMMA due to plasticizing effect. The poling field was limited to approximately 70 V μm^{-1} in DAN/BPA-PC and DAN/PMMA, due to electrical breakdown. Loss of guest molecules was observed around the T_g . The amount of loss is strongly dependent on temperature and time.

A guest-host interaction occurs in DAN/BPA-PC. This interaction is likely to be hydrogen bonding between the acetanilide group in DAN and the carbonyl group in BPA-PC. An enhancement of one order of magnitude occurs in the experimental electro-optic coefficient of 20% DAN/BPA-PC with respect to theoretical value. This enhancement may be due to the hydrogen bonding interaction. The thermal stability of DAN/BPA-PC sample is unexpectedly good for a guest-host system. Over nine months, only 30-40% relaxation occurred in a corona poled DAN/BPA-PC sample, while a complete relaxation occurred in the other examined guest-host systems within a few hours or days. The thermal stability of the DAN/BPA-PC system is comparable to poled and annealed side-chain systems and cross-linked materials.

4.14 References

- 1- Oudar, J.L., J. Chem. Phys. **67**, (1979), 446
- 2- R.J.Tweig and K.Jain in Non-linear Optical Properties of Organic and Polymeric Materials, edited by D.J.Williams (American Chemical Society, Washington,DC, 1983), ASC Symp. Ser. 233, 57.
- 3- Hutson J., private communication
- 4- Gray D., private communication
- 5- Uemiya T., N. Uenishi and S. Umegaki, J. Appl. Phys., **73**, (1993), 12-15
- 6- Kerkoc P., M. Zgonik, K. Sutter, C.H. Bosshard, P. Gunter, Appl. Phys. Lett., **54**, (1989), 2062-2064
- 7- Norman P.A., D. Bloor, J.S. Obhi, S.A. Karaulov, M.B. Hursthouse, P.V.

- Kolinsky, P.J. Jones and S.R. Hall, *J. Opt. Soc. Am. B*, **4**, (1987), 1013-1016
- 8- Kolinsky P.V., R.T. Bailey, F.R. Cruickshank, D. Pugh, J.N. Sherwood, G.S. Simpson and K.B.R. Varna, *J. Appl. Phys.*, **71**, (1992), in press
- 9- Cross, G.H., Oldroyd, A.R. and Worboys, M.R., *Opt. Comm.*, **74**, (1989), 425-429
- 10- Bailey R.T., F.R. Cruickshank, P.J. Halfpenny, D. Pugh, J.N. Sherwood and G.S. Simpson, Molecular crystals in "Principles and Applications of Nonlinear Optical Materials", Munn R.W. and C.N. Ironside, Eds., (1993), Glasgow, U.K., p. 169
- 11- Polymer Handbook, 3rd edition, Eds. J. Brandrup and E.H. Immergut, Wiley Inter-science, 1989.
- 12- Karakus Y., D. Bloor, G.H. Cross, *J. Phys. D: Appl. Phys.*, **25**, (1992), 1014-1018
- 13- Sachio Yasufuku, *IEEE, Electrical Insulation*, **8**, (1992), 7-15
- 14- Freitag D., G. Frengler, and L. Morbitzer, *Angew. Chem. Ed. Engl.*, **30**, (1991), 1598-1610
- 15- Illers K.H., H. Breuer, *Kolloid-Z.*, **176**, (1961), 110
- 16- Reading F.P., J.A. Faucher, R.D. Whitman, *J. Polym. Sci.*, **54**, (1961), 556
- 17- Yee A.F. and S.A. Smith, *Macromolecules*, **14**, (1981), 54-64
- 18- Kohler, Wener, D.R. Robello, P.T. Dao, C. S. Willand and D.J. Williams, *J. Chem. Phys.*, **93**, (1990), 9157-9166
- 19- Singer K.D., T.C. Kowalczyk, P.A. Cahill, and L.A. King, *Mol. Cryst. Liq. Cryst. Sci. Technol -sec. B: Non-linear Optics.*, **3**, (1992), 3-12
- 20- Kobayashi T., K. Minushima, S. Nomura, S. Fukaya, and A. Ueki, *Proc. SPIE*, **1147**, (1989)
- 21- Gulloty R.J., Langhoff C.A. and Bales S.E., *Proc. SPIE*, **1337**, (1990), 258-270
- 22- Hayden L.M., G.F. Sauter, F.R. Ore, P.L. Pasillas, J. M. Hoover, G.A. Lindsay and R.A. Henry, *J. Appl. Phys.* **68**, (1990), 456-465
- 23- Malhotra B.D. and R.A. Pethrick, *Eur. Polym. J.*, **19**, (1983), 457
- 24- Kumar U., J.M.J. Frechet, T. Kato, S. Ujiie, and K. Timura, *Angew. Chem. Int. Engl.*, **31**, (1992), 1531-1533
- 25- Knable G., H. Franke and W. F. X. Frank, *J. Opt. Soc. Amer. B*, **6**, (1989), 761

5.1 Introduction

Previous studies have shown that side-chain polymers are candidate organic materials for commercial devices due to the high second order non-linearity and the long term thermal stability [1-6]. High non-linearity in side-chain type polymers is due to the high concentration of NLO chromophores, and also to the high $\mu\beta$ of the NLO side-chains.

Ye and coworkers reported functionalised NLO polymers in reference [1]. They functionalised poly (p-hydroxystyrene) to varying levels with DR1 and hemicyanine. Poling of these materials at $30 \text{ V}\mu\text{m}^{-1}$ gave a d_{33} of $1.1 \times 10^{-12} \text{ mV}^{-1}$ and $0.4 \times 10^{-12} \text{ mV}^{-1}$ (at $1.064 \mu\text{m}$) respectively. Although the $\mu\beta$ of these two materials are about the same, the SHG efficiency in the first sample is twice as high. This difference is attributed to the ionic nature of the second material. Ye et al. [Chapter 2 ref. 27] used the same (PS) backbone for different NLO chromophores {(PS)CH₂-DR (DR, 2-[4-[(4-nitrophenyl)azo]-N ethylanilino]ethoxy)), (PS)CH₂-DASP (DASP, 4-(4-(dimethylamino)styryl) pyridinium iodide)} and (PS)O-NPP. They obtained a d_{33} of $1.1 \times 10^{-12} - 7.5 \times 10^{-12} \text{ mV}^{-1}$ (at $1.064 \mu\text{m}$), for poling fields of $30\text{-}160 \text{ V}\mu\text{m}^{-1}$. A 30% relaxation in the SHG response of poled and annealed (PS)O-NPP (NPP N-(nitrophenyl)-L-prolinyl) films at room temperature in 33 days was found. Dai et al. [Chapter 2 ref. 28] reported higher SHG efficiency ($d_{33} = 27.2 \times 10^{-12} \text{ mV}^{-1}$, at $1.064 \mu\text{m}$) in their functionalised PPO-(NPP)_x (PPO poly(2,6-dimethyl-1,4-phenylene oxide). The glass transition temperature, T_g , of this polymer is around $173 \text{ }^\circ\text{C}$. Dai and his coworkers have also reported that stability of samples poled with contact poling is twice as high than with corona poled samples.

Copolymers with methyl methacrylate or side-chain substituted methacrylates containing dyes have been reported [4-10]. Chen et al. [2] reported a copolymer of methylmethacrylate and 4-[4-(-methylacryloxy)octyloxy 2 methylphenyliminomethyl] cyanobenzene, (copolymer 1), with a T_g of $89 \text{ }^\circ\text{C}$. Despite the low concentration of

NLO chromophores (10% weight/volume), the corona poled copolymer **1** gave a d_{33} of 3×10^{-12} mV⁻¹. Another (similar type) of polymer was reported by Sohn et al. [3] with a high second order coefficient $d_{33} = 7.4 \times 10^{-8}$ esu (31×10^{-12} mV⁻¹). Haas et al. [4] fabricated an EO waveguide device using methacrylic chain polymers with NLO chromophores attached as side-chains through variable length spacer groups. Poling of this side-chain material (for $200 \text{ V}\mu\text{m}^{-1}$ at the T_g of the polymer) gave an EO coefficient r_{33} of 98 pmV^{-1} (at 632.8 nm). This apparently large value results partly from resonance enhancement and partly from a factor of π missing in the equation they used to calculate the EO coefficient. Larger second harmonic d coefficients and high thermal stability of poling induced alignment were reported [5,Chapter 2 ref. 33]. Hill et al. [5] reported a stable high SHG coefficient (55×10^{-12} mV⁻¹) in poled poly(4-(4-nitrophenylazo)-N,N-methyl-ethyl-acrylesters).

Shuto et al. [6] reported the largest $\chi^{(2)}$ value of 419.1×10^{-12} mV⁻¹ ever observed for poled polymer systems on corona poled thin films of a methacrylate polymer containing a dicyanovinyl-terminated, dimethyl-substituted diazo dye. The thermal stability of this poled side-chain polymer is excellent even at 80 °C. At 80 °C only 20-25% relaxation in the initial value of the EO coefficient occurred within 150 days.

Many authors suggest that the exact form of the decay function obeys a bi-exponential curve [1,2]. The general characteristic of the relaxation function seen in these reports is that of a fast initial relaxation which occurs in a short time (a few minutes) and a slow relaxation over a long period (months). Man and Yoon [Chapter 2 ref. 31] attempted to improve the thermal stability of poled side-chain polymers through design of the molecular structure and adjustment of the T_g . They have shown in P2ANS/BMA (25/75 and 50/50) and P2ANS/MMA 25/75 copolymers (with T_g s of 68, 93 and 112 °C, respectively) that the long term relaxation slows with the increase in T_g . At 60 °C the SHG response relaxed over 2×10^4 minutes, to, respectively, 80% and 40% of its initial value in the case of T_g s of 112 °C and 93 °C. For the first material complete relaxation occurred in the SHG response over a few minutes. Man and Yoon also show that in the

case of annealed samples the short term thermal stability of the SHG response is increased compared to quenched samples.

In this chapter electrical poling studies of two side-chain polymers are presented. First, a commercially available polymer, poly 4-vinylpyridine, P-4VP, was studied for the first time. Second, a homopolymer, MO3ONS was studied for its poling and EO properties and compared to P-4VP. Figure 5.1 shows the structural formulae of these side-chain polymers.

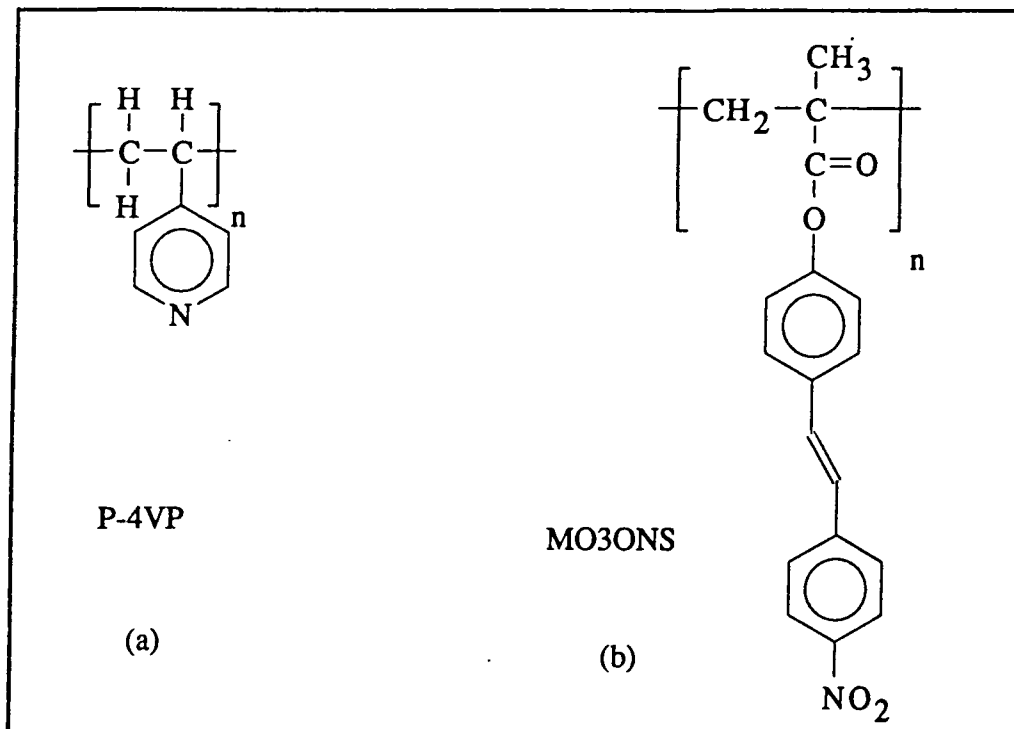


Figure 5.1: The structural formulae of the side-chain polymers, (a) P-4VP, and (b) MO3ONS

In P-4VP the polar pyridine group is directly bonded to the backbone by a single C-C bond. This cannot allow reorientations of the side groups which are independent of the backbone and any alignment must therefore involve rotations around the C-C bonds on the chain.

Pyridine has a similar structure to benzene (figure 5.1), but one of the CH groups of benzene has been replaced by a nitrogen atom. Pyridine is basic due to having a 'lone pair' of electrons and forms salts with acids. Like benzene, pyridine is aromatic. It is a

flat molecule with bond angles 120 degree and with carbon-carbon bond lengths of 1.39 Å. Each of five carbon atoms contributes one π electron to complete the aromatic sextet [8,9].

MO3ONS is a homopolymer of 4-(3-methacryloyloxypropoxy)-4'-nitrostilbene monomer where the oxynitrostilbene side group is attached to the backbone by a short, $(\text{CH}_2)_3$, aliphatic linkage (see Figure 5.1). This side-chain polymer was supplied by Hoechst-Celanese Research Division, Summit, N.J. USA.

5.2 Sample preparation and Characterisation

3 g. of P-4VP was dissolved in 20 ml of isopropyl alcohol, IPA, (which corresponds to a weight to weight proportion of 18%). The solutions were filtered through 3 μm pore size Millipore filters. A thin film of this polymer was prepared when an ITO coated glass slide was withdrawn (with a 20 mm minute^{-1} speed) from the solution. The sample was dried at 90 °C under vacuum for 24 hours. The thickness measured by a Tencor surface profiler was 2 μm . The refractive index of P-4VP was given [10] as 1.568 (at 632.8 nm). The relative permittivity of P-4VP was measured at room temperature and at the poling temperature (122 °C) and found to be $\epsilon_{\text{R.T.}} = 2.7$ and $\epsilon_{\text{Tp}} = 2.45$ respectively. Figure 5.2 shows the absorption spectrum of P-4VP. This material has an excellent transmission in the visible region. The glass transition temperature of P-4VP was found through differential scanning calorimetry (for a heating rate of 10 °C minute^{-1}) and was 145 °C (see figure 5.3).

A 20% w/w solution of MO3ONS in cyclohexanone was prepared and filtered. Thin films of MO3ONS were prepared by spin coating. For 1300 rpm 2 μm thick films were achieved. The samples were dried at 110 °C under vacuum for 2 hours. The measured refractive index by prism coupling was 1.600 at 632.8 nm. This material shows a strong absorption peak at 400 nm (figure 5.4).

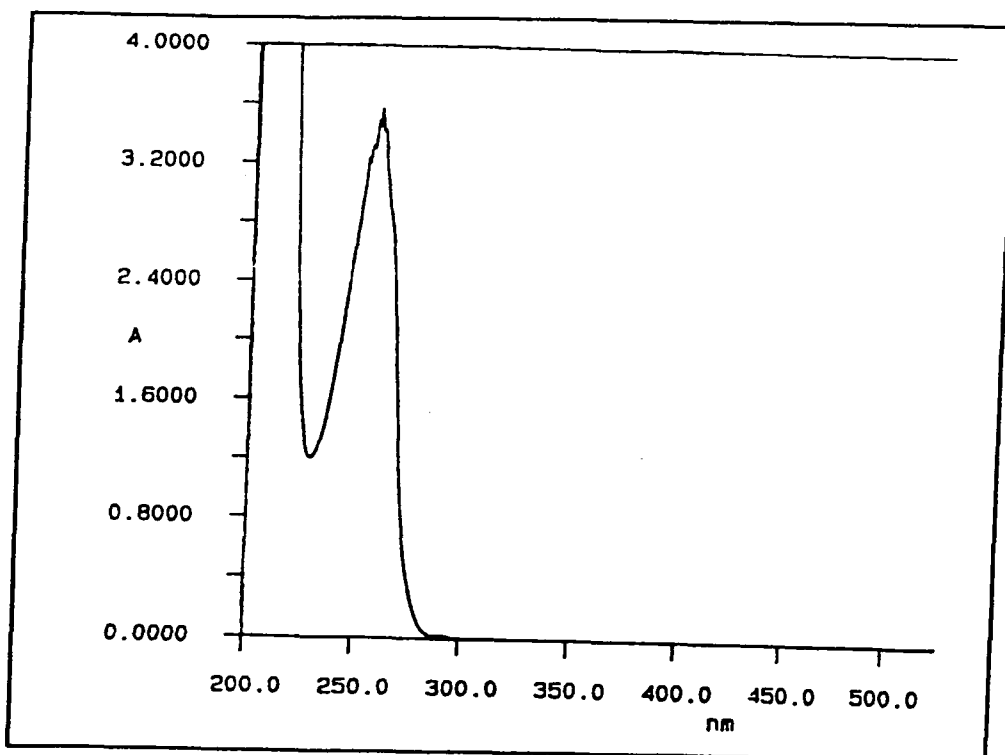


Figure 5.2: The absorption spectrum of P-4VP thin film

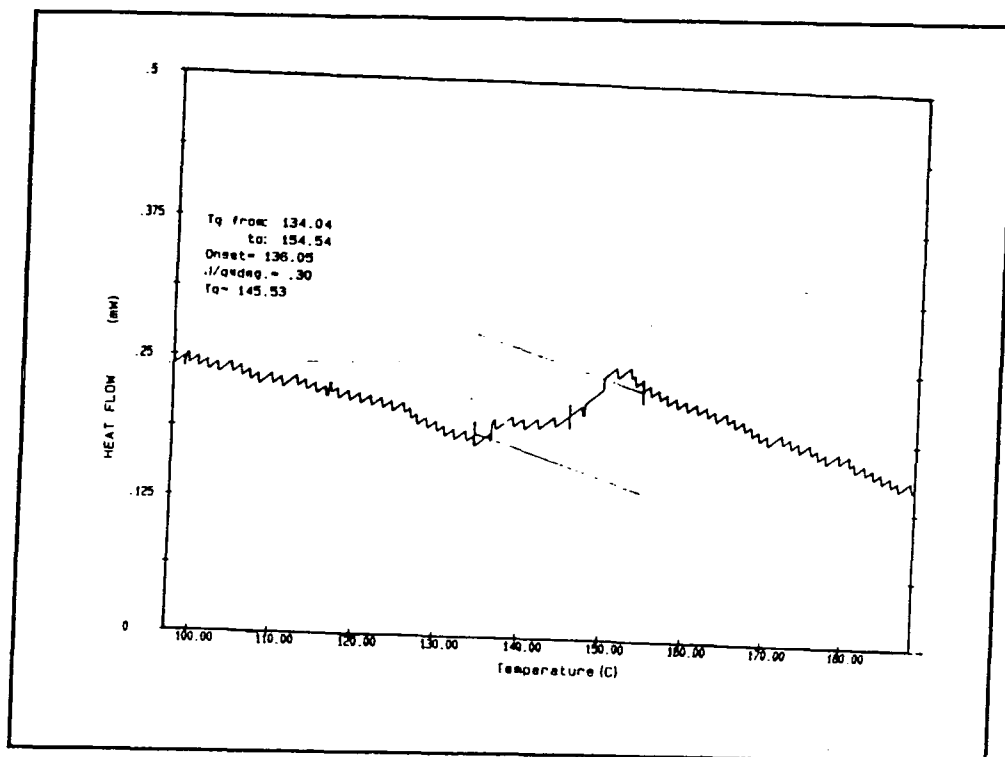


Figure 5.3: DSC of P-4VP (heating rate is $10\text{ }^{\circ}\text{C min}^{-1}$)

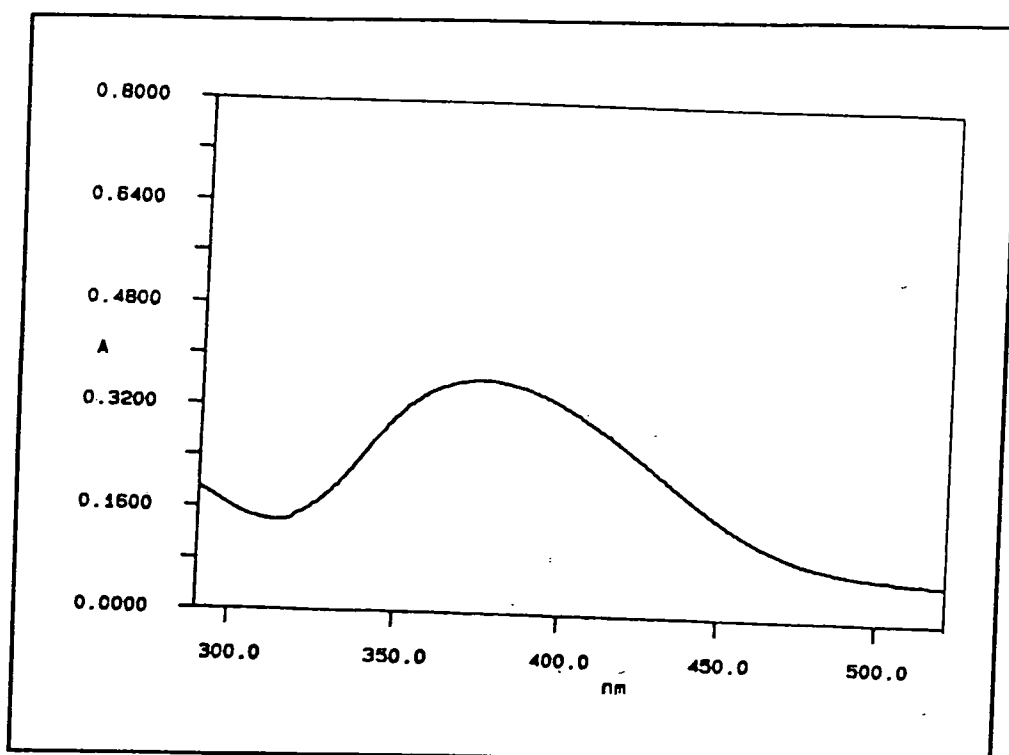


Figure 5.4: The absorption spectrum of MO3ONS film

5.3 Poling of P-4VP

5.3.1 Initial studies

P-4VP samples were poled at various fields and temperatures. Both fixed electrode poling and corona poling techniques were used. Table 5.1 shows the poling conditions and the measured EO coefficients for the samples poled with both methods.

No of the sample	E_p ($V\mu m^{-1}$)	T_p ($^{\circ}C$)	Poling Time (minutes)	EO coeff. (r_{33}) ($10^{-12} mV^{-1}$)
1	10.0	100	15	0.014
2	23.0	100	15	0.017
3	56.0	116	12	0.042
4	60.0	102	5	0.31
5	88.0	122	15	0.47
6	90.0	122	10	0.18
7	-	134	3	0.055

Table 5.1: Measured EO responses (at 632.8 nm) for the poled P-4VP samples (1-6 fixed electrode poled samples, 7 corona poled sample)

Three important points can be drawn from table 5.1. The first is that in P-4VP the EO response found was higher for the samples poled at 122 °C compared to 100 °C. Polar alignment will increase when the poling temperature becomes close to the T_g of the material. T_g of P-4VP is around 145 °C.

The second is that the corona poled sample gives a smaller EO response than the fixed electrode poled samples. This is unusual since much higher poling fields can usually be maintained by corona poling. The low poling efficiency of P-4VP samples by corona poling is not understood. It may be due to the penetration of the ions, which are produced by high field, into the sample. If this is the case the ions would not stay on the surface of the polymer and a high field cannot be established across the sample.

The third and the most important one is that there were irregularities between the poling conditions and the subsequent linear EO coefficients. It is clear that despite the poling temperature being higher in sample 3 than in sample 4, the EO coefficient is around 8 times smaller. The irregularity seen in the samples 5 and 6 is clearer. Both samples were poled at the same temperature for more or less the same poling time, however the EO response was three times smaller in the case of the sample which was poled at higher poling field. This irregularity between poling conditions and subsequent EO responses was seen in other cases which are not included in the table.

It is known [11] that isopropyl alcohol, IPA absorbs water. This is due to the hygroscopic character (infinite solubility in water) of IPA. Dissolved water in IPA may cause some ions (like H_3O^+ , CO_3^{2-}). The possible chemical reactions are shown in figure 5.5. The presence of ions may result in the above mentioned irregularities in the EO response of poled P-4VP films.

In order to see the effect of dissolved water on the polar induced alignment in 'wet' P-4VP samples, some 'dry' P-4VP samples were prepared by using distilled IPA, dried by means of molecular seive pellets. Poling of 'dry' and 'wet' P-4VP samples were carried out at various temperatures and fields.

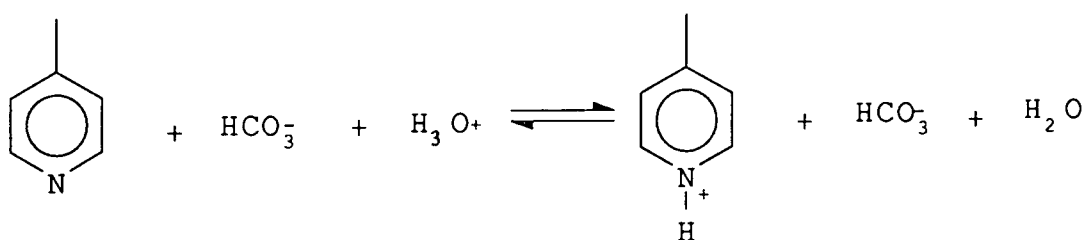


Figure 5.5: Possible mechanism for quaternisation of P-4VP

5.3.2 Current Density versus Temperature Characteristics

Figure 5.6 shows the current density/temperature relationship of both P-4VP samples. In the 'wet' P-4VP the current started to increase at relatively low temperatures (50 °C). At temperatures above 100 °C a two order of magnitude current increase occurred. During the 15 minutes of poling time at 125 °C, a one order of magnitude current decrease was observed. When the temperature was reduced, a current decrease occurred around 100 °C. Below this temperature the current further decreased steadily to smaller values.

In the 'dry' sample, however, the current increase was negligible up to 100 °C. Nevertheless above 100 °C a very sharp current increase again occurred. Over 15 minutes of poling time, a one order of magnitude current decrease was seen, but during cooling of the sample, the current did not change.

By comparing the *J/T* characteristics of 'wet' and 'dry' P-4VP we can see that there are at least two sources of current which contribute to the total current density. The first, and smaller contribution, is that attributed to ions (in 'wet' P-4VP). It can be seen in figure 5.6 that above 40 °C a slow current increase occurs in 'wet' P-4VP. In 'dry' P-4VP no current increase occurs around this temperature. The current increase becomes apparent at temperatures above 90 °C. It can also be seen from the cooling process that

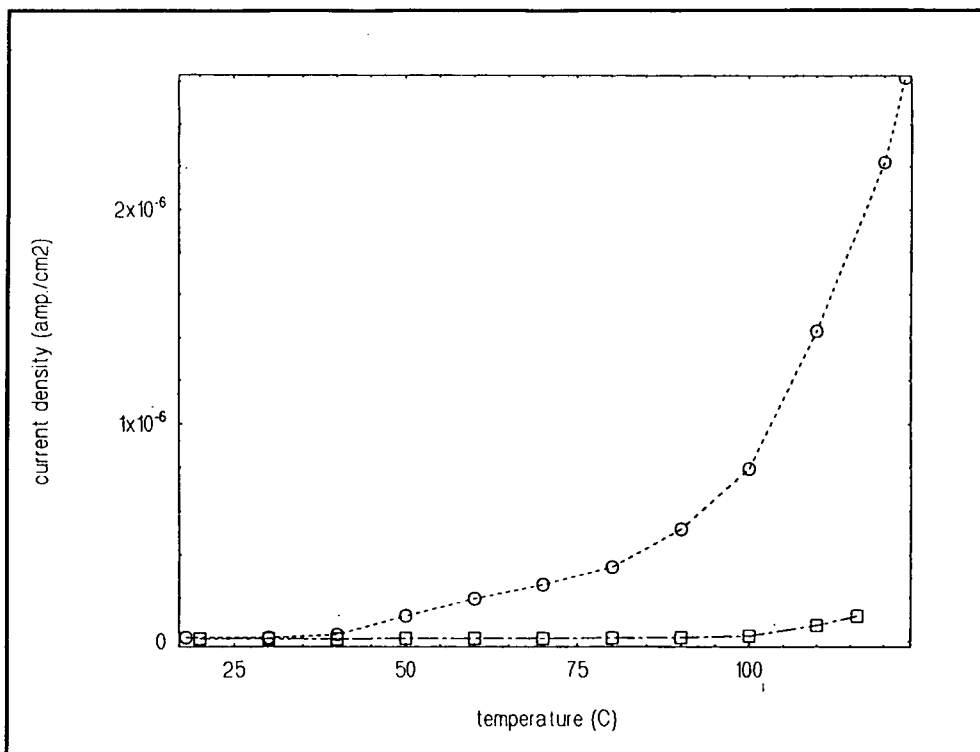
a small reduction occurs in the current density of the 'wet' P-4VP, whereas no change in the current density of the 'dry' P-4VP is observed.

The second and the most dominant one may be due to the polarisation current which would occur above 100 °C in both 'wet' and 'dry' P-4VP (near to the T_g). It is not proven that this is the polarisation current, but, because this current increase was seen in both 'dry' and 'wet' P-4VP in the same temperature range and reproducibly, this is not a unreasonable suggestion.

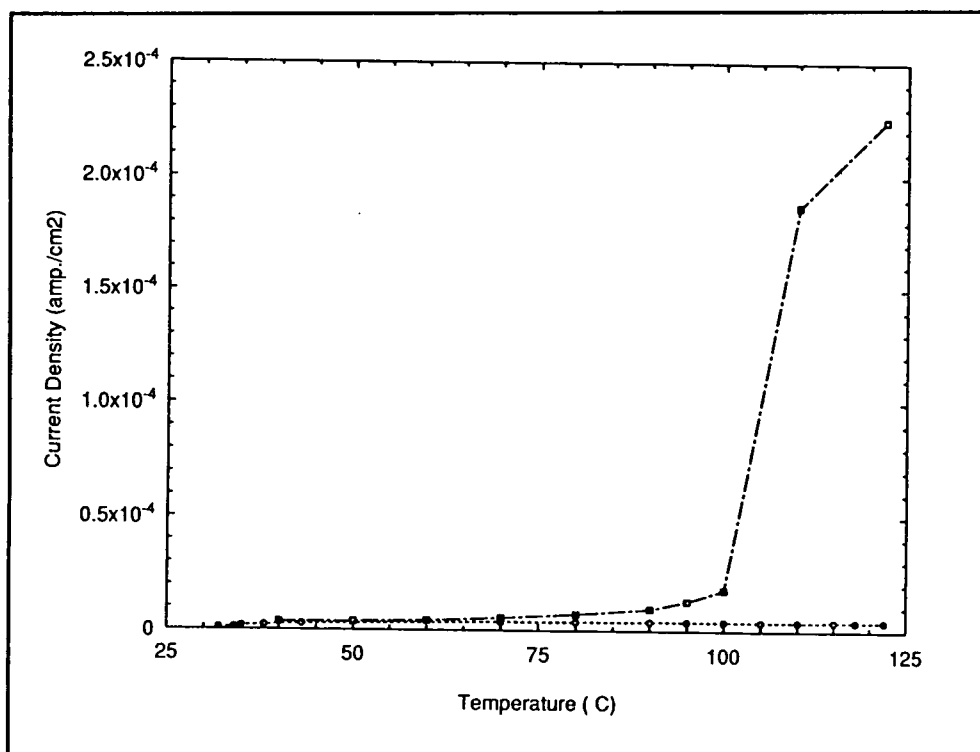
In the current density/temperature relationship of 'wet' and 'dry' P-4VP samples (figure 5.6) it has been seen that above 100 °C a huge increase in current density occurs. This high current will reduce the effective poling field. In order to prove this the following experiments were carried out.

5.3.3 Poling at Different Temperatures

It is of interest to investigate the alignment achieved for fixed poling times and fields but at various temperatures and to this end the data in figure 5.7, which relates to P-4VP, is presented. The optimum poling temperature is around 100 °C which is below the T_g of the polymer. The EO response decreases at temperatures over 100 °C. The reduction in EO response with the increase in temperature is due to an increase in current density. Increase in current reduces the effective poling field and causes a subsequent reduction in the EO response.



(a)



(b)

Figure 5.6: The current density/temperature relationship of (a) 'wet' P-4VP (open circles, heating; open squares, cooling cycle), and (b) 'dry' P-4VP (open squares, heating; open circles, cooling cycle)

5.3.4 Poling of 'dry' and 'wet' P-4VP Samples at Various Fields

A 7 μm thick 'dry' P-4VP and a 2 μm thick 'wet' P-4VP sample was poled at 125 °C for 10-15 minutes. The poling field was varied from 7-50 $\text{V}\mu\text{m}^{-1}$ in the case of 'dry' P-4VP and 7-118 $\text{V}\mu\text{m}^{-1}$ in the case of the 'wet' sample. After each poling r_{33} was measured. Figure 5.8 shows r_{33} vs. poling field for these samples. As can be seen r_{33} varies linearly with the poling field in both samples. This single result also shows that the poling efficiency in 'dry' P-4VP is higher than 'wet' P-4VP (twice in this particular case). This is further evidence of the existence of ions within the 'wet' P-4VP. The increase in the current density at the poling temperature in the 'wet' sample indicates a reduction in the effective poling field. This explains the subsequent reduction of the poling efficiency in the 'wet' P-4VP sample.

5.3.5 Stability of Polar Alignment in Poled 'dry' and 'wet' P-4VP

Following the poling of the 'dry' and 'wet' P-4VP samples, the relaxation of polar alignment over time (500 hours) was studied. Figure 5.9 shows the normalised EO coefficient versus time characteristics of these samples.

In the case of poled, 'dry' P-4VP, the EO response relaxed only by approximately 6% within 500 hours (which is not shown in figure 5.9). By contrast in poled, 'wet' P-4VP, a very sharp relaxation occurred in a few hours. The EO response relaxed to 70% of its initial value. Then it relaxed by a further 50% over 100 hours.

The excessive relaxation of the dipolar order in the 'wet' films would then be due to ionic conduction. The precise mechanisms for this have not been fully explored and require further work. Presumably due to the low number of the ions in the 'dry' P-4VP the relaxation of the poling induced alignment was very stable.

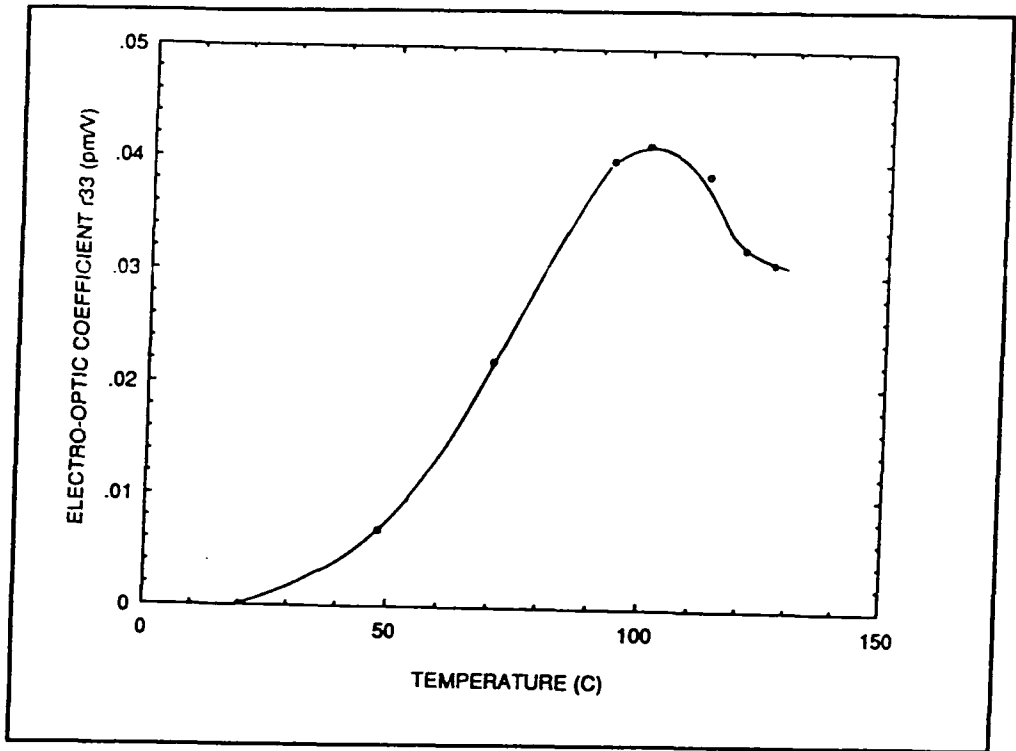


Figure 5.7: The r_{33} vs. poling temperature for a poled ($E_p = 21 \text{ V}\mu\text{m}^{-1}$) 'wet' P-4VP sample

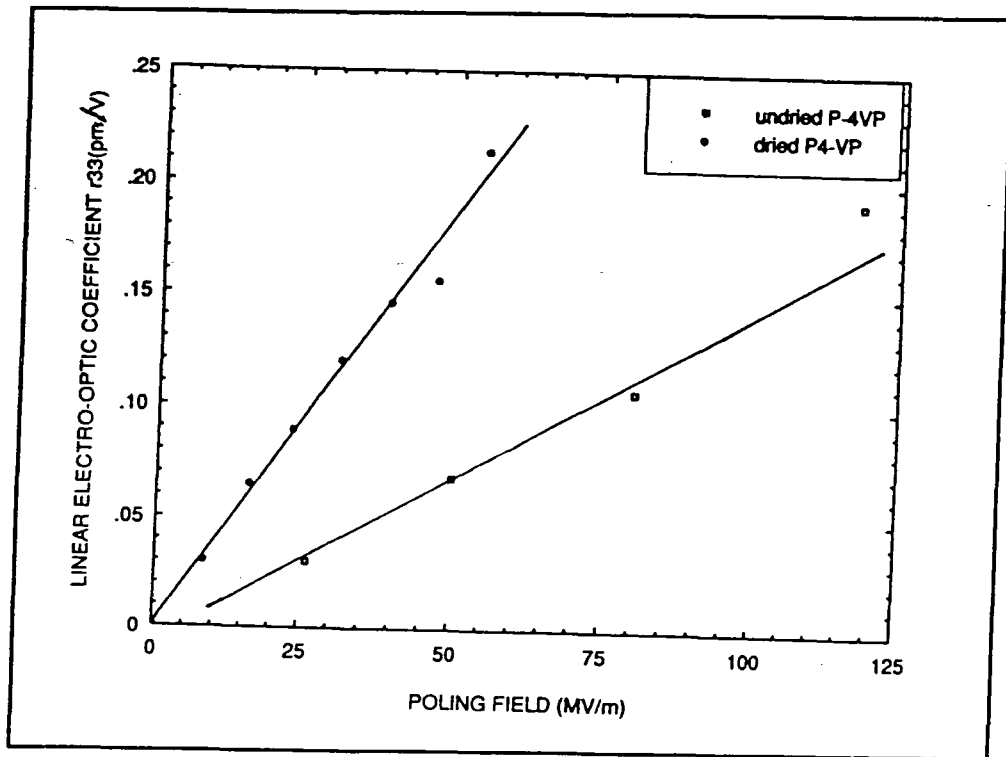


Figure 5.8: The r_{33} vs. poling field relationship of 'wet' and 'dry' P-4VP samples ($T_p : 120 \text{ }^\circ\text{C}$ in both samples)

5.3.6 Theoretical comparison

In an attempt to quantify and understand the origin of the EO response in P-4VP the values calculated for μ_z and β_{zz} were examined. The zero frequency value for β_{zz} , $\beta(0)_{zz}$, for pyridine is $1.1 \times 10^{-40} \text{ m}^4\text{V}^{-1}$ and the ground state dipole moment, $\mu_z = 1.9 \text{ D}$, ($6.34 \times 10^{-30} \text{ Cm}$) as calculated using the AM1 model [Chapter 4 ref. 3]. In the literature, [13] the ground state dipole moment of pyridine is given as 2.26 D (in liquid phase). The calculated μ_z (according to AM1 model) is smaller than the literature value. This is due to the fact that the value obtained in the AM1 model is a gas phase value and thus take no account of the influence of local fields. The product, $\mu\beta$ (theory), can be regarded as an ideal figure of merit for the molecular properties and is calculated to be $7 \times 10^{-70} \text{ Cm}^5\text{V}^{-1}$.

The experimental r_{33} value ($0.2 \times 10^{-12} \text{ mV}^{-1}$, at 122 °C for $50 \text{ V}\mu\text{m}^{-1}$, for a 'dry' P-4VP, figure 5.8) can be used to calculate the product, $\mu\beta$ (experimental), by appropriate substitution into equation 2.16.

The number density, N , of non-linear moieties, assumed to be the pyridine side groups, was calculated from the monomer formula weight and an assumed polymer density of 1 gcm^{-3} . A survey of the densities of related substituted vinyl polymers [16] shows that this is reasonable. This gives $N = 6 \times 10^{21} \text{ cm}^{-3}$.

Substituting the experimental values for r_{33} , T_p and E_p into equation 2.16 and using the measured relative permittivity of P-4VP at room temperature ($\epsilon_r(0) = 2.7$) and at the poling temperature ($\epsilon_r'(0) = 2.5$) we find; $\mu\beta$ (experimental) $7.0 \times 10^{-69} \text{ Cm}^5\text{V}^{-1}$. Comparison with the theoretical value which calculates the electronic properties for isolated molecules, immediately shows a discrepancy. The experimental product is enhanced by ten times the theoretical value. In making this comparison, we do not necessarily imply that the microscopic electronic properties themselves have been altered, although this remains a possibility. An alternative way of expressing the enhancement is to use gas phase values for β_{zz} and μ_z in equation 2.18 and calculate the expected r_{33} , as was done earlier for the guest-host systems. This leads to a value,



r_{33} (theory) = $0.018 \times 10^{-12} \text{ mV}^{-1}$ which compares with the experimental value of $0.2 \times 10^{-12} \text{ mV}^{-1}$.

Thus it seems that in this polymer system there is some enhancement in the polar order, over and above that predicted on the free dipole theory.

We note that the low frequency relative permittivity of P-4VP is approximately equal to the square of the refractive index which supports the validity of the assumption implied in equation 1.11. A contribution to the low frequency EO response can be expected, although where this has been previously invoked to explain the differences between r_d and $r(0)$ the differences have relatively minor (a factor of 2 in reference 7). The most important assumption made in the thermodynamic model is that the side groups re-orient independently from each other. This assumption is only valid for dilute systems where the separation between dipoles is large enough to neglect dipole-dipole interactions. In P-4VP the large number density of pyridine side groups suggests a high probability of close mutual contact between groups which could therefore be responsible for some co-operative phenomena similar to that found in piezoelectric materials such as PVDF. This behaviour requires further study.

5.4 Poling of MO3ONS

Poling of a film of MO3ONS (see figure 5.1) a more conventional side-group polymer was studied in comparison with P-4VP samples. A $2 \mu\text{m}$ thick MO3ONS sample was poled at about the glass transition temperature of this polymer ($105 \text{ }^\circ\text{C}$). The poling conditions and the measured r_{33} are shown in table 5.2. The value obtained for the EO coefficient is moderately high but reflects the size of poling field applied to thin films. With a better sample preparation much higher poling fields may be applied and subsequently much higher EO responses can be achieved. It is found that in MO3ONS the figure of merit ($\frac{r_{33}}{E_p}$) is about 24 times higher than that of 'dry' P-4VP and 60 times

higher than 'wet' P-4VP. This of course is due to the higher nonlinearity of the side group in MO3ONS. The stability of poling induced alignment was also studied in MO3ONS compared to 'wet' P-4VP. The relaxation of polar alignment of these two samples (at room temperature) is shown in figure 5.10.

The stability of polar alignment in MO3ONS is much better compared to 'wet' P-4VP. For MO3ONS, the r_{33} coefficient falls to 70% of its initial value after 10 hours. The EO response was stable thereafter at room temperature for at least 2200 hours (not shown). In comparison to 'dry' P-4VP, the short term relaxation in MO3ONS is poor. A 30% relaxation occurs in MO3ONS over 10 hours while there is no detectable relaxation in 'dry' P-4VP. P-4VP may thus have advantages over MO3ONS particularly when the range of optical transparency is concerned. The absorption edge in P-4VP is in the UV region whereas that of MO3ONS is close to 400 nm [figure 5.2 and 5.4]. These difference may be of consequence for frequency doubling applications particularly if very long interaction lengths can be achieved.

Material	E_p ($V \mu m^{-1}$)	T_p ($^{\circ}C$)	Time (minutes)	EO coeff. r_{33} (pmV^{-1})
MO3ONS	25	105	10	2.41
P-4VP ('dry')	25	122	10	0.10
P-4VP ('wet')	25	125	10	0.04

Table 5.2: The poling conditions and the measured EO coefficients at 632.8 nm

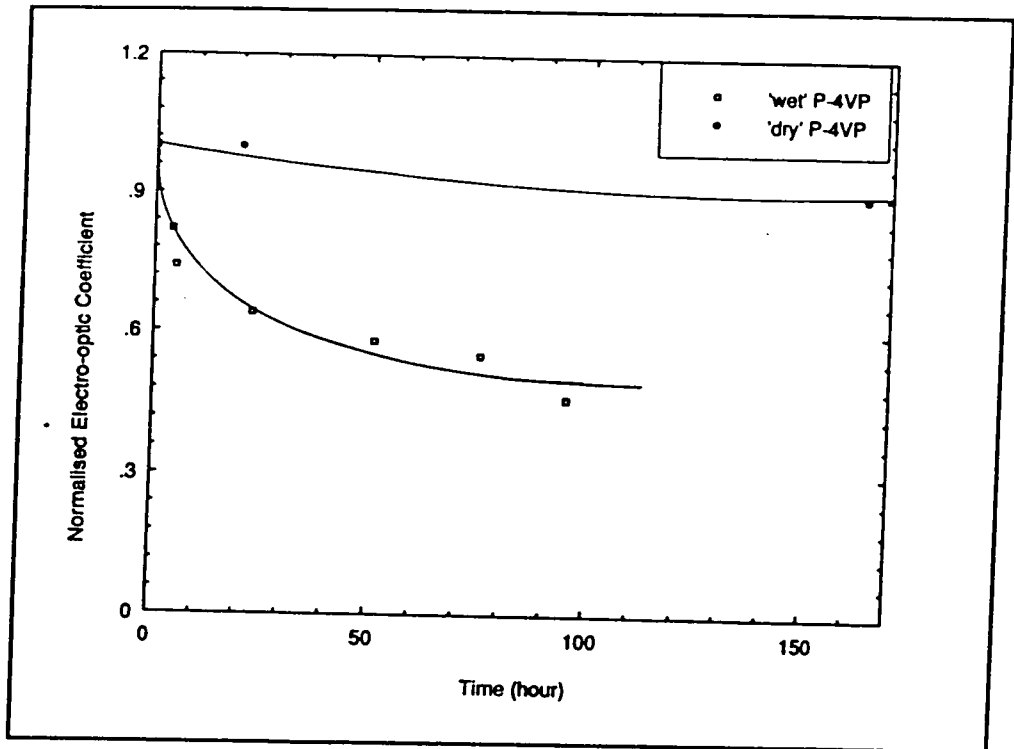


Figure 5.9: The thermal relaxation of polar alignment in 'wet' and 'dry' P-4VP samples at $T = 20\text{ }^\circ\text{C}$ (poling conditions for the 'wet' P-4VP, $E_p = 88\text{ V}\mu\text{m}^{-1}$, $T_p = 120\text{ }^\circ\text{C}$ and 'dry' P-4VP, $E_p = 28\text{ V}\mu\text{m}^{-1}$, $T_p = 125\text{ }^\circ\text{C}$)

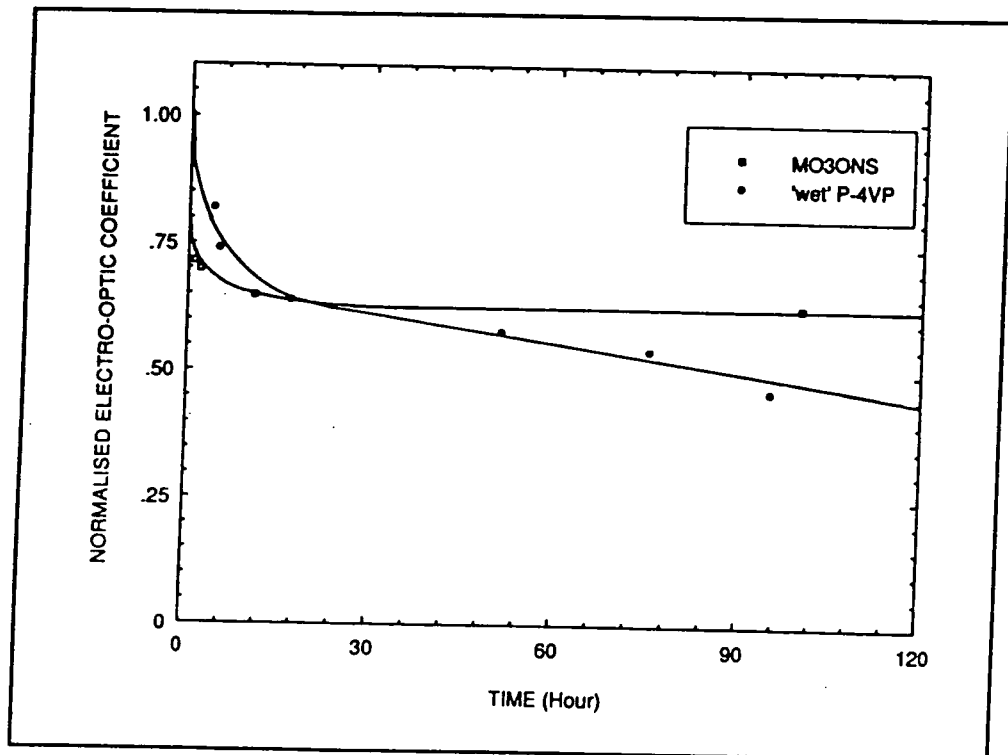


Figure 5.10: The thermal relaxation of polar alignment in MO3ONS with compared to 'wet' P-4VP (at $T = 20\text{ }^\circ\text{C}$)

5.5 Conclusions

It has been shown for the first time that thin films of P-4VP exhibit reasonable EO response following poling. The experimental EO coefficient is ten times higher than the theoretical EO coefficient which indicates some enhancement in polar order.

It is proposed that due to the hygroscopic character of IPA some ions are present in the solution of P-4VP from which films were prepared. This proposal is supported by the results found from the comparative poling study on 'dry' and 'wet' P-4VP. The poling efficiency was twice as high in the 'dry' P-4VP sample than in a 'wet' one. In addition the stability of polar alignment was much better in 'dry' P-4VP samples compared to 'wet' samples. In 550 hours only a 6% relaxation occurred in the EO response.

Another side-chain polymer, MO3ONS was studied and compared to P-4VP. This material shows higher EO responses compared to P-4VP. Poled MO3ONS films show reasonably high long term thermal stability. After 30% initial relaxation the EO response was stable for more than 1100 hours.

5.6 References

- 1- Ye C., T.J. Marks, J. Yang, and G.K. Wong, *Macromolecules*, **20**, (1987), 2324
- 2- Chen Y., M. Rahman, T. Takahashi, B. Mandal, J. Lee, J. Kumar, and S. Tripathy, *Japan. J. Appl. Phys.*, **30**, (1991), 672-676
- 3- Sohn J.E., K.D. Singer, M.G. Kuzyk, W.R. Holland, H.E. Katz, C.W. Dirk, M.L. Schilling, and R.B. Commizoli, in "Non-linear Optical Effects in Organic Polymers", (Eds. J. Messier, F. Kajzar, P. Prasad, and D. Ulrich) *Nato ASI Series*, 162, Kluwer, Dordrecht, (1989), 291
- 4- Haas D., H. Yoon, H.T. Man, G. Cross, S. Man, N. Parsons, *Proc. SPIE*, **1147**, (1989), 222-232
- 5- Hill J.R., P. Pantelis, P.L. Dunn and G.J. Davies, *Proc. SPIE*, **1147**, (1989), 165- 176

- 6- Shuto Y., A. Michiyuki, and T. Kaino, *IEEE Transactions Photonics Technology Letters*, **3**, (1991), 1003-1005
- 7- Singer K.D., M.G. Kuzyk, and J.E. Sohn, *J. Opt. Soc. Am. B*, **4**, (1987), 968
- 8- Lloyd D., "A First Course in Organic Chemistry", John Wiley & Sons, England, (1989), 302-303
- 9- McMurry M.J., "Organic Chemistry", Brooks/Cole Publishing Company
Monterey, California, (1984), 463-464
- 10- Wells P.J. and D. Bloor, *Proc. SPIE* , **58**, (1989), 1018
- 11- Riddick and Bunger, "Organic Solvents Physical Properties and Methods of Purification", 3rd edition, Vol.2, (1970), John Wiley & Sons. Inc. USA., 150

6.1 Introduction

It may be expected that the number density of NLO chromophores and the stability in the poling induced alignment can be increased in main-chain polymers in comparison to guest-host or side-chain polymers. This is due to the fact that each main-chain unit can contain one NLO chromophore and thus the rigidity of the main-chains may slow down the thermal relaxation of the polar alignment. A few reports have been published previously on main-chain NLO polymers [1-10]. In these reports the main-chain polymers are mostly head-to-tail type that is, all the chromophore dipole moments point in the same general direction along the polymer backbone [figure 6.1 (a)]. In an individual chain the effective dipole moment is increased for a main-chain type material in comparison with a side-chain polymer, because of the head-to-tail assembly of chromophores.

Following poling, main-chain NLO polymers can exhibit significant frequency doubling coefficients (32 pmV^{-1} [3]), comparable to those of side-chain polymers. In addition they can show an improvement in stability over side-chain NLO polymers. Meyrueix et al. [4] reported a very stable alignment in their moderately ($50 \text{ V}\mu\text{m}^{-1}$) poled main-chain type polymer. They reported less than 10% relaxation within 120 days at room temperature.

Studies of these materials are important in understanding the mechanisms of decay in induced nonlinearities in poled polymers, since the decay in side-chain NLO polymers is often attributed simply to segmental rotation of the side groups which might occur independent of the chain backbone motion. Unlike the side-chain type materials, the main-chain materials must relax by reorientation of the polymer chain.

The stability of induced polar order in some main-chain polymers has been studied in parallel with dielectric relaxation studies [3,5]. Teraoka et al. [3] have seen two relaxation modes in two main-chain polymers, BISA-NA (diglycidylbisphenol A -4-

nitroaniline) and BISA-DMNPDA (diglycidylbisphenol A- N,N'-dimethyl(4-nitro-1,2-phenylenediamine). These are an α relaxation, attributed to the glass transition and a β -relaxation, attributed to local segmental motion of the main-chain. Kohler et al. [5] have studied and compared the dielectric relaxation of a series of five different polymers containing the same nonlinear optical chromophore where this is included either as a guest, as a side-chain, or as a main-chain group. In all cases the relaxation of the chromophores is coupled to the glass transition which indicates an α process. They have also found an additional slow relaxation mode at frequencies below the α peak in the two types of main-chain polymer studied.

Early main-chain NLO polymers had low glass transition temperatures (60-90 °C) [5,6] which is not desirable for electro-optic device applications. Much effort has been spent on synthesising new main-chain NLO polymers with high glass transition temperatures. Fuso et al. [7] have synthesised a copolymer containing cis-and trans-1,4-cyclohexyldimethyl units with a T_g of 102 °C. Nalwa et al. [8] reported a novel organic polymeric system of urea having no pendant NLO chromophores, instead NLO active urea moieties constitute the main polymer backbone. This polymer has a T_g around 123 °C and is highly soluble in a variety of organic solvents. This material shows an absorption maximum at 253 nm (and the cut-off wavelength is around 307 nm). This unique optical transparency gives superiority over other polymers from an applications point of view. Recently, new main-chain NLO polymers with much higher glass transition temperatures (168 - 183 °C) have been reported by Mitchell et al. [9]. These authors also report in the same study that high molecular weight copolymer ($M_n = 30,200$) possessed an even higher glass transition temperature (187 °C).

Recent new work by Xu et al. [10] reports on the stability of poled and cross-linked main-chain NLO polymer. In this main-chain polymer, the NLO units are combined with a flexible segment which increases the poling efficiency. The dipolar alignment is made easier (compared to the head-to-tail main-chain polymers) because the polymer chains are random coil conformations instead of extended rigid chains (figure 6.1 b). After corona poling a d_{33} of 80 pmV⁻¹ was obtained. A poled and cross-linked sample showed

no detectable relaxation in the SHG response over 1200 hours while a poled but not cross-linked sample showed complete relaxation in a few hours.

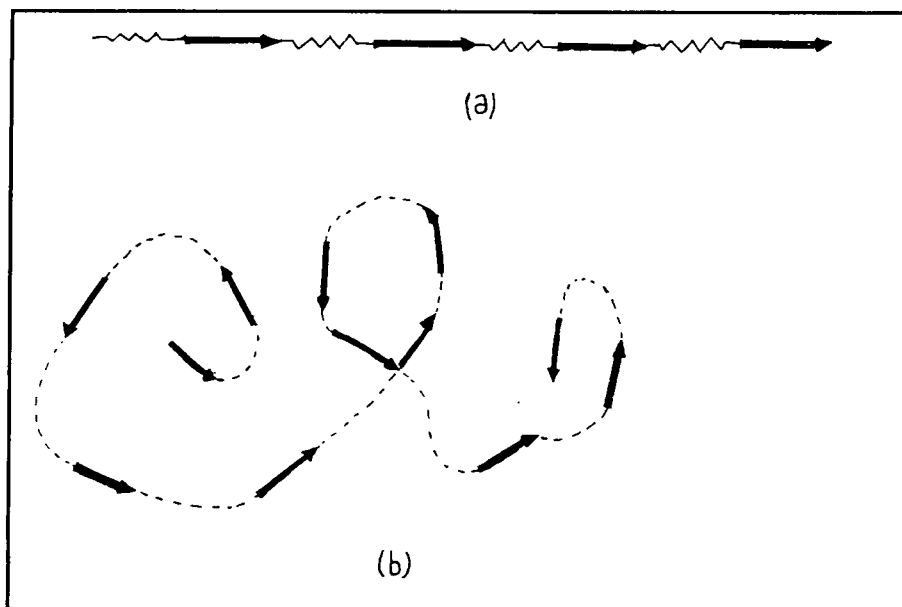


Figure 6.1 : (a) Head-to-tail type dipolar arrangement, (b) Random coil conformation in a main-chain which has flexible segments

This chapter describes poling studies on a new polycarbosilane main-chain type polymer, where the NLO group is contained in a segment in the polymer chain which adopts a rigid 'V' conformation. This polymer was supplied by Dr William Douglas, currently at Unite Mixte, Universite de Montpellier, France [11].

6.2 Synthesis and film deposition

A series of diethynyl diphenylsilicon homopolymers substituted with donor- π -acceptor model chromophores were synthesised by Corriu et al. [12] and the structure of the material chosen for initial studies is shown in figure 6.2. This polymer does not decompose or undergo any observable phase changes (including a glass-to-rubber transition) up to 234 °C (figure 6.3). At this temperature an exothermic transition occurs which may be related to new bond formation in the material. The low molecular weight

($M(w) = 9000$) means that chains are on average 24 units long and thus it is preferable to describe the secondary structure as oligomeric.

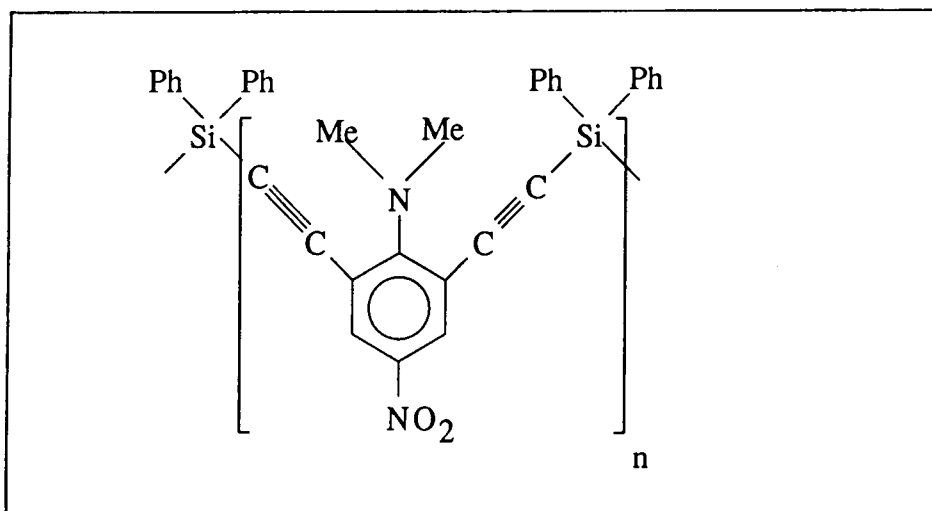


Figure 6.2 : Structure of the rigid 'V' main-chain polymer

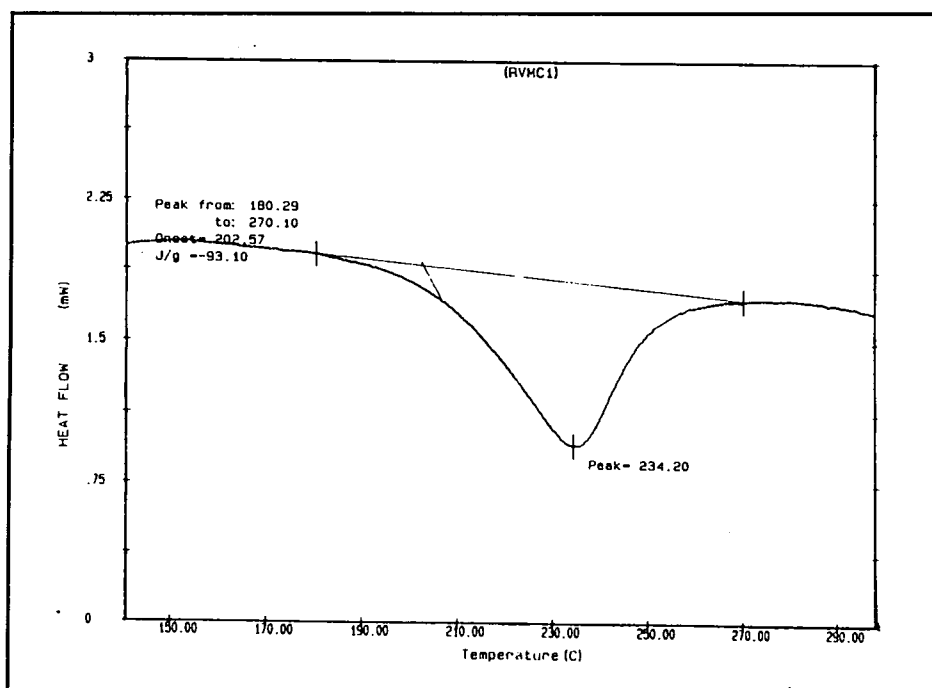


Figure 6.3: DSC scan of rigid 'V' (heating rate is $10\text{ }^\circ\text{C minutes}^{-1}$)

Solutions of 17% w/w of the polymer were prepared in 1,2,3 -trichloropropane. To remove dust particles and any coagulant the solution was filtered through a 0.5 μm pore size Millipore disposable filter. Thin films of this polymer were prepared via spin coating at 1300 rpm on an ITO coated glass slide. The samples were dried in an oven under vacuum at 80 $^{\circ}\text{C}$ for 1-2 hours. Thickness measurements were carried out by a Tencor surface profiler. The samples used in this experiment were around 1 μm thick. For parallel plate poling and reflection EO measurements (sections 3.4.1 and 3.5) a silver top electrode was evaporated on the surface of the polymer sample. Figure 6.4 shows the absorption spectra of this main chain polymer. A sharp peak was seen at around 396 nm and is ascribed to the two-level transition of the dimethylaminonitroaniliny, DMNA, chromophore group.

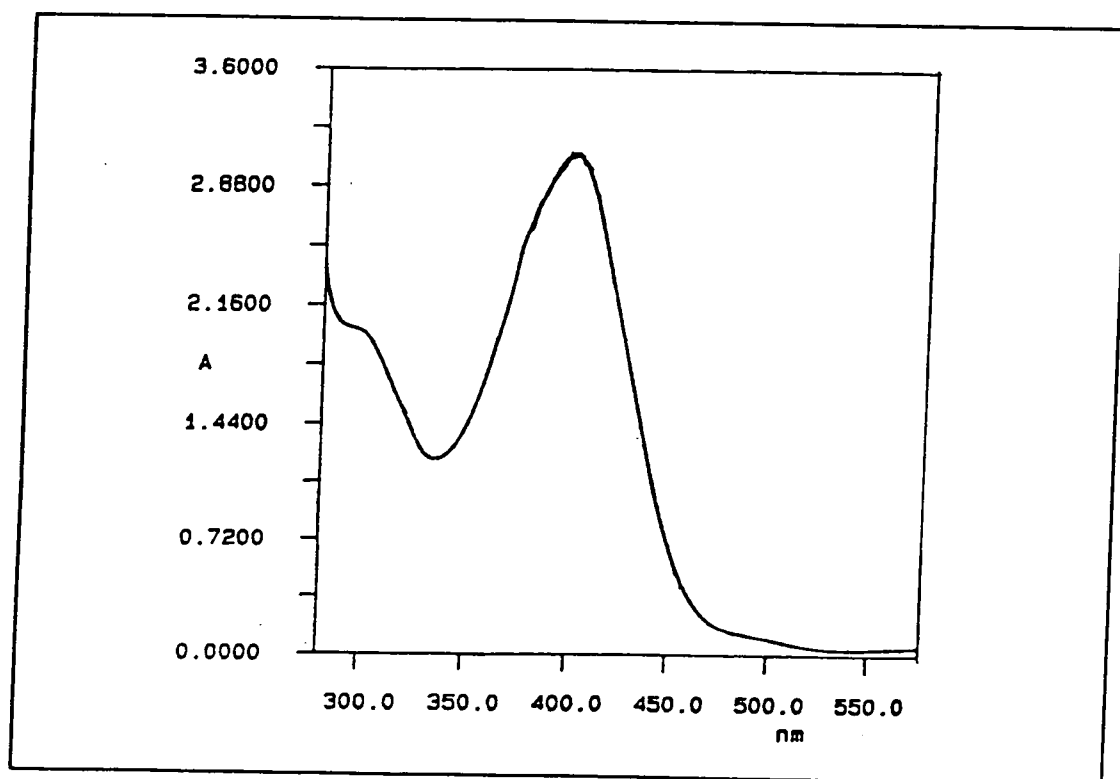


Figure 6.4 : The absorption spectrum of the rigid 'V' main-chain polymer

The refractive index of the sample was calculated from the spacing of interference fringes seen in transmission studies. The estimated refractive index in the visible region $n = 1.87 \pm 0.03$.

6.3 Poling of Rigid 'V' Main-Chain Polymer

This polymer is not of the 'glassy' type, and no glass/rubber transition is seen above room temperature. In an attempt to identify an optimum temperature for poling the rise in current which occurs during the heating cycle in fixed electrode poling was followed. The current density increase was very small and much less than that found for DAN/BPA-PC [Chapter 4 ref. 12] as described in chapter 4. Figure 6.5 shows the J/T relationship for a poling field of $11.7 \text{ V}\mu\text{m}^{-1}$.

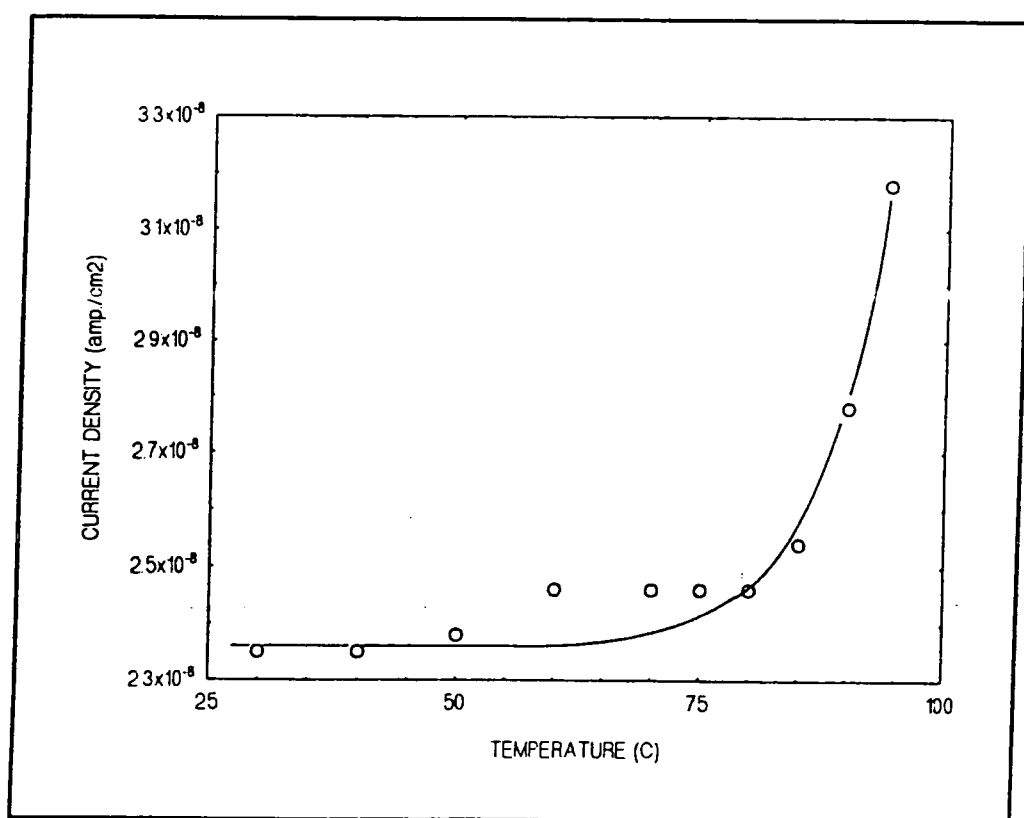


Figure 6.5 : The current density/temperature relationship of rigid 'V' main-chain polymer

In a further attempt to find the optimum poling temperature, fixed electrode poling of a $1.2 \mu\text{m}$ thick sample was carried out at various temperatures. The poling field ($11.7 \text{ V}\mu\text{m}^{-1}$) and the poling time (10 minutes), were kept constant in each poling experiment. After poling, the electro-optic coefficient was measured. The efficiency of poling measured via the electro-optic effect versus poling temperature is shown in

figure 6.6. The poling response increased up to 85 °C the maximum temperature studied. The poling field vs. the EO response characteristics of rigid 'V' main-chain polymer were also studied. Figure 6.7 shows the r_{33} vs. $E(p)$ relationships for films poled at 85 °C. A linear relation can be seen between the EO coefficient and the poling field. Higher fields could not be applied because of electrical breakdown problems.

6.4 Thermal stability of poled rigid 'V' film

Figure 6.8 shows the relaxation of a fixed electrode poled sample of rigid 'V' over a period of 200 hours. Over 30 hours the EO response relaxes to 85% of its initial value. A further 10% relaxation occurs within 100 hours. After the initial relaxation the EO response was stable for more than 200 hours. In the relaxation studies of either the fixed electrode or corona poled samples there was no significant rapid decay of the alignment. This shows that the decay of the alignment may not be governed strictly by the size and distribution of free volume. The relaxation mechanism (which was modelled with a single exponential) may be controlled by segmental main-chain rotation.

6.5 SHG Measurements on Corona Poled Samples

A 1.2 μm thick sample was corona poled, for a -5 kV needle voltage at 85 °C for 30 minutes, with a tip-to-plane distance of 1.5 cm. Immediately after poling second harmonic generation measurements were carried out.

Figure 6.9 shows the angular dependence of second harmonic light (at 532 nm) in transmission through a corona poled film for 'p' (horizontal) incident light and 'p' transmitted second harmonic. The angular dependence of the second harmonic intensity is typical of uniaxial symmetry. The absence of a signal at normal incidence (found for both p-p and s-p polarisation) shows that there are no in-plane components to the non-

linear polarisation. Thus the assumed symmetry is $C_{\infty v}$ and in the absence of absorption at the second harmonic frequency (and thus where Kleinmann symmetry is valid), the expected ratio between d_{33} and d_{13} ($= d_{15}$) is very close to 3:1. The measured d_{33} coefficient was 2.34 pmV^{-1} which corresponds to an r_{33} of approximately 1.43 pmV^{-1} . This is perhaps a surprisingly small value when considering the much higher expected fields obtained from the corona process. The r_{33} measurements following fixed electrode poling at $17.5 \text{ V}\mu\text{m}^{-1}$ gave 0.8 pmV^{-1} . If the linear relationship between r_{33} and poling field still applies in the case of corona poling then a field of only $31.3 \text{ V}\mu\text{m}^{-1}$ is predicted [13].

6.6 Comparison with theory

The theoretical model discussed in chapter 2 section 3 was applied to interpret these results further. The ground state dipole moment μ and β of DMNA were calculated using an AM1 semiempirical molecular orbital model. The value obtained for the ground state dipole moment is; $\mu = 2.368 \times 10^{-29} \text{ Cm}$, and $\beta = 88 \times 10^{-40} \text{ m}^4\text{V}^{-1}$. Using these values and the values of the experimental variables in equation 2.16 leads to a calculated r_{33} of 16 pmV^{-1} . The difference in this theoretical value and that obtained experimentally (0.8 pmV^{-1}) indicates that only 1/20 of the dipolar groups undergo free rotation during poling. The average number of chain ends given by an average chain length of 24 repeat units is given by $N(\text{AV}) = \frac{N}{12}$. The use of this reduced effective number of the NLO groups in part may explain the observed discrepancy. Other reasons require further investigation. These include the possibility of errors associated with the estimation of the effective poling fields. This has particular significance in view of the high conductivity reported for a doped sample of a polymer in this series [12] and thus gives rise to the possibility of some intrinsic or impurity assisted conductivity acting to dissipate the poling field.

6.7 Conclusion

The first in a series of thermally stable silicon-containing polymers where a nonlinear optical (NLO) dipolar group is held in a rigid 'V' segment has been studied for electrical poling and second-order properties.

The restriction to rotation of the NLO groups in the chain means that chain-end groups only play the major role during the alignment process. Comparisons with the 'free gas' model theory tend to support this observation.

Moderately high EO response ($r_{33} = 0.8 \times 10^{-12} \text{ mV}^{-1}$ for a poling field of $17 \text{ V}\mu\text{m}^{-1}$) has been achieved with contact poling. This material shows a very stable EO response at room temperature. Only a 30% relaxation was observed over 200 hours.

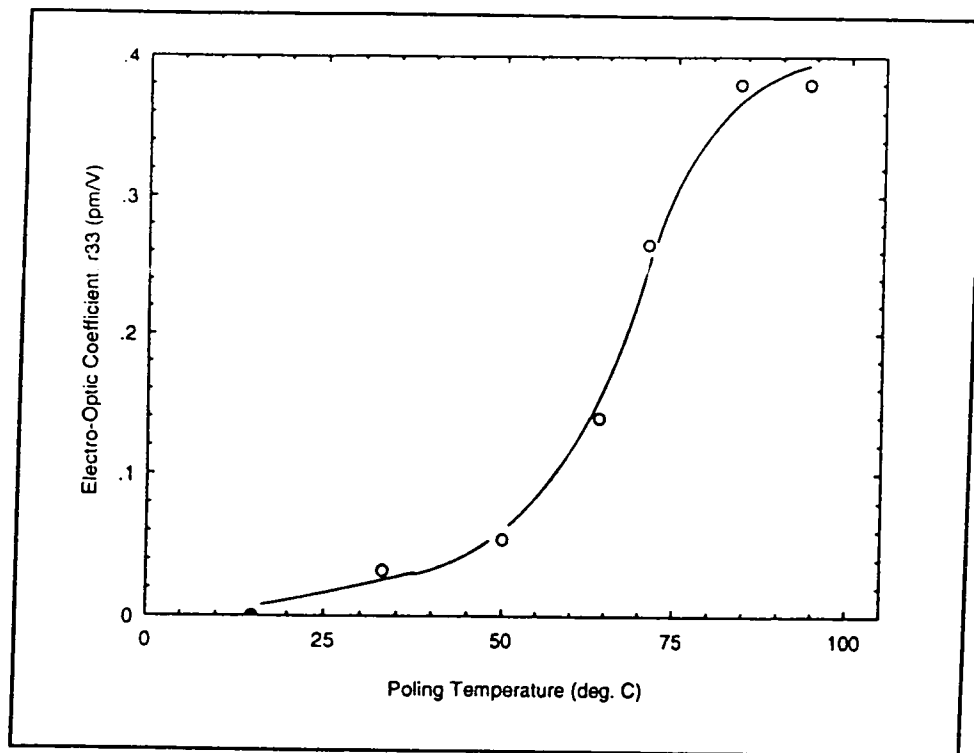


Figure 6.6: The r_{33} vs. T_p of rigid 'V' main-chain polymer

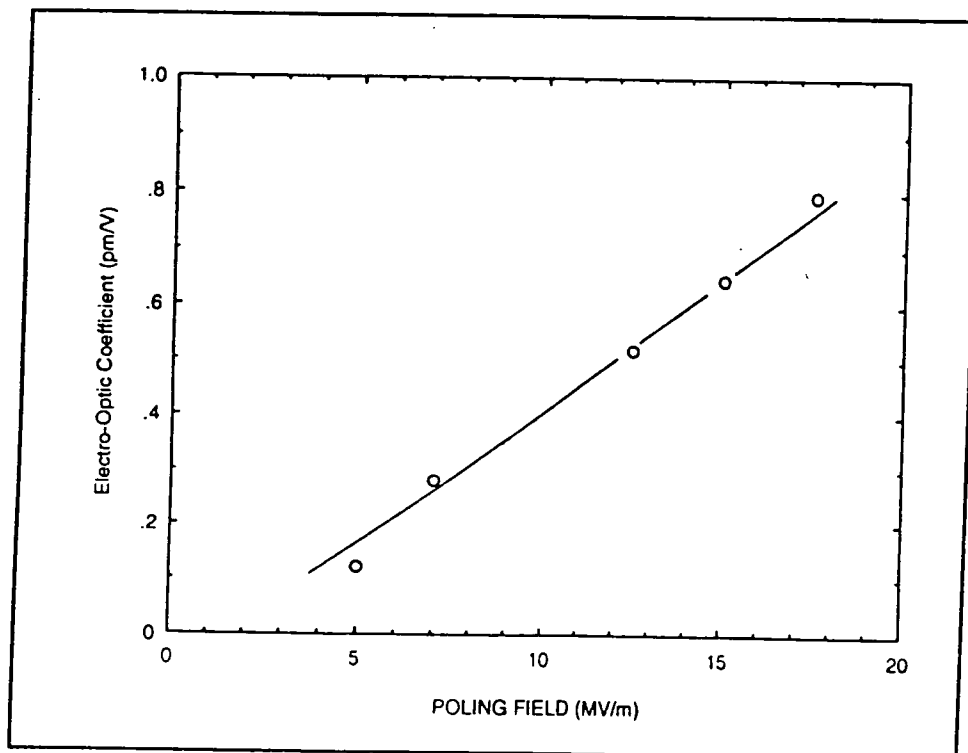


Figure 6.7: The r_{33} vs. E_p of rigid 'V' main-chain polymer

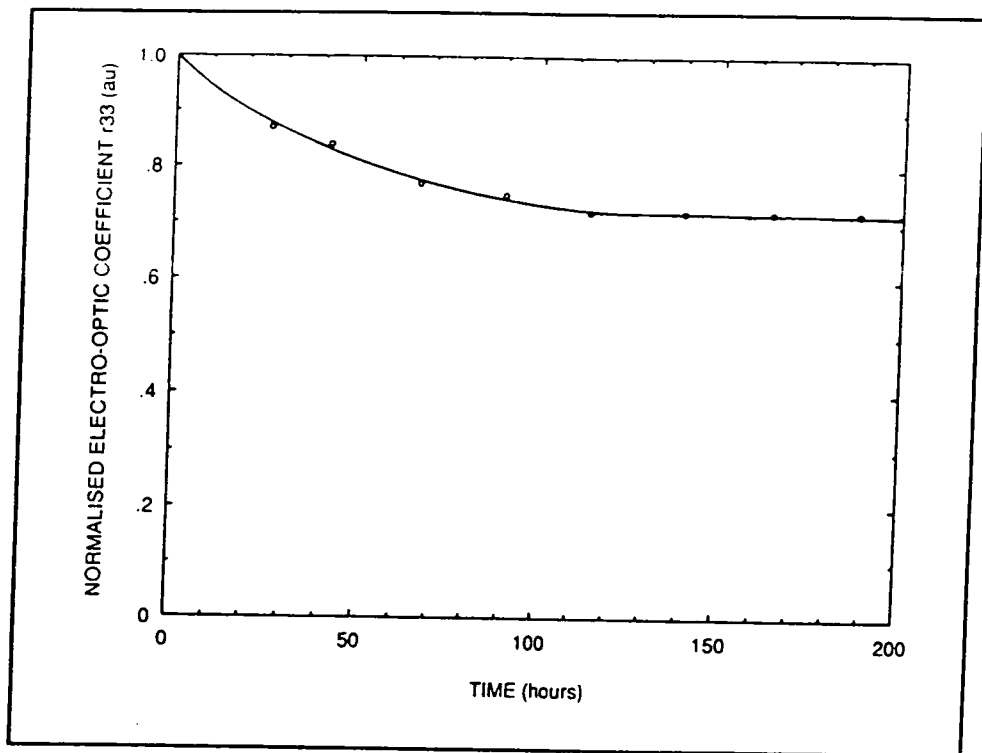


Figure 6.8: The thermal relaxation of poled rigid 'V' shaped main-chain polymer (at room temperature)

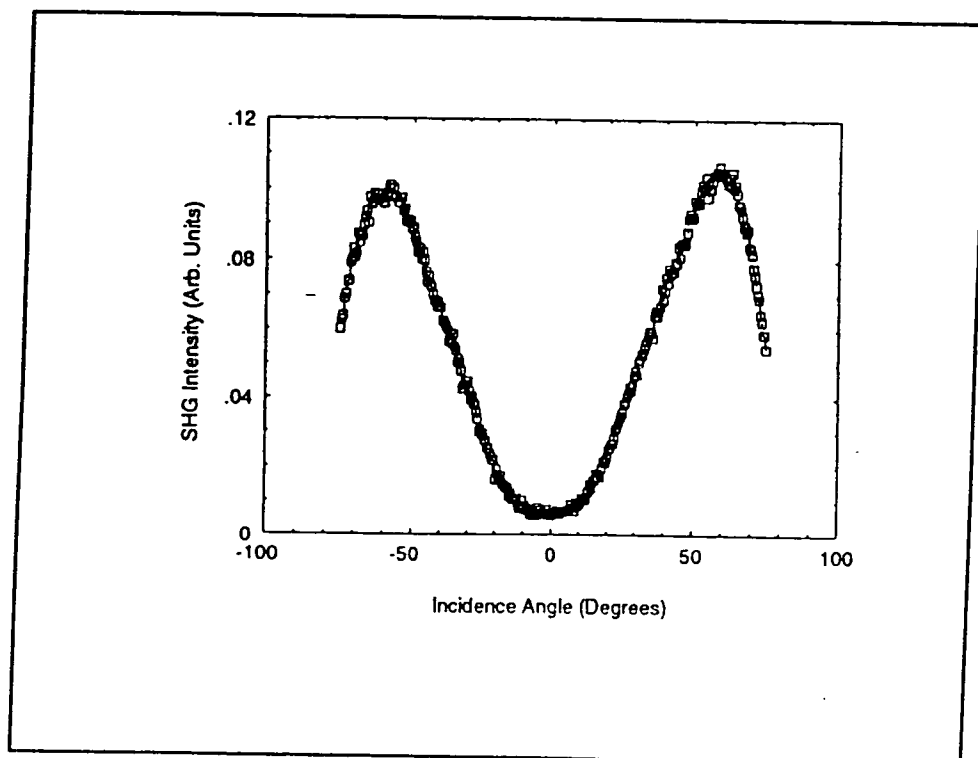


Figure 6.9: The angular dependence of the second harmonic light (for 'p' incident and 'p' transmitted)

6.8 References

- 1- Green G.D., J.I. Weinschenk, Mulvaney J.E., H.K. Jr. Hall *Macromolecules*, **20**, (1987), 722
- 2- Katz H.E., M.L. Schilling, *J. Am Chem. Soc.*, **111**, (1989), 7554
- 3- Teraoka I., D. Jungbauer, B. Reck, D.Y. Yoon, R. Twieg and C.G. Wilson, *J. Appl. Phys.* **69**, (1991), 2568-2576
- 4- Meyrueix R., G. Mignani, and G. Tapolsky, *Organic Molecules for Non-linear Optics and Photonics* Edited by J. Meissier, F. Kajzar, and P. Prasad, **194**, (1991), 161-176.
- 5- Kohler W., D.R. Robello, C.S. Willand, D.J. Williams, *Macromolecules*, **24**, (1991), 4589-4599.
- 6- Kohler W., D.R. Robello, P.T. Dao, C.S. Willand, D.J. Williams, *J. Chem. Phys.*, **93**, (1990), 9157.
- 6- Stenger-Smith, J.D., J.W. Fischer, R.A. Henry, J.M. Hoover, G.A. Lindsay, L.M. Hayden, *Macromol. Chem. Rapid Commun.* **11**, (1990), 141.
- 7- Fuso F., A.B. Padias, H.K. Jr. Hal, *Macromolecules*, **24**, (1991), 1710
- 8- Nalwa H.S., T. Watanabe, A. Kakuta, A. Mukoh and S. Miyata, *Polymer Communication* pre-print,
- 9- Mitchell M.A., J.E. Mulvaney, H.K. Hall, S.C. Jr. Willand, H. Hampsch, and D.J. Williams, *Polymer Bulletin*, **28**, (1992), 381-388
- 10- Xu C., Wu B., L.R. Dalton, P.M. Ranon, Y. Shi and W.H. Steier, *Macromolecules*, **25**, (1992), 6716-6718
- 11- Polymer supplied by W. Douglas, currently at Unite Mixte, the Universite de Montpellier, France
- 12- Corriu R.J.P., W.E. Douglas, Z.-X. Yang, F. Garnier, and A.J. Yasser, *Organomol. Chem.*, **417**, (1991), C50
- 13- Cross G.H., Y. Karakus, D. Gray, D. Bloor, R.J.P. Corriu, W.E. Douglas, Z.-X. Yang, *SPIE Proc.* **1775**, (1992), 144-153.

7.1 Summary of The Work

For the guest-host systems it was shown that bisphenol-A polycarbonate, BPA-PC is a 'polar' electret. Poled at 120 °C, for 80 V μ m⁻¹, BPA-PC gave an EO coefficient, r_{33} , of 0.03 pmV⁻¹. Two different NLO guest molecules, DAN and NMBA, were doped into BPA-PC at various concentrations. Up to 20% (w/w) of guest molecules were doped into BPA-PC and PMMA and no phase separation was observed. The DSC scans of undoped and doped BPA-PC and also PMMA have shown that the glass transition temperature of doped samples is reduced by an amount proportional to doping level. For example the T_g of 20% (w/w) DAN doped BPA-PC occurs at 90 °C which is equivalent to a depression of 55 °C due to the plasticizing effect. The optimum poling temperature for 20% (w/w) DAN doped BPA-PC was 80 °C and for 20% (w/w) DAN doped PMMA was 55 °C. Those temperatures at which the highest polar alignment were achieved are close to the T_g of these samples. A linear relationship was seen between the EO response and poling field (at a fixed poling temperature and time) for both DAN doped samples. The EO response slightly increased with poling time up to 4-5 minutes. Above 5 minutes quite a significant decrease was seen in the EO response of the poled guest-host samples especially at temperatures either at T_g or above T_g . It is suggested (in chapter 4) that this reduction in EO response originates from loss of guest molecules at temperatures above T_g . Second harmonic generation measurements on corona poled guest-host samples have shown that the high frequency EO coefficients are close to the low frequency EO coefficient. This indicates that the phonon contributions at low frequencies are not important. The most important conclusion is that a guest-host interaction occurs between DAN guest molecules and BPA-PC host which may account for an order of magnitude increase in experimental EO coefficient in comparison to theoretical value. This guest-host interaction is hydrogen bonding (figure 4.25). The

poled DAN doped BPA-PC samples show excellent thermal stability. Both short and long term thermal stability of alignment in this material is unexpectedly high for a guest-host system and can be comparable to annealed guest-host and side-chain polymers. Over 30 hours only a 9% relaxation was observed. For very long term stability, over nine months, less than 40% relaxation was observed in a corona poled 20% (w/w) DAN doped BPA-PC thin film. By contrast in DAN doped PMMA and NMBA doped BPA-PC a very sharp relaxation was observed in a few hours time. This high thermal stability in DAN doped BPA-PC is attributed to hydrogen bonding coupled with stable polar order in the host.

As far as the long term thermal stability is concerned the DAN/BPA-PC system may suffice for electro-optic device requirements. However this material system shows high long term stability only at room temperature. For integrated electro-optic device applications materials which have high thermal stability at operating temperatures of 80 °C (sometimes above 80 °C) are needed. The 20% DAN/BPA-PC system fails to answer this requirement with the present conditions. Another important requirement is a high EO coefficient. This is necessary so that low voltages may achieve the desired birefringence. The EO response achieved for a poled 20% DAN/BPA-PC system is rather small (1-2 pmV⁻¹).

It was shown here for the first time that a commercially available side-chain polymer, poly-4-vinyl pyridine, P-4VP may be poled. Poled P-4VP films show a moderate EO response following poling ($r_{33} = 0.28 \text{ pmV}^{-1}$ at $\lambda = 632.8 \text{ nm}$; for $E_p = 50 \text{ V}\mu\text{m}^{-1}$). It was suggested that dissolved water in isopropanol, IPA, causes some ions within the polymer. A comparative poling study between 'dry' and 'wet' P-4VP has shown that the poling efficiency is higher in the former. In 'wet' P-4VP samples for poling temperatures over 100 °C the EO response decreases with the increase in temperature. The decrease in the EO response is due to an increase in current density. The increase in current density may be due to a high ion population in 'wet' P-4VP samples. The effective poling field in 'wet' samples is reduced by increased current density. The thermal stability of poled 'dry' P-4VP was also improved compared to the 'wet' one. In 'wet' P-4VP the

polar alignment relaxed to 70% of its initial value within 500 hours at room temperature. By contrast in poled 'dry' P-4VP only a 6% relaxation was observed over the same time interval. A more conventional side-chain polymer MO3ONS was also studied in comparison with P-4VP. High EO responses were achieved in MO3ONS due to higher nonlinearities. It was found that the figure of merit ($\frac{r_{33}}{E_p}$) is about 24 times higher in MO3ONS than in P-4VP. P-4VP, however, has clear advantages over MO3ONS particularly where the range of optical transparency is concerned. The absorption edge in P-4VP is in the UV region whereas that of MO3ONS is close to 400 nm. The high energy absorption edge is particularly important for frequency doubling applications.

Although it was shown that there appears to be a relationship between ions and the low poling efficiency, this is surely not the only reason for the low poling efficiency seen in P-4VP. Other types of experiments (such as insitu-SHG) need to be done in order to understand the poling and relaxation mechanisms in P-4VP.

A rigid 'V' shaped main chain polymer was studied. This polymer is not a glassy type since there was no glass to rubber transition seen from room temperature up to 234 °C. Following poling this material gives a moderate EO response ($r_{33} = 0.8 \text{ pmV}^{-1}$ at, $\lambda = 632.8 \text{ nm}$; for $E_p = 17 \text{ V}\mu\text{m}^{-1}$). A calculated EO coefficient, r_{33} , based on gas law particle statistics has given 16 pmV^{-1} which is 20 times higher than the experimental value. This observed discrepancy between theoretical and experimental r_{33} is due to the reduced effective number of NLO groups. Only chain end groups contribute to the polar alignment. The average number of chain ends given by an average chain length of 24 repeat units is given by $N_{AV} = \frac{N}{12}$. The other reason for the mismatch may be the errors associated with the estimate of effective poling field.

The shape of the SHG envelope (from angle dependent SHG studies) in rigid 'V' was broader in comparison to DAN/BPA-PC. The shape of the SHG envelope in DAN/BPA-PC was sharp and $\frac{d_{31}}{d_{33}}$ ratio was $\frac{1}{3}$. The extra broadness in the SHG

envelope from rigid 'V' materials may therefore indicate a deviation from the 1:3 relationship assumed. The upper limit of broadening of the envelope function occurs in LB films. In LB films all the molecules are aligned.

In the relaxation studies of either fixed electrode or corona poled rigid 'V' samples there was no significant rapid decay of the alignment. So the decay may not be governed strictly by the size and distribution of free volume. The relaxation mechanism (which was modelled with a single exponential) may be controlled by segmental main-chain rotation. The polar alignment relaxes to 85% of its initial value within 30 hours at room temperature. After this initial relaxation the EO response was stable for at least 200 hours.

7.2 Ideas For Future Work

Poled and cross-linked guest-host, side-chain and main chain polymers show very high and very stable $\chi^{(2)}$ response. Cross-linked polymer samples are good candidate materials for integrated optical device applications. For device applications materials which have physically and chemically stable second order nonlinearity at operating temperatures are required. For example, operation at up to 125 °C may be required with even higher storage temperatures. Poled DAN/BPA-PC systems therefore do not give an answer to device requirements at higher temperatures. The long term thermal stabilities at higher temperatures may be achievable in other guest-host systems which have the potential for hydrogen bonding and higher T_g . For instance for DAN guest molecules, TMBPA, a polycarbonate with T_g of 203 °C, could be used. Hydrogen bonding, however, has its own temperature limitations. Above 130-150 °C the hydrogen bonds break. For temperature requirements over 120 °C the materials which have a potential for hydrogen bonding may not be appropriate for device applications. For moderately high (80-100 °C) temperatures these systems may give a satisfactory answer.

For better understanding of the poling dynamics and the thermal stability of P-4VP samples, ions of a known type and concentration may be introduced into the polymer and the poling efficiency studied with comparison to ion concentration. To increase the

magnitude of the EO response in P-4VP, guest NLO molecules may be introduced into the polymer. If the guest molecule has a hydrogen bonding capability with the pyridine groups, this not only will increase the magnitude of EO response but also will increase the thermal stability of poling induced alignment. It was seen that fixed electrode poled samples show higher EO responses than the corona poled samples. This is not easily understood since much higher poling fields may be achieved with corona poling. Low poling efficiency in corona poled samples may be due to a possible interaction between the ions created and subsequent ion transport in the polymer. If the majority of the ions do not stay on the surface of the polymer sample, it would not be possible to maintain a high field across to the film. The poling of P-4VP samples could be carried out at different poling conditions. For instance the polarity of the high voltage can be changed from (-) to (+). By doing that different type of ions may be produced and this may give an opportunity to test the previous suggestion.

The simultaneous thermally stimulated discharge current, TSD, and second harmonic generation technique could be used to study the poling and relaxation dynamics of rigid 'V' main-chain polymer. TSD measures the thermally stimulated release of the polarisation. The weak side of TSD is the difficulty of assigning the observed relaxation peaks to specific motions at the microscopic level. This can be partly overcome by measuring simultaneously the second harmonic signal. This technique could give useful information about relaxation process of the poled rigid 'V' polymers, since this material has no discernible glass transition temperature above room temperature.

APPENDIX I

The electro-optic effect is defined through the change in the electric impermeability induced by an applied electric field is given by

$$B_{IJ}(E) - B_{IJ}(0) = \left[\frac{1}{\epsilon(E)} \right]_{IJ} - \left[\frac{1}{\epsilon(0)} \right]_{IJ} \equiv r_{JK} E_K$$

where B_{IJ} is the impermeability tensor, E_K the applied electric field.

The linear EO effect can also be defined through the change in the optical susceptibility

$$\Delta\chi_{IJ} = \Delta\epsilon_{IJ} = -\epsilon_{II} \Delta B_{IJ} \epsilon_{JJ}$$

where ϵ_{IJ} is the dielectric tensor

The induced polarisation is then given by

$$P_I(t) = \epsilon_o \Delta\chi_{IJ} E_J(t) = -\epsilon_o \epsilon_{II}(\omega_1) \epsilon_{JJ}(\omega_1) r_{JK} E_J(t) E_K(t)$$

if $\chi_{IJ} = 0$ when $I \neq J$.

The electric fields are defined as

$$\begin{aligned} E_J(t) &= E_J \cos(\omega_1 t + \phi_1) \\ &= \frac{1}{2} [e_J(\omega_1) \exp(-i\omega_1 t) + e_J^*(-\omega_1) \exp(i\omega_1 t)] \text{ and} \end{aligned}$$

$$\begin{aligned} E_K(t) &= E_K \cos(\omega_2 t + \phi_2) \\ &= \frac{1}{2} [e_K(\omega_2) \exp(-i\omega_2 t) + e_K^*(-\omega_2) \exp(i\omega_2 t)] \end{aligned}$$

where $e_i(\omega)$ are the Fourier amplitudes of the electric fields including the overall phase.

Taking $\omega_1 = \omega$ and $\omega_2 = 0$, the polarisation at the optical frequency is then

$$P_I(\omega) = -\epsilon_o \epsilon_{II}(\omega) \epsilon_{JJ}(\omega) r_{JK} e_J^\omega e_K^0$$

If a similar analysis is carried out in the notation of a second order nonlinear optical susceptibility defined through

$$P_I(t) = \epsilon_0 \chi_{IJK}^{(2)} E_J'(t) E_K'(t)$$

$$\text{where } E_{J,K}'(t) = \frac{1}{2} [e_{J,K}(\omega_1) \exp(-i\omega_1 t) + e_{J,K}(\omega_2) \exp(-i\omega_2 t) + \text{c.c.}]$$

then the following relationship between the nonlinear susceptibility and the EO coefficient is obtained

$$\chi_{IJK}^{(2)}(-\omega; \omega, 0) = -\frac{1}{2} \epsilon_{II}(\omega) \epsilon_{JJ}(\omega) r_{JK}(-\omega; \omega, 0)$$

where $\epsilon_{II}(\omega) = n_I^2$, the principal indices of refraction. For typical doped poled polymer films, all principal indices are nearly identical. The $\chi^{(2)}$ is then related to the EO coefficient by

$$\chi_{IJK}^{(2)}(-\omega; \omega, 0) = \frac{1}{2} n^4 r_{JK}(-\omega; \omega, 0)$$

APPENDIX II

$$\Delta\Psi = \frac{2\pi n^3 V}{\lambda \cos \theta'} (r_{33} \sin^2 \theta' + r_{13} \cos^2 \theta' - r_{13}) \quad 3.13$$

By using the relation between r_{33} and r_{13} as $r_{33} = 3r_{13}$ (note: In some polymers having restriction to chain motion, this assumption may not strictly apply) we have

$$\Delta\Psi = \frac{2\pi n^3 V r_{33}}{\lambda \cos \theta'} \left(\sin^2 \theta' + \frac{1}{3} \cos^2 \theta' - \frac{1}{3} \right) \quad A-1$$

and carrying out the mathematical calculations in parentheses

$$\Delta\Psi = \frac{2\pi n^3 V r_{33}}{3\lambda} \left(\frac{3\sin^2 \theta' + \cos^2 \theta' - 1}{\cos \theta'} \right) \quad A-2$$

We can use $\sin^2 \theta' + \cos^2 \theta' = 1$ to proceed with the simplification

$$\Delta\Psi = \frac{2\pi n^3 V r_{33}}{3\lambda} \left(\frac{3\sin^2 \theta' + \cos^2 \theta' - \sin^2 \theta' - \cos^2 \theta'}{\cos \theta'} \right) \quad A-3$$

where $\sin \theta'$ and $\cos \theta'$ are given in terms of known parameters (θ and n) as;

$$\sin \theta' = \frac{\sin \theta}{n} \quad A-4$$

$$\cos \theta' = \left(1 - \frac{\sin^2 \theta}{n} \right)^{\frac{1}{2}} \quad A-5$$

When the above equations A-4 and A-5 are substituted into A-3, the relative phase difference takes the simpler form

$$\Delta\Psi = \frac{4\pi n^3 V r_{33}}{3\lambda} \left(\frac{\sin^2 \theta}{n(n^2 - \sin^2 \theta)^{\frac{1}{2}}} \right) \quad \text{A-6}$$

The transmission factor of a cross-polarised EO modulator is given in equation 3.14. By substituting A-6 into equation 3.14 and using the small angle approximation the linear electro-optic coefficient r_{33} will be given as

$$r_{33} = \frac{3\lambda I_m}{4\pi n^2 V_m I_o} \frac{(n^2 - \sin^2 \theta)^{\frac{1}{2}}}{\sin^2 \theta} \quad \text{3.15}$$

Publications

- P.1 Karakus Y., D. Bloor, and G.H. Cross, "Enhanced Linear Electro-optic Response and Enhanced Stability of Thermo-poled 'guest-host' Polycarbonate Thin Films", J. Phys. D: Appl. Phys., 25, (1992), 1014-1018.
- P.2 Karakus Y., G.H. Cross, and D. Bloor, "Electro-optics in Moderately Doped Thermopoled Polymer Waveguides", ISE 7 Proc., (1991), 827-832
- P.3 Karakus Y., G.H. Cross, D. Bloor, W.E. Douglas, R.J.P. Corriu, and Z.-X. Yang, "Rigid 'V' Silicon-Containing Oligomers: $\chi^{(2)}$ Properties", OMNO Proc. (1992), in print.
- P.4 G.H. Cross, Y. Karakus, D. Gray, D. Bloor, W.E. Douglas, R.J.P Corriu and Z.-X. Yang, "Cooperative Processes in Polar Ordered Polymers", SPIE Proc., 1775, (1992), 144-153.
- P.5 G.H. Cross, Y. Karakus, and D. Bloor, "Electro-optics in Thermopoled Polymer Films", IEEE, Transactions on Electrical Insulation, 28, (1993), 136-142.
- P.6 Bloor D., G.H. Cross, Y. Karakus, and D. Gray, "Poled Electro-optical polymers displaying collective effects", OMNO, Proc. (1992), in print.
- P.7 R.J.P. Corriu, W.E. Douglas, Z.-X. Yang, Y. Karakus, G.H. Cross, and D. Bloor, "Preparation of diphenylsilene polymers containing main chain acetylene and (hetero)aromatic groups. $\chi^{(2)}$ Nonlinear Optical and other properties", submitted to J. Organomet. Chem., (1993).

